Transverse Deck Reinforcement for Use in Tide Mill Bridge

By

Sasha N. Bajzek

Thesis submitted to the Faculty of the Virginia Polytechnic Institute and State University in partial fulfillment of the requirements for the degree of

Master of Science

In

Civil Engineering

Carin L. Roberts-Wollmann, Chair

Thomas E. Cousins

Cristopher D. Moen

February 8, 2013

Blacksburg, Virginia

Keywords: Hybrid-Composite Beam, Tide Mill Bridge, Skewed Bridge, Deck Design

Transverse Deck Reinforcement for Use in Tide Mill Bridge

Sasha N. Bajzek

ABSTRACT

The objective of the research presented in this thesis was to study and optimize the transverse deck reinforcement for a skewed concrete bridge deck supported by Hybrid Composite Beams (HCB's). An HCB consists of a Glass Fiber Reinforced Polymer outer shell, a concrete arch, and high strength seven wire steel strands running along the bottom to tie the ends of the concrete arch together. The remaining space within the shell is filled with foam. The concrete arch does not need to be cast until the beam is in place, making the HCB very light during shipping. This lowers construction costs and time since more beams can be transported per truck and smaller cranes can be used. HCB's are quite flexible, so AASHTO LRFD's design model for bridge decks, as a one-way slab continuous over rigid supports, might not apply well to the HCB's deck design.

A skewed three HCB girder bridge with a reinforced concrete deck and end diaphragms was built in the laboratory at Virginia Tech. Concentrated loads were applied at locations chosen to maximize the negative and positive moments in the deck in the transverse direction. The tests revealed that the transverse reinforcement was more than adequate under service loads.

An Abaqus model was created to further study the behavior of the bridge and to help create future design recommendations. The model revealed that the HCB bridge was behaving more like a stiffened plate at the middle section of the bridge, indicating that the flexibility of the girders needed to be considered.

ACKNOWLEDGEMENTS

I would first like to thank Dr. Carin Roberts-Wollmann, Dr. Tommy Cousins, and Dr. Christopher Moen for the opportunity to work on this project and for all of their support and guidance. It was a really amazing experience getting to be a part of the design, construction, and testing of a full scale HCB bridge.

I would also like to thank John Hillman and Mike Zicko. Their knowledge and enthusiasm for their work is infectious, and it was an absolute pleasure getting to talk to them about their work.

I would like to greatly thank Dr. Dave Mokarem, Brett Farmer, and Dennis Huffman for all of their help in the lab during my testing. They are always willing to help and answer questions, and I could not have completed my testing without them.

I would like to thank Tao Zou for teaching me how to use Abaqus, and always motivating me to take a try. He is an amazing teacher and I appreciate all of his help.

Finally, I am very grateful to my family and friends for loving and supporting me though this whole project. I could not have done this without them.

All pictures were taken by the author.

TABLE OF CONTENTS

LIST OF FIGURES

LIST OF TABLES

CHAPTER 1: INTRODUCTION

1.1 General

With the number of structurally deficient bridges in the United States increasing, now is the time for innovation and creativity in the design of bridges. One such innovation is the Hybrid Composite Beam (HCB), invented by John Hillman in 1996. HCB's both maximize the efficiency of common construction materials and decrease the construction costs. They are already being used in bridges across the country, and the Virginia Department of Transportation (VDOT) is planning on using HCB's for the first time in the Tide Mill Bridge. VDOT funded Virginia Tech to conduct research on a test HCB bridge in the lab to make sure the design is adequate and to provide design recommendations.

1.2 Research Objective

The Tide Mill Bridge is to be replaced by a bridge utilizing Hybrid Composite Beams (HCB's). The objective of this research is to study the behavior of a skewed bridge deck in a bridge with HCB's, and use that information to optimize the transverse deck reinforcement. Loads were applied to the deck at locations chosen to maximize the negative and positive moments in the deck in the transverse direction. Also, an Abaqus model was created to further study the behavior of the bridge and to help with the development of other design recommendations.

1.3 Tide Mill Bridge

The Virginia Department of Transportation (VDOT) will be replacing the current Tide Mill Bridge with Virginia's first bridge to incorporate HCB's (Figure 1-1). It is located on state route 205 in Colonial Beach, VA. The current bridge has a forty five degree skew and spans approximately 52 ft. The new bridge was designed by the engineering firm Parsons Brinckerhoff.

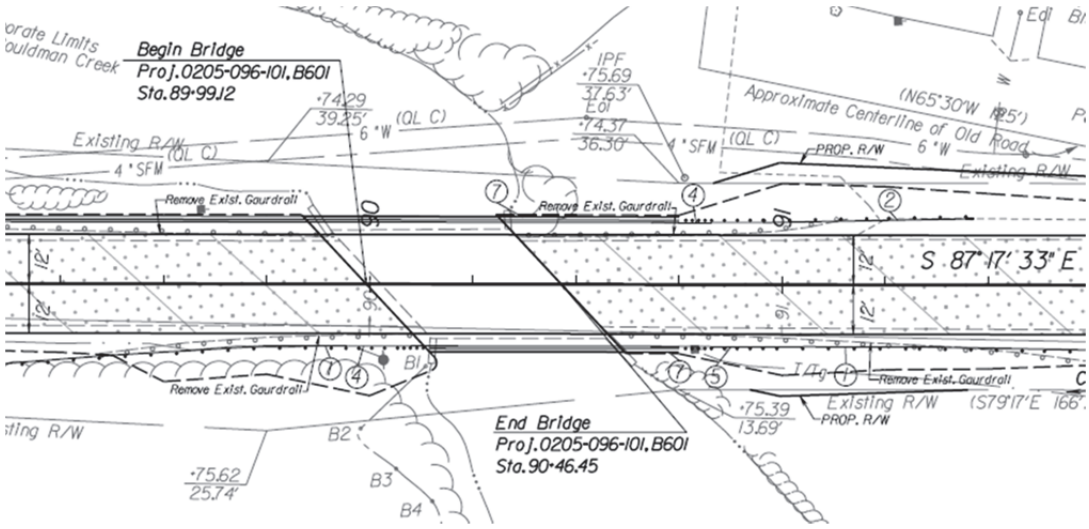

Figure 1-1: Tide Mill Bridge (Ahsan, 2012) Used with permission of Jason Stull, Parsons Brinckerhoff (2013)

1.4 Introduction to Hybrid-Composite Beams

The Hybrid-Composite Beam was invented by John Hillman and is a system that combines the stiffness and strength of concrete and steel with the lightweight and corrosion resistant properties of fiber reinforced polymers (Hillman). A HCB consists of a Glass Fiber Reinforced Polymer (GFRP) outer shell, a self-consolidating concrete arch, and high strength seven wire steel strands that run along the bottom of the beam and tie the ends of the concrete arch together as seen in Figure 1-2. The remaining space within the shell of the beam is filled with low-density foam, making a HCB very lightweight before the concrete arch is placed. Shear reinforcement is embedded into the concrete arch and protrudes out of the top of the HCB and into the concrete deck.

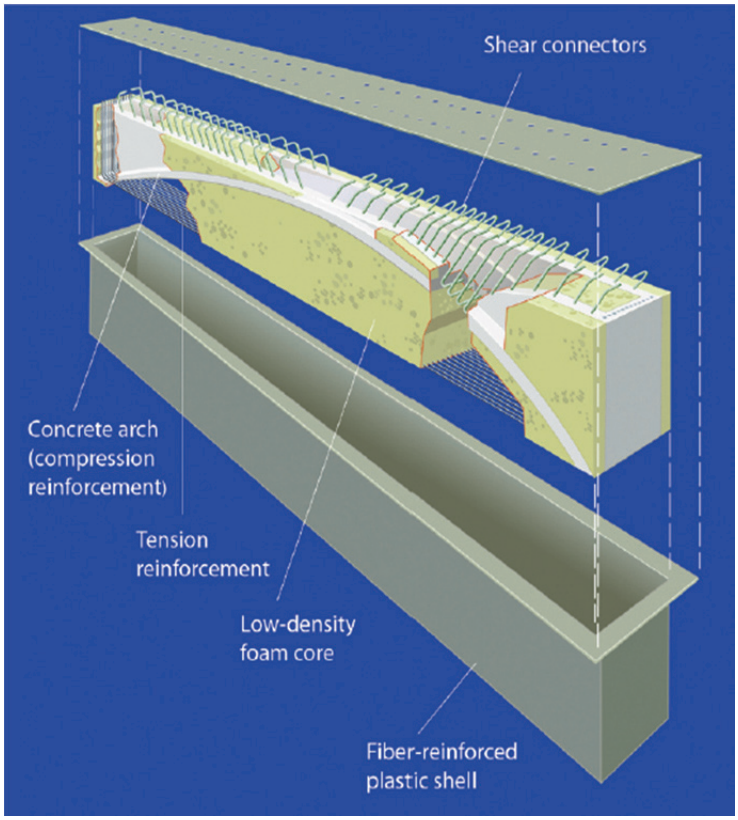

Figure 1-2: Hybrid-Composite Beam (Hillman) Used under fair use, 2013

One advantage of using HCB's is that they can be transported and set in place before adding the concrete to create the arch. Before the arch concrete is placed, the beams weigh approximately 10 percent of the weight of an equivalent concrete beam and 33 percent of the weight of an equivalent steel beam (Hillman). This allows for lower shipping and erecting costs because more beams can be placed on a truck and smaller cranes can be used. Another advantage of HCB's is their sustainability. With its encapsulating GFRP shell, HCB's do not rust, spall, or need painting, and provide a 100+ year service life (Hillman). The current disadvantage of using HCB's is that they are such a new product. Because they are so new, there is not much experience in designing structures with them with is one of the reasons for this research.

HCB's can be used in bridges spanning up to 120 ft, marine structures, roofs, and decks. HCB's have already been used in bridges in Illinois, Maine, and New Jersey. The bridge shown in Figure 1-3 is the 540 ft long Knickerbocker Bridge located in Boothbay, Maine, which is the longest HCB bridge constructed thus far. (POPSCI, 2011)

Figure 1-3: Knickerbocker Bridge (POPSCI, 2011) Used under fair use, 2013

1.5 Introduction to Skewed Bridge Decks

Skewed bridges are bridges where the major axis of the substructure is not perpendicular to the longitudinal axis of the superstructure (PCI). Approximately two-thirds of all bridges nationwide are skewed (AASHTO C4.6.2.1.1). Some reasons for the use of a skewed bridge design are: complex intersections, manmade or natural obstacles, mountainous terrain, and space limitations. Skewed bridges behave differently than rectangular bridges. According AASHTO C.4.6.2.1.1, "skew generally tends to decrease extreme force effects, it produces negative moments at corners, torsional moments in the end zones, substantial redistribution of reaction forces, and a number of other structural phenomena that should be considered in design."

1.6 Scope

The type of structure considered in this study is a skewed single-span bridge over flexible beams. The supporting flexible girders tested and modeled in this research project are Hybrid Composite Beams. The slab is terminated at the outer web of the outer beam so there is no overhang. All of the girders are assumed to be parallel and have identical properties. The effects of barriers, curbs and parapet walls are ignored.

CHAPTER 2: LITURATURE REVIEW

2.1 Overview

This literature review covers the behavior of bridge decks including skewed bridge decks. The history of bridge deck design methods is also covered, from Westergaard's 1930 paper to current studies in bridge deck design with flexible beams. Finally, overviews of various bridge deck design methods are presented.

2.2 Deck Behavior

2.2.1 Beam-and-Slab Decks

A beam-and-slab deck is one where a thin continuous slab is supported by longitudinal beams. When loaded, the slab acts compositely with the longitudinal beams and the load is transfer longitudinally to the supports. Also, the load is distributed transversely from the most heavily loaded beams to the neighboring beams. There are two main types of beam-and-slab decks: 'contiguous beam-and-slab' decks where the beams are at close centres or touching and 'spaced beam-and-slab' decks where the beams are at wide centres. The beams in spaced beam-and-slab decks are usually spaced between 6 ft and 12 ft center to center. (Hambly, 1991)

2.2.2 Contiguous Beam-and-Slab Bridge Decks

The Tide Mill Bridge and the test bridge have a girder spacing of 4 ft with the beams touching one another. This type of beam-and-slab system falls under the category of contiguous beam-and-slab bridge decks. These types of decks deflect in a smooth wave when a load is placed on it, and the load distribution behavior is similar to an orthotropic slab with longitudinal stiffening as seen in Figure 2-1. (Hambly, 1991)

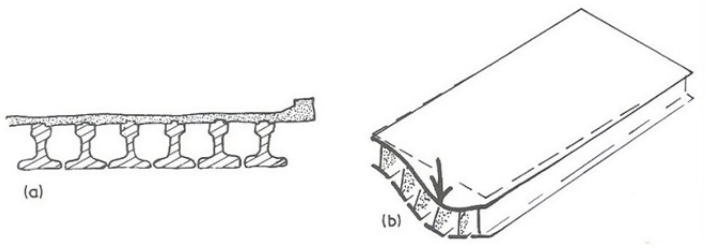

Figure 2-1: (a) Contiguous Beam-and-Slab Deck and (b) Deflection (Hambly, 1991) Used under fair use, 2013

2.2.3 Skew Deck Behavior

In bridge decks with significant skew, there is a non-uniform distribution of reactions at the supports. The greatest reactions usually occur at the obtuse corners and the smallest reactions occur at the acute corners. In some bridges with a large skew angle, uplift can even occur at the acute corners. The high reactions in the obtuse corners lead to high shear forces. (O'Brien & Keogh, 1999).

2.2.4 Skewed Bridge Conceptual Design

When a skewed bridge is loaded, the load tends to be carried to the supports via the shortest path. Because that shortest path is usually to the obtuse corners, the obtuse corners are more heavily loaded than the acute corners. The principle stress caused by bending and torsion in the horizontal plane is in the direction between the girder axis and the normal to the support axes. (Menn, 1990)

A skewed bridge's behavior is determined by the ratio of torsional stiffness to bending stiffness. Because the edges perpendicular to the longitudinal axis of the bridge deflect differently, the cross section twists. Figure 2-2 shows the twisting action a skewed bridge may undergo, with the first part of the figure showing the undeformed shape of the bridge and the deflected shape right below it. The next part of the figure shows the forces, moments, and torsion at the ends of the girders. The last part of Figure 2-2 shows the stresses in the lower fibres of a girder with the adjacent dashed rectangle representing the undeformed girder and the solid rectangle showing the girder after twisting. (Menn, 1990)

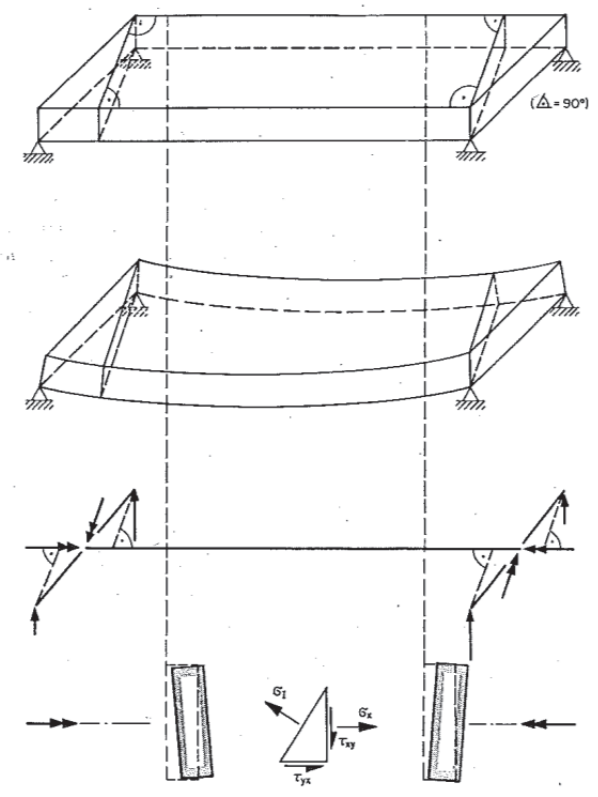

Figure 2-2: Structural Behavior of Skew Girder Bridges (Menn, 1990) Used under fair use, 2013

The behavior near the supports at the ends of the beams of skew bridges includes a force couple and longitudinal bending moments cause by the compatibility torsional moments. Figure 2-3 shows rotations are possible at the girder ends. The rotations occur about the vector ω_n, which is perpendicular to the support axis, and are restrained by the end diaphragm. (Menn, 1990)

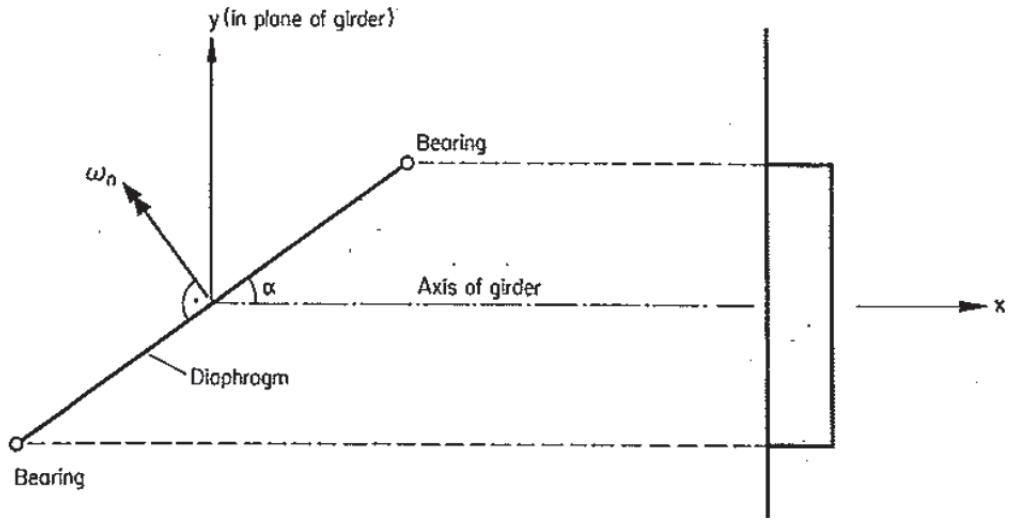

Figure 2-3: Model of Supports of Skew Box Girder Bridges (Menn, 1990)

2.3 History of Slab Design Methods

2.3.1 Timber to Concrete

The history of bridge decks began in the 20th century. Since the earliest settlements in colonial times and well into the 1920s, timber was the primary material used for decks and stringers. However, with the introduction of concrete bridges, concrete decks seemed more prudent. Reinforced concrete became the primary material for bridge decks when motor vehicles became the dominant mode of transportation in America. Reinforced concrete was well established as a building material and knowledge of how to design with it was widespread by the 1930s. (Bettigole & Robinson, 1997)

2.3.2 Westergaard

In March 1930, H. M. Westergaard's article titled "*Computation of Stresses in Bridge Slabs due to Wheel Loads*" was published in *Public Roads Magazine*, and became the basis for standards of design for reinforced concrete bridge decks. Westergaard's article went into great detail deriving and presenting formulas, tables, and diagrams using plate theory to be used to find the bending and twisting moments in bridge decks at various locations under different loads. (Westergaard, 1930)

Westergaard's calculations were conducted by treating the slab as being supported on beams parallel to the direction of y as shown in Figure 2-4. He considered the slab to extend infinitely

far in the directions of +y and –y with no beams or edges in the direction of x. Westergaard's theory also considers the beams supporting the slab as nondeflecting supports that can be treated as simply supported or fixed edges for the slab. Therefore, the deflections of the beams are ignored.

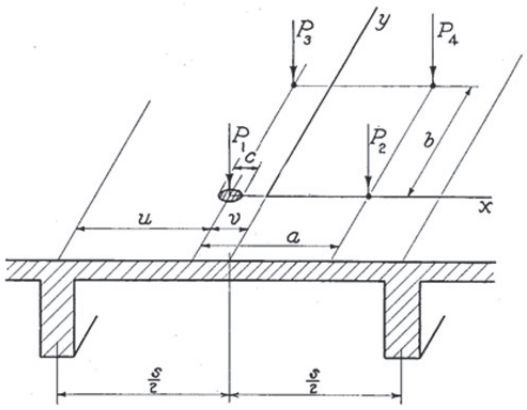

Figure 2-4: Slab Supporting Wheel Loads (Westergaard, 1930) Used under fair use, 2013

Westergaard used two theories of flexure of slabs: ordinary theory and special theory. Ordinary theory is based off of Bernoulli and Navier's assumption of the plane cross section of a beam remaining plane and normal to the elastic curve of a beam. Westergaard deemed this assumption as acceptable for slabs used commonly in bridges with the exception of "expressing the stresses produced by a concentrated load in its immediate vicinity." In this case, he used special theory, which treats the load as a distributed load over the area of a circle with an equivalent diameter. Doing so allows ordinary theory to once again be used. (Westergaard, 1930)

Westergaard provided a derivation of the fundamental equations of ordinary theory of flexure of slabs, which lead to the conclusion that the problem of ordinary theory of flexure of the slab is to find a solution of Lagrange's equation ($N * \Delta^2 z = w$) that satisfies the special conditions existing at the boundary of the investigated area. The boundary conditions are: the bending moments (M_x and M_y), the twisting moment (M_{xy}), the vertical shears (V_x and V_y), and the reactions (R_x and R_y). Figure 2-5 shows the twisting moments and the shears at the edge of the slab. (Westergaard, 1930)

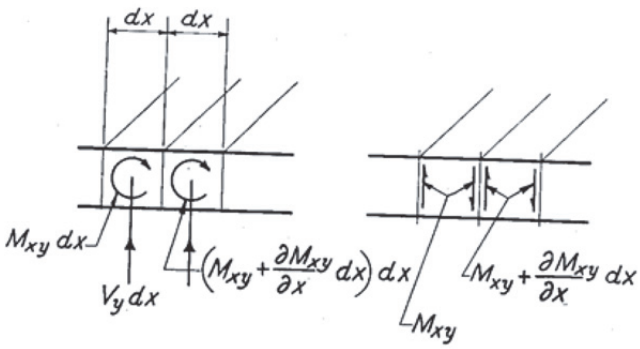

Figure 2-5: Twisting moments and Shears at Edge (Westergaard, 1930) Used under fair use, 2013

The first load case Westergaard considered was the case of a wheel load at the center as seen in Figure 2-6 with simply supported edges. He developed an equation which he then graphed (Figure 2-7) to determine the values of the coefficients of moments at the center ($\frac{M_{ox}}{P}$ and $\frac{M_{oy}}{P}$) in the directions of x and y. With a known value of the applied load, P, and the value from the graph, the bending moments can be obtained with the unit being moment per unit width such as $\frac{in.-lb}{in.}$ or $\frac{ft-lb}{ft}$. (Westergaard, 1930)

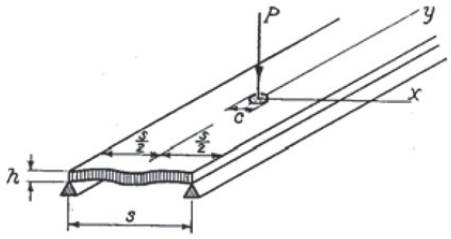

Figure 2-6: Wheel Load at Center (Westergaard, 1930) Used under fair use, 2013

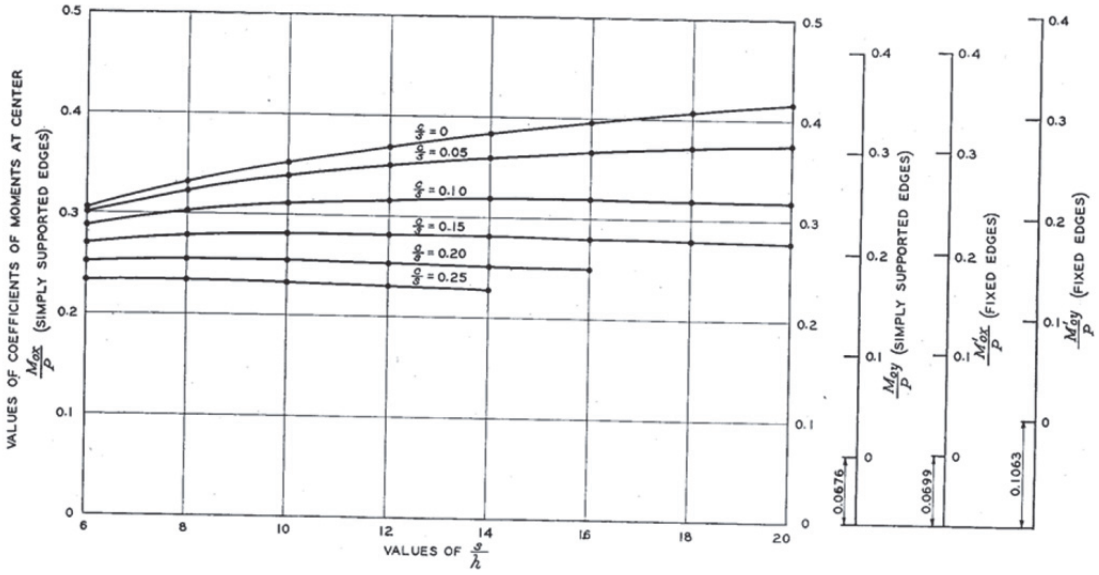

Figure 2-7: Coefficients of Bending Moments in Directions of x and y Produced at Center of Slab by a Central Load P Distributed Uniformly Over the Area of a Small Circle with Diameter c (Westergaard, 1930) Used under fair use, 2013

Westergaard went on to discuss the effective width, b_e. He stated that the moment could be produced as the maximum moment per unit of width in a simple beam with span s and width b_e when the load P is applied at the center of the span and distributed over the width of the beam. If the effects of Poisson's ratio are ignored, the bending moment may be assumed to be distributed uniformly over the width. Westergaard defined the effective width with the equation, $b_e = \frac{P*s}{4*M_{0x}}$. He then graphed values of the effective width for varying ratios of span to thickness as shown in Figure 2-8. The straight lines on the right side can be used as an approximation for the curves and follow the equation, $b_e = 0.58s + 2c$. (Westergaard, 1930)

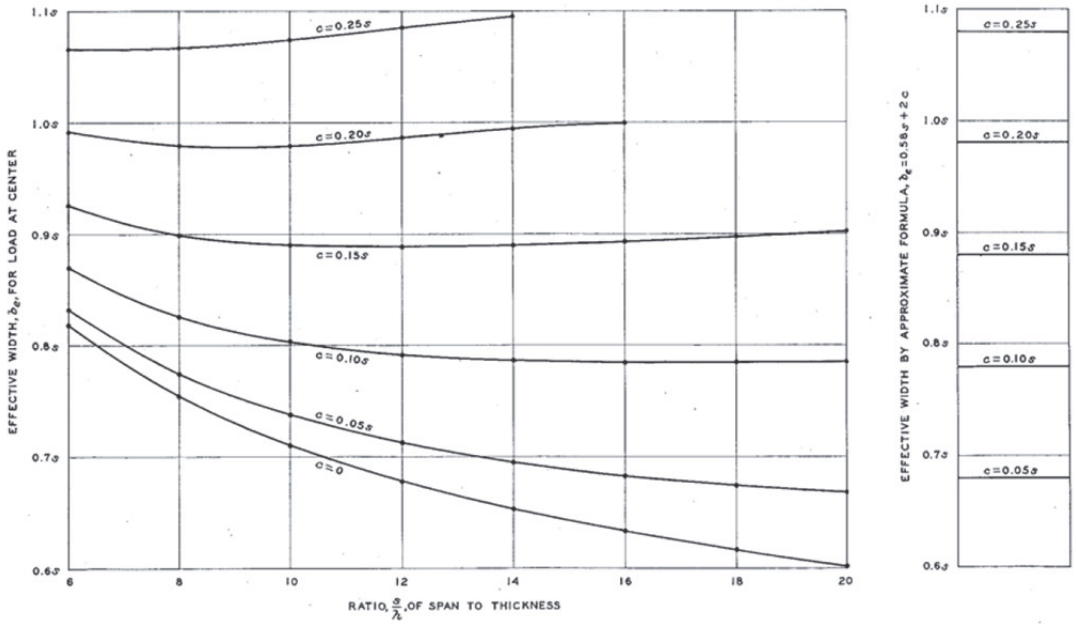

Figure 2-8: Effective Width, b_e, for Central Load Distributed Uniformly Over the Area of a Small Circle with Diameter c (Westergaard, 1930) Used under fair use, 2013

Westergaard then went on to determine equations and graphs for: moments computed for case of two wheel loads on line in direction of span, moments computed for two loads on center line, moments computed at center for load at any point and at any point for load at center, moments produced at point of application of one load by two other loads, and combined effects of four loads. He also investigated: the changes caused by introduction of beam in direction z, effects of changing from simply supported edges to fixed edges, a slab cantilevered from a single fixed edge, and reactions. (Westergaard, 1930)

2.3.3 Newmark

Beginning in 1936, the University of Illinois started a research program to attempt to answer some questions regarding the design of highway bridges. Newmark and Siess summarized the results which were obtained by a combination of mathematical analyses and laboratory tests. In 1938, Newmark developed a method that correctly accounted for the actions of a slab continuous over noncomposite supporting girders. He derived it from the moment distribution method developed by Hardy Cross. The solution obtained from this method is in the form of an infinite trigonometric series with each term being determined from numerical calculations involving fixed-end moment, stiffness, and carry-over factors applied to an analogous continuous beam. Newmark and Siess were then able to determine the structural behavior and distribution of load

for a large number of right slab-and-girder bridges by using Newmark's method to analyze them. The analytical results of their study are what the well-known S/5.5 wheel load fraction is based upon. This method is limited, however, because it does consider composite action, girder torsion, or skew of bridges. (Marx, Khachaturian, & Gamble, 1986)

2.3.4 Standardization

In the 1950s, the design of bridge decks became standardized with a set of typical plan drawings published by the Bureau of Public Roads. These drawings showed the typical details for reinforced concrete decks for several types of bridges, and created the policy for bridge engineers to primarily choose reinforced concrete as the material of choice for bridge decks. Therefore, in 1956, when the elements of bridges were being standardized for the Interstate Highway System's program to build 41,000 miles of new bridges and highways, there was no further discussion to standardize bridge decks. Individual states developed their own standards based on AASHTO specifications, also focusing primarily on reinforced concrete design for bridge decks. (Bettigole & Robinson, 1997)

While the standardization of deck design has the benefits of saving time and money when designing, it also has its disadvantages. Because it restricts bridge design to a set of standards, it also restricts innovation. (Bettigole & Robinson, 1997) For example, in Newmark's paper "Design of I-beam Bridges" in 1949, Newmark studied the behavior of bridge decks and found that girder deflections should be included in the calculations for slab design moment. (Cao, 1996) However, today girder deflections are still not accounted for in deck design.

2.4 Slab Design Methods

2.4.1 Overview of Design Methods for Slabs in Slab-Girder Bridges

Three methods for designing slabs are: the analytical strip method approach, the empirical approach, and the yield-line method. These methods can be used to proportion the slab and generally give different designs that are acceptable for use. The strip method represents a lower bound representation of the carrying capacity and gives results on the safe side, which is preferable in practice. Whereas the yield-line method is an upper bound method and therefore errs on the unsafe side. (Nilson, Darwin, & Dolan, 2004) There has also been research done to

develop new methods of designing the top mat of transverse reinforcement for decks on flexible beams.

2.4.2 Strip Method

When a deck has an aspect ratio of 1.5 or above, it may be considered a one-way slab system. For example, the Tide Mill Bridge will be using 44 ft long beams at a 4 ft girder spacing, so it will have an aspect ratio of 11.0, qualifying for one-way slab behavior. One-way slabs carry loads in a beamlike manner to the girders and the main issue is to determine the strip width of the deck used for analysis and design. (Barker & Puckett, 2007) The effective strip width is the width over which one axle of the design truck or tandem acts. (TXDOT, 2010) Near the point of application of a load, the effect on the deck is high, but this dissipates the further away from the load a point is in the longitudinal direction. The strip width is the effective width of the deck affected by the load. Table 2-1 shows the equations in Table 4.6.2.1.3-1 of AASHTO (2012) used to determine strip widths for concrete decks, where S is the girder spacing (ft) and X is the distance from load to point of support (ft). The values are based on past experience, and practical experience and research may lead to refinement. (AASHTO, 2012)

Table 2-1: AASHTO Strip Widths for Concrete Decks (AASHTO, 2012) Used under fair use, 2013

Type of Deck	Direction of Primary Strip Relative to Traffic	Width of Primary Strip (in.)
Concrete:		
• Cast-in-place	Overhang	45.0 + 10.0X
	Either Parallel or Perpendicular	+M: 26.0 + 6.6S -M: 48.0 + 3.0S
• Cast-in-place with stay-in-place concrete formwork	Either Parallel or Perpendicular	+M: 26.0 + 6.6S -M: 48.0 + 3.0S
• Precast, post-tensioned	Either Parallel or Perpendicular	+M: 26.0 + 6.6S -M: 48.0 + 3.0S

Shown in Figure 2-9 (a), is an example of a strip and its strip width, SW. Figure 2-9 (b) shows the bridge's deflection in the transverse direction when it is loaded to create maximum positive moment. This deflection is a combination of the local effects shown in Figure 2-9 (c)

and the global effects shown in Figure 2-9 (d). The local effects consist of the bending of the strip due to the wheel loads on the strip and the global effects consist of the bending of the strip from the displacement of the girders. The global effect is usually very small compared to the local effects, and may be neglected. The strip may then be analyzed using classical beam theory with the assumption that the girders are a rigid support. (Barker & Puckett, 2007) (AASHTO 4.6.2.1.5)

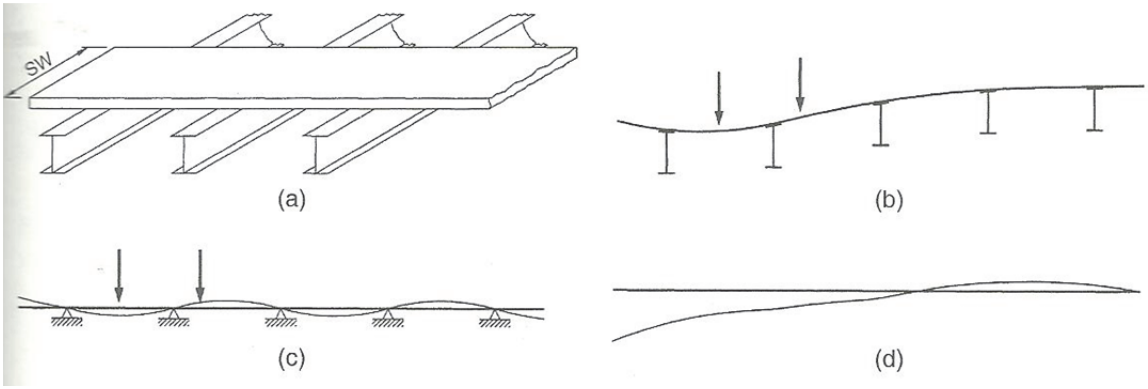

Figure 2-9: (a) Idealized Design Strip (b) Transverse Section Under Load (c) Rigid Girder Model (d) Displacement Due to Girder Translation (Barker & Puckett, 2007) Used under fair use, 2013

The procedure for determining the maximum positive and negative live load moments in a bridge deck in the transverse direction using the strip method approach begins by finding the strip widths. Table 4.6.2.1.3-1 in AASHTO (2012) as shown in Table 2-1 may be used to find the strip widths for the positive and negative moment regions. Next, using the strip model of the slab with the girders acting as infinitely rigid supports and the deck acting as a continuous beam over those supports, the maximum positive and negative bending moments of the model are determined using any beam analysis method such as moment distribution. Once the critical moments are determined, they are divided by their respective strip widths to calculate the moments per foot which is used for design. (Barker & Puckett, 2007) According to AASHTO Section 4.6.2.1.1, the maximum positive moments in any deck panel between the girders is used for all positive moment regions, and the maximum negative moments in any deck panel between the girders is used for all negative moment regions. (AASHTO, 2012)

2.4.3 Empirical Approach

The empirical approach assumes that limits states are satisfied as long as a few simple rules regarding deck thickness and reinforcement details are satisfied. Analysis is not required. (Barker & Puckett, 2007) The empirical approach is further discussed in Section 2.5.1 with information from AASHTO.

2.4.4 Yield-Line Method

In the yield-line method, the slab is assumed to behave inelastically and have enough ductility to sustain the applied load until a plastic collapse mechanism is reached. A collapse mechanism occurs through a system of plastic hinges called yield lines which form a pattern in the slab, creating the mechanism. Different yield-line patterns are tried until the minimum load needed to create a collapse mechanism is determined. The two methods of yield-line analysis are the equilibrium approach and the energy approach. The energy approach is described here as it is the upper-bound approach. (Barker & Puckett, 2007)

The assumptions and fundamentals of yield-line theory are:

“

- In the mechanism, the bending moment per unit length along all yield lines is constant and equal to the moment capacity of the section.
- The slab parts (area between yield lines) rotate as rigid bodies along the supported edges.
- The elastic deformations are considered small relative to the deformation occurring in the yield lines.
- The yield lines on the sides of two adjacent slab parts pass through the point of intersection of their axes of rotation

“ (Barker & Puckett, 2007)

When using the yield line method, it is assumed that the distribution of reinforcement is already known for the system. Therefore, it is more of an analysis tool, and when used for design, an iterative approach must be taken. The capacities of various trial sections are calculated with different reinforcement designs until a satisfactory design is chosen. (Nilson, Darwin, & Dolan, 2004)

2.4.5 Grillage Method

One of the best ways to model a deck is to model it as a thin plate using a biharmonic equation. This method, however, has limited solutions available for girder-supported systems, and therefore, approximate techniques and numerical models have been created. The most common of these are grillage, finite-element, and finite-strip methods. In the early 1960s, grillage models became popular with the advancement of the digital computer. (Barker & Puckett, 2007)

The grillage method, which is based on the stiffness matrix approach, consists of transforming a bridge deck structure into an equivalent system of beams that are rigidly connected at nodes. The beams have equivalent flexural and torsional stiffness with the members they represent and the nodes that connect them are continuous for rotation in all directions. Any applied loads must be converted into equivalent nodal loads in order to be applied to the system. (Gupta & Dhir)

There are five main steps to obtain design responses with a grillage model:

“

i. Idealization of physical deck into equivalent grillage
ii. Evaluation of equivalent elastic inertia of members of grillage
iii. Application and transfer of loads to various nodes of grillage
iv. Determination of force responses and design envelopes
v. Interpretation of results

” (Gupta & Dhir)

Choosing the grillage mesh requires consideration of the structural behavior of the particular deck and it is difficult to create a set of rules. Figure 2-10 shows some examples of grillage meshes for different types of bridge systems. The different types and spacings of the girders for each example are considered when choosing the layout of the grillage mesh. Some examples of grillage meshes for skewed decks are also shown in Figure 2-11 and Figure 2-12. (Hambly, 1991)

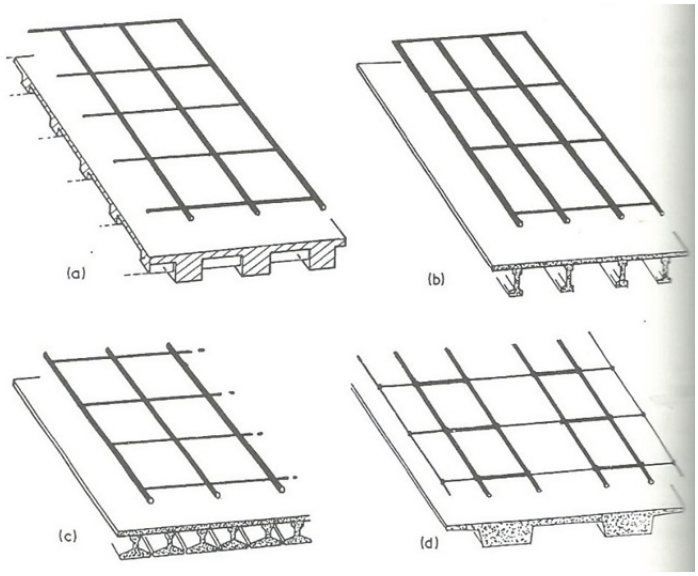

Figure 2-10: Grillage Mesh Examples (Hambly, 1991) Used under fair use, 2013

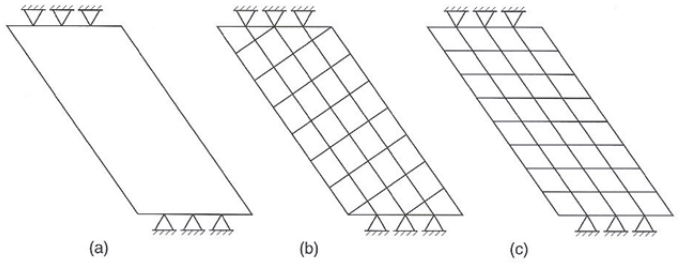

Figure 2-11: Grillage Mesh for Long and Narrow Bridge Decks with Large Skew (a) Plan View, (b) Grillage Layout, (c) Alternative Grillage Layout (O'Brien & Keogh, 1999) Used under fair use, 2013

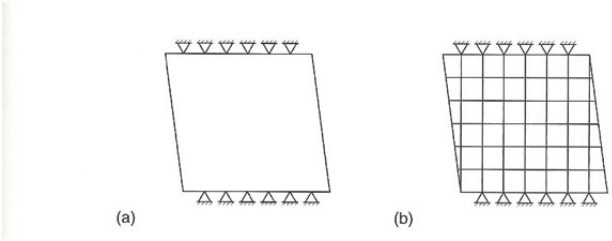

Figure 2-12: Grillage Mesh for Short and Wide Bridge Decks with Small Skew (a) Plan View, (b) Grillage Layout (O'Brien & Keogh, 1999) Used under fair use, 2013

The longitudinal grillage member section properties are calculated about the centroid of the section it is representing and include the composite section. Figure 2-13 shows the part cross-section and the amount of each deck represented by the appropriate longitudinal grillage member for three beam-and-slab decks. The transverse grillage member section properties only represent

the slab and are calculated as if for a slab. For instance, the moment of inertia $I = \frac{(b*d^3)}{12}$ and $C = \frac{(b*d^3)}{6}$. If a diaphragm is included, an estimate must be made of the width of slab acting as a flange. (Hambly, 1991)

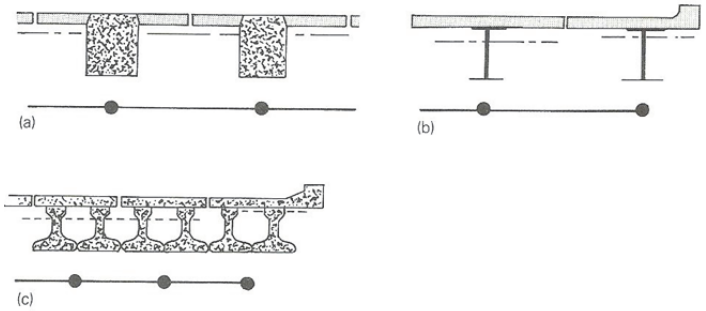

Figure 2-13: Sections Represented by Longitudinal Grillage Members (Hambly, 1991) Used under fair use, 2013

Using grillage models has both advantages and disadvantages. The advantages of using a grillage model is that the results can be easily interpreted and equilibrium can easily be checked. Also, a grillage model can be used with any program with plane grid or space frame capabilities. Critics on the other hand, consider grillage models nonrigorous and point out that the method requires experience in order to obtain mesh designs and refinement that yield good solutions. (Barker & Puckett, 2007)

2.4.6 Finite Element Method

The finite-element method is a versatile and powerful numerical method. It is most commonly based on a stiffness approach where a system of equilibrium equations is created and solved for the displacements at the degrees of freedom. There are many different types of elements with many different numbers of degrees of freedom and response characteristics available to use in modeling. (Barker & Puckett, 2007) Two examples of meshes for skewed decks are shown in Figure 2-14.

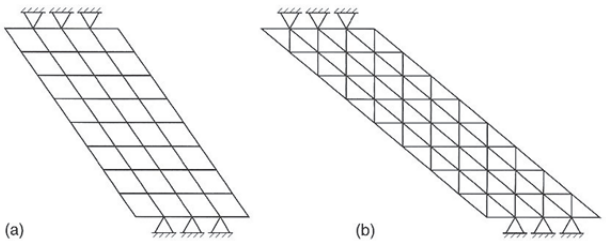

Fig. 6.37 Alternative finite-element meshes: (a) skewed quadrilateral finite elements; (b) alternative triangular elements

Figure 2-14: Finite-Element Meshes for Skewed Decks (O'Brien & Keogh, 1999) Used under fair use, 2013

There are both 2D and 3D finite-element models. The 2D model is simpler and has fewer degrees of freedom. For example, a plate element contains three degrees of freedom per node. A 3D model may use shell elements that combine the in- and out-of plane effects with six degrees of freedom per node. (Barker & Puckett, 2007)

It is recommended to do an equilibrium check when using a finite-element model in order to check for any errors.

2.4.7 New Methods for Deck Design on Flexible Beams

In deck design, AASHTO currently ignores the effect of girder deflections and uses one-way bending to calculate the required size and number of top mat transverse reinforcing bars. This method is conservative especially in the case of flexible beams, and therefore research has been done to study and account for the flexibility of girders in the design of the top reinforcement of bridge decks.

2.4.7.1. Cao 1996

It has been observed that often the cracks in the deck surface are in the transverse direction and not the longitudinal direction, indicating that the cracks were due to shrinkage and not flexure. Therefore, various research projects have been conducted to determine the need for top mat reinforcement such as research done by Beal in 1982 and Fang et al. in 1990. They found that the negative bending moments and top tensile stresses in bridge decks are usually very low and much less than the positive bending moments and bottom tensile stresses. (Cao, 1996)

Cao's research explores the idea that the amount of top mat reinforcing in bridge decks can be greatly reduced. Cao investigated the behavior of an actual four-span highway bridge and

analyzed the behavior of the bridge deck with the finite-element method. In all of Cao's experimental tests, the maximum tensile strain in the top transverse reinforcement was always less than 40με. This is about 30% of the expected cracking strain of the deck concrete. Cao's finite-element model predictions closely followed the experimental tests and the model was used to conduct further tests with a single test truck and two model trucks. From all of his testing and modeling, Cao found that the top transverse reinforcement was not required in a properly designed deck for sustaining negative bending moment from traffic loads. However, some shrinkage and temperature cracks were observed in top of the bridge deck and therefore Cao recommended further study of the reinforcement required to prevent cracking due to temperature and shrinkage. (Cao, 1996)

While Cao's research is a good benchmark for study of design of bridge decks on flexible beams, it was based on plate theory which ignores the number of loaded lanes, and the equations Cao used were based on only one wheel load at the midspan of the deck. The research in the following section takes into account more variables than Cao's research by looking into the effects of girder spacing, the span length of the girders, the width of the roadway and various patterns of traffic. (Tangwongchai, Anwar, & Chucheepsakul, 2011)

2.4.7.2. Flexural Responses of Concrete Slab over Flexible Girders

Tangwongchai, Anwar, and Chucheepsakul developed a method for finding the maximum negative moment in the transverse direction in bridge decks with flexible beams. They carried out a finite-element based parametric study that focused on the effect of girder flexibility due to patterns of moving loads and created empirical relationships to find the maximum slab moment at any point along the girder span. Using their method reduces the maximum moment compared to the AASHTO values, and therefore requires less reinforcement, reducing the cost of the bridge deck by at least 30%. (Tangwongchai, Anwar, & Chucheepsakul, 2011)

Tangwongchai's finite-element model (FEM) was validated by comparing the deformations and forces from the model to the experimental results from testing done by Fang et al. This experiment was chosen because it provided a full-scale test with realistic boundary conditions. Both the deflections of the girders and the maximum transverse moments of Tangwongchai's

model were acceptable when compared to the test results. (Tangwongchai, Anwar, & Chucheepsakul, 2011)

Various bridge deck geometries were used in the parametric study. In order to use the AASHTO 2004 Table A4.1-1 for deck slabs, it is required that the deck be supported by at least three girders with a deck width of at least 14 ft. Therefore, tests were run with three to five girders that had a spacing (S) of 8 ft, 10 ft, and 12 ft. The deck thickness was set to be 8 in. and the overhang was set to 3.28 ft. (Tangwongchai, Anwar, & Chucheepsakul, 2011)

The different bridge layouts were loaded with various vehicle patterns consisting of HS-20 design trucks. The loading condition was expressed by the ratio $N = N_L / N_G$, where N_L is the number of transverse traffic lanes and N_G is the number of girders. The results reported were for the load configurations that produced the maximum negative moment in the transverse direction. (Tangwongchai, Anwar, & Chucheepsakul, 2011)

The maximum moments (M) were found at a location ¼ of the top flange width from the center line of the girder with length L at a loading position of y from the girder's support at a maximum wheel load of P. The maximum moments M were determined for each of the three girder spacings, S, at loading position y/L for the cases of one loaded lane ($N = 0.33$) and two to five loaded lanes ($0.40 \leq N \leq 1.00$). Figure 2-15 shows how the ratios of M/P are mostly sensitive to y/L only when they seem to be influenced by N and S. It also shows that the AASHTO LRFD Specifications have a much higher design moment than one that takes into account the flexibility of the girders. (Tangwongchai, Anwar, & Chucheepsakul, 2011)

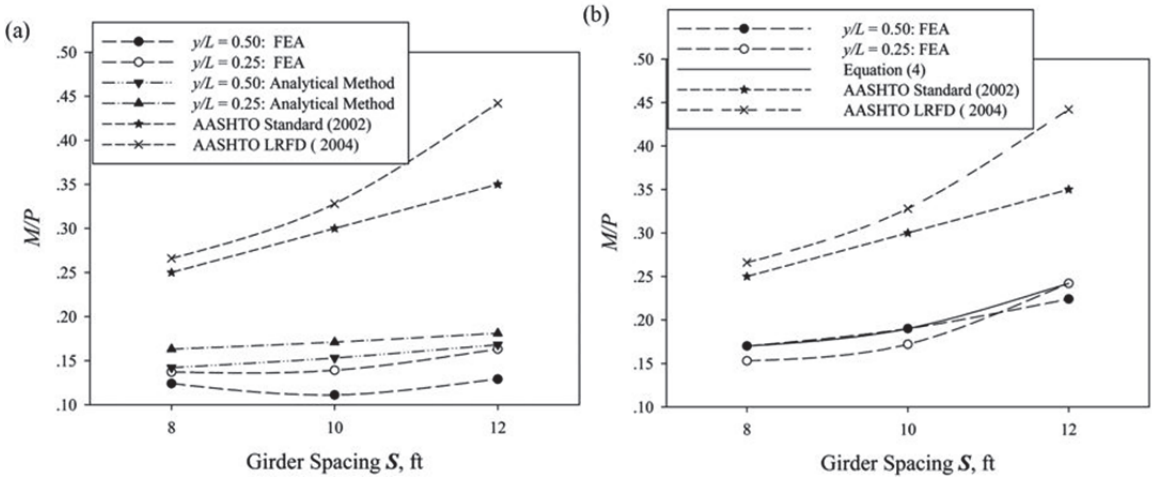

Figure 2-15: Variation of Normalized Moment M/P with Respect to S for Various Numbers of Girders and Loaded Lanes: (a) N = 0.33 (N_L =1 and N_G =3), (b) 0.40 ≤ N ≤ 1.00 (N_L = 2-5 and N_G = 3-5) (Tangwongchai, Anwar, & Chucheepsakul, 2011) Used under fair use, 2013

When N is less than 0.33, the deck slab deflects more flexibly which was both stated by Cao and seen in the graph on the left in Figure 2-15. This flexibility leads to more global deformation of the slab and smaller transverse moments. The opposite effect is seen when N is greater than 0.33. Local deformation occurs in the slab with rigid support behavior which leads to higher moments. (Tangwongchai, Anwar, & Chucheepsakul, 2011)

The following proposed equations do not include the impact factor IM from AASHTO, which is to be included in calculations later. Using a curve fitting technique, a relationship was determined for M with an R-square value of 0.95. The relationship M/P = 0.41 – 0.062S + $0.004S^2$ was determined from the governing cases in second graph in Figure 2-15. A second set of relationships was determined for the maximum transverse bending moment M in the slab in terms of S and y/L as follows:

For S = 8 ft: $M = \left\{ 0.150 - 0.048\frac{y}{L} + 0.048 \left(\frac{y}{L}\right)^2 \right\} P$

For S = 10 ft: $M = \left\{ 0.159 - 0.096\frac{y}{L} + 0.096 \left(\frac{y}{L}\right)^2 \right\} P$

For S = 12 ft: $M = \left\{ 0.246 - 0.059\frac{y}{L} + 0.059 \left(\frac{y}{L}\right)^2 \right\} P$

The three values shown for S are the spacing used in this study. For different values of S,

interpolation or the previous relationship may be used. For all of these relationships, P is a single wheel load, $N \leq 1.00$, stiffness ratio $D_x/D_y \leq 0.025$, $S/L \leq 0.02$, $S/t \leq 18$ and $0.25 \leq y/L \leq 0.75$. (Tangwongchai, Anwar, & Chucheepsakul, 2011)

Figure 2-16 shows the ratio between the required reinforcement area A_s and the temperature reinforcement area A_{Temp} calculated with several methods. It shows that the empirical method proposed by Tangwongchai has a much lower A_s / A_{Temp} ratio compared to the values obtained from AASHTO and in some cases, only the reinforcement for temperature may be required. Tangwongchai found that for a practical range of deck slab ($S \leq 12$ ft), when the flexibility of the beams is taken into account in the flexible zone there is a savings of at least 30% compared to the AASHTO Standard. (Tangwongchai, Anwar, & Chucheepsakul, 2011)

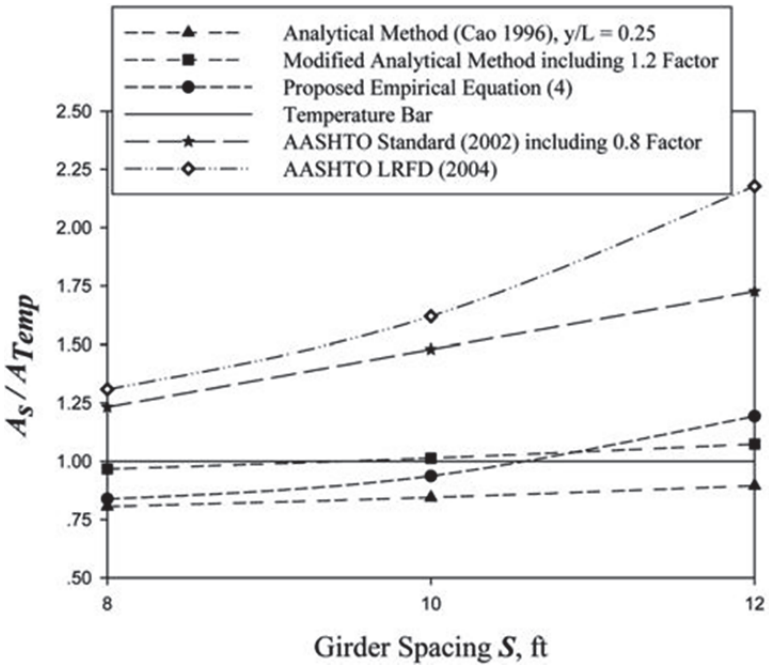

Figure 2-16: Comparison Reinforcement Areas As with the Minimum Atemp Excluding Impact (Tangwongchai, Anwar, & Chucheepsakul, 2011) Used under fair use, 2013

2.5 AASHTO

There are two methods of deck design presented in AASHTO (2012), empirical design and traditional design. AASHTO also specifies reinforcement requirements for control of cracking and temperature and shrinkage.

2.5.1 Empirical Design Method

Through extensive research into concrete deck slab behavior, it was observed that it is internal arching that primarily resists concentrated wheel loads instead of flexure. This complex internal membrane stress is made possible through the cracking of concrete in the positive moment region and the consequent upward shift of the neutral axis in that part of the slab. In-plane membrane forces develop from the lateral confinement from the surrounding concrete slab, rigid appurtenances, and supporting components acting compositely with the slab. An internal compressive dome is created that fails through punching shear when the perimeter of the wheel footprint is overstressed. The specified minimum amount of isotropic reinforcement adequately provides the global confinement needed to develop the arching effects and resist the small amount of local flexure. Tests have shown that the empirical design method provides a factor of safety of 8. (AASHTO C9.7.2.1)

Certain requirements must be met in order to use the empirical design method. They are described in AASHTO Section 9.7.2.4 and some of them include:

“

- Cross-frames or diaphragms are used throughout the cross-section at lines of support
- The supporting components are made of steel and/or concrete
- The deck is fully cast-in-place and water cured
- The ratio of effective length to design depth does not exceed 18.0 and is not less than 6.0
- The specified 28-day strength of the deck concrete is not less than 4.0 ksi

“ (AASHTO, 2012)

There are four layers of isotropic reinforcement required by the empirical design method with the outermost layers in the direction of the effective length. The effective length depends upon the type of slab. The effective length of a slab that is monolithic with walls or beams is the face-to-face distance. The effective length of a slab that is supported on steel or concrete girders is the distance between flange tips plus the flange overhang, which is the distance from the extreme flange tip to the face of the web. (AASHTO 9.7.2.3)

The minimum amount of steel required is 0.27 $\frac{in^2}{ft}$ for each bottom layer of reinforcement and 0.18 $\frac{in^2}{ft}$ for each top layer of reinforcement. The reinforcement should be placed as close to the outside surface as allowed by the required concrete cover, and the maximum allowed spacing of the reinforcement is 18 in. The reinforcement should be all straight bars, except where hooks are required, and should be Grade 60 or higher. For decks with at least a 25 degree skew, the specified amount of steel in both directions should be doubled in the end zone. (AASHTO 9.7.2.5)

2.5.2 Traditional Design

The traditional design for concrete bridge decks using AASHTO is based on flexure. The live load force effect is to be determined using the approximate methods of Article 4.6.2.1 or the refined methods of Article 4.6.3.2. The approximate method or strip width method is described in Section 2.4.2. (AASHTO C9.7.3.1)

In addition to providing equations for determining the strip widths in AASHTO Table 4.6.2.1.3-1, AASHTO (2012) also provides a table with the live load moments for the positive and negative regions in AASHTO Table A4-1. The moments provided in the table were determined using the equivalent strip method for slabs supported on parallel girders and can be used for interior bays. The multiple presence factors and the dynamic load allowance are included in the tabulated moments. To qualify to use AASHTO Table A4-1, the deck must be supported by at least three girders and have a width of at least 14.0 ft between the centerlines of the exterior girders. VDOT includes a copy of this table in Chapter 10 of the VDOT Bridge Manual, which is shown in Appendix A. When calculating negative moments, the distance between the center of the girders to the location of the design section is determined by AASHTO Article 4.6.2.1.6. It states that for monolithic construction, closed steel boxes, closed concrete boxes, open concrete boxes without top flanges, and stemmed precast beams, the design section is at the face of the supporting component. For steel I-beams and steel tub girders, it is at one-quarter the flange width from the centerline of support. For precast I-shaped concrete beams and open concrete boxes with top flanges, the design section is at one-third the flange width, but not exceeding 15.0 in., from the centerline of support. (AASHTO, 2012)

Distribution reinforcement is required in bridge decks in order to account for the lateral distribution of live loads, with lateral implying a direction transverse to the main reinforcement. (Tonias & Zhao, 2007) The amount of distribution reinforcement is determined as a percentage of the primary reinforcement for the positive moment. When the primary reinforcement is parallel to traffic, $\frac{100}{\sqrt{S}} \leq 50\%$, and when the primary reinforcement is perpendicular to traffic, $\frac{100}{\sqrt{S}} \leq 67\%$, where S is the effective span length described in Section 2.5.1. (AASHTO 9.7.3.2)

2.5.3 Skewed Decks

AASHTO Section 9.7.1.3 states that if the skew angle is less than 25 degrees, then the primary reinforcement should be placed in the direction of the skew. If skew angle is greater than 25 degrees, the primary reinforcement should be placed perpendicular to the main supporting components. The commentary describes the reason for this is to prevent cracking due to the lack of reinforcement acting in the direction of the principal flexural stresses as seen in Figure 2-17.

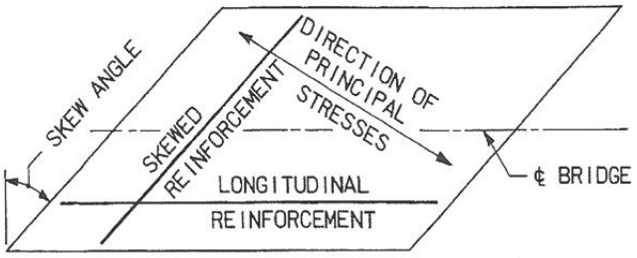

Figure 2-17: AASHTO Reinforcement Layout (AASHTO, 2012) Used under fair use, 2013

2.5.4 Control of Cracking

In Article 5.7.3.4 of the 2004 AASHTO LRFD Bridge Design Specifications, the crack control reinforcement shall be designed according to AASHTO 5.7.3.4 unless the deck is designed according to the empirical method in article 9.7.2. Cracking can occur under any load condition including thermal effects and the following equation provides a distribution of reinforcement that should control cracking:

$f_{sa} = \frac{Z}{d_c * A}^{\frac{1}{3}} \leq 0.6 * f_y$ where:

d_c = depth of concrete measured from extreme tension fiber to center bar located closest

A = area of concrete having the same centroid as the principal tensile reinforcement and bounded by the surfaces of the cross-section and a straight line parallel to the neutral axis, divided by the number of bars

Z = crack width parameter

The provision above was changed in the 2005 Interim Revisions, and now in AASHTO Article 5.7.3.4 of the 2012 version the following equation is used:

$s \leq 700\frac{\gamma_e}{\beta s\, fs} - 2d_e$ where:

s = spacing in layer closest to tension force

f_s = tensile stress in steel at service load limit state (ksi)

$$\beta_s = 1 + \frac{d_e}{0.7 * (h - d_e)}$$

d_e = thickness of concrete cover measured from extreme tension fiber to center of the flexural reinforcement

h = overall depth of component

γ_e = exposure factor (1.00 for Class 1 exposure and 0.75 for Class 2 exposure)

2.5.5 Temperature and Shrinkage

Reinforcement is required for temperature and shrinkage stresses near the surfaces of concrete that are exposed to daily temperature changes and in structural mass concrete. This reinforcement may be in the form of bars, welded wire fabric, or prestressing tendons. When bars or welded wire fabric is used, the area of reinforcement per foot on each face and each direction shall satisfy $A_s \geq \frac{1.30bh}{2(b+h)f_y}$ and $0.11 \leq A_s \leq 0.60$ where: A_s is the area of reinforcement in each direction and each face ($\frac{in.^2}{ft}$), b is the least width of component section (in.), h is the least thickness of component section (in.), and f_y is the yield strength of reinforcing bars.

The spacing of the temperature and shrinkage reinforcement shall not exceed:

“

- 3.0 times the component thickness, or 18.0 in.
- 12.0 in. for walls and footings greater than 18.0 in. thick
- 12.0 in. for other components greater than 36.0 in. thick

“ (AASHTO 5.10.8)

2.6 VDOT

2.6.1 Deck Design

Chapter 10 of the VDOT Bridge Manual establishes the practices and requirements for the design and detailing of concrete deck slabs. It states that the design shall be in accordance with LRFD Sections 3, 4, 5, 9, 13, and VDOT Modifications, and that the empirical method is not to be used. (VDOT)

The main reinforcement can be designed using the Deck Design Table on File No. 10.01-4 shown in Appendix A. To choose the main reinforcement bar spacing and deck thickness, one just needs to lookup the values corresponding to the type of beam used and the center-to-center stringer/girder spacing. (VDOT)

The main reinforcing bars consist of alternating truss-type slab bars with straight top and bottom bars. The design of a truss-type bar uses the assumption that the bridge girders may be treated as rigid supports for the deck, creating maximum positive moments in the deck between the girders and maximum negative moments in the deck above the girders. A truss-type bar is bent so that it is near the top of the deck over the girders to resist the negative bending moment, and it is also bent so that it is near the bottom of the deck between the beams to resist the positive bending moment as seen in Figure 2-18. Truss-type bars are used in a design to make it more efficient by placing the reinforcement in the location where it is needed to resist flexure across the width of a bridge deck. The way the truss-type bar dimensions are determined is shown in Figure 2-19. S is the span length that is used in the Deck Design Table File No. 10.01-4 mentioned above, and S_t is the span length used to determine the geometry of the truss bar. The designation, t, includes a ½ in. monolithic wearing surface. (VDOT)

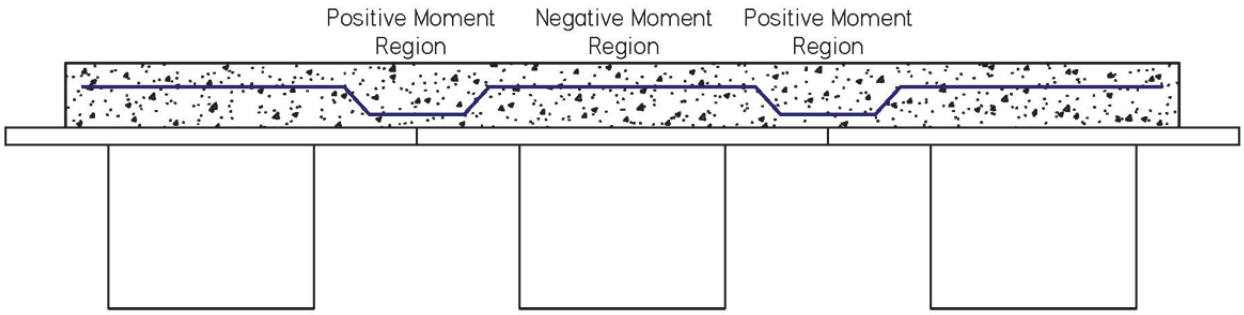

Figure 2-18: Truss Bar

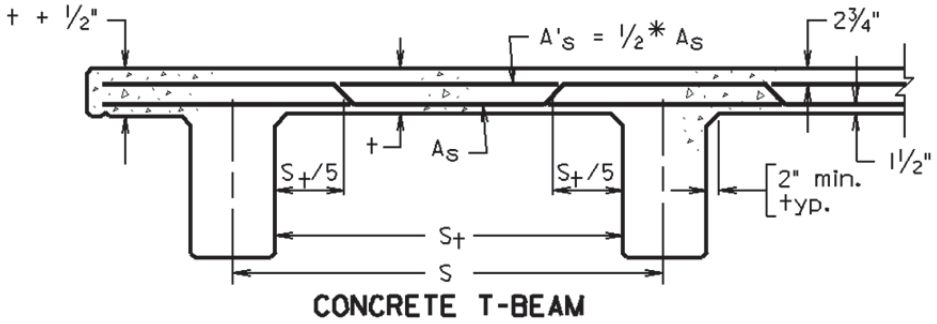

Figure 2-19: Transverse Section (VDOT) Used with permission of VDOT (2013)

2.6.2 Skewed Decks

The VDOT Bridge Manual states that if the skew angle is less than or equal to 20 degrees, the main reinforcement should be placed parallel to the slab ends with truss bars alternating with straight bars top and bottom (VDOT).

For skew angles over 20 degrees, the VDOT Bridge Manual states that the main reinforcement should be placed perpendicular to the bridge centerline. Where full-length across the width of the bridge main reinforcement is required, truss bars should be alternated with straight bars top and bottom as shown in Figure 2-20. The middle section of Figure 2-20 shows the alternation of truss bars with straight bars by using a dashed line for the truss bars and straight lines where straight top and bottom bars are used. At the end sections, the main reinforcement should be straight bars top and bottom, with special consideration given to reinforcing the ends of the slab with additional bars parallel and close to the end diaphragms (VDOT).

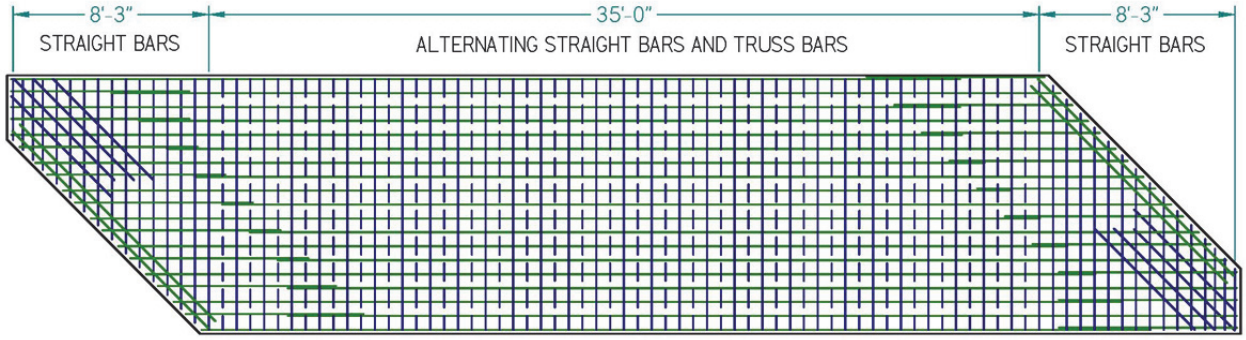

Figure 2-20: Region Where Truss Bars are Used

2.7 Summary

In summary, the current deck design methods used by AASHTO follow Westergaard in that they ignore the deformations of beams and treat them as rigid supports. This assumption leads to conservative top transverse reinforcement in the flexible zones of bridges using flexible beams. Research has been done to develop empirical equations to determine the maximum negative moment in the transverse direction for bridge decks with flexible beams. These equations yield smaller moments than the conservative AASHTO values, and therefore less reinforcement is required and the cost of bridge decks is reduced.

CHAPTER 3: DECK DESIGNS OF TIDE MILL AND TEST BRIDGE

3.1 Tide Mill Bridge Deck Design

3.1.1 Design Parameters

The deck for the new Tide Mill Bridge was designed by Parsons Brinckerhoff using Volume V Part 2 of the VDOT Bridge Manual, which will be referred to as the VDOT Bridge Manual for the remainder of this section and is included in Appendix A. The parameters for the design were a ½ in. non-structural wearing surface, a beam spacing of 4 ft – ¼ in., a 2 ft overhang past the centerline of the exterior girders, a deck width of 32 ft - 6 in., and a deck thickness of 7.5 in. The deck concrete was specified to have a concrete compressive strength of 4 ksi. The deck reinforcing steel was specified to have yield strength equal to 60 ksi.

3.1.2 Deck Design

The spacing of the HCB girders is about 4 ft; therefore, the thickness of the deck was chosen to be 7.5 in. from the table on Sheet 1 of the VDOT Bridge Manual shown in Appendix A. With a span length of about 4 ft, the flexural reinforcing steel required was determined to be No. 5 bars with 7 in. spacing for both positive and negative moment, following the Deck Design Table on Sheet 4 of the VDOT Bridge Manual shown in Appendix A. The design called for alternating two straight bars near the top and bottom of the deck with a truss bar. The dimensions of the truss bars followed the Concrete T-Beam figure on Sheet 2 of the VDOT Bridge Manual shown in Appendix A. The distribution steel was determined to be No. 4 bars at 7 in. top and bottom in accordance with Sheet 10 of the VDOT Bridge Manual shown in Appendix A. Figure 3-1 and Figure 3-2 show the interim plans for the deck slab plan and cross section for the Tide Mill Bridge.

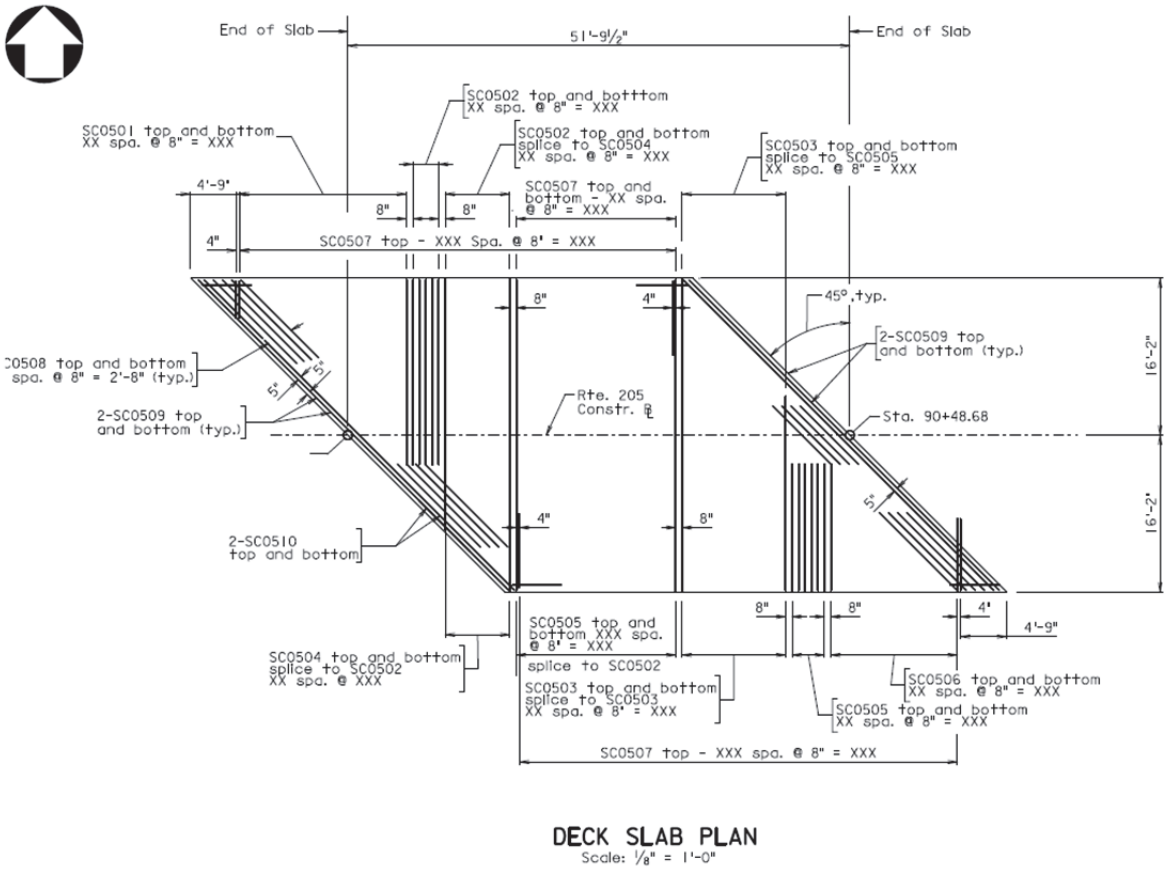

Figure 3-1: Deck Slab Design ((VDOT), Virginia Department of Transportation, 2011) Used with permission of Jason Stull, Parsons Brinckerhoff (2013)

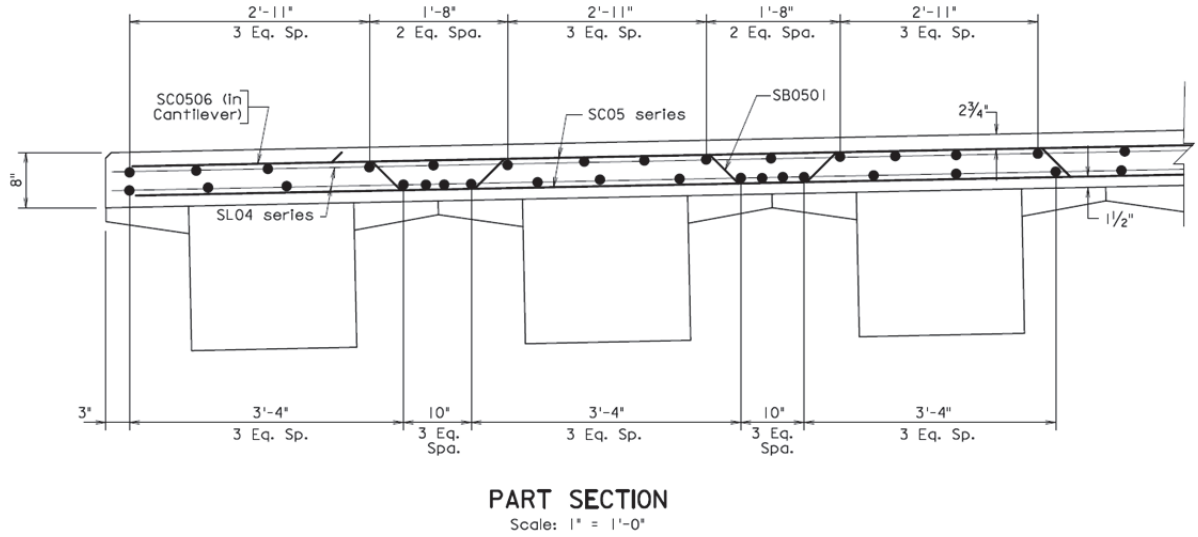

Figure 3-2: Bridge Cross Section ((VDOT), Virginia Department of Transportation, 2011) Used with permission of Jason Stull, Parsons Brinckerhoff (2013)

3.2 Test Bridge Deck Design

The design for the test bridge was very similar to the design for the new Tide Mill Bridge and is shown in Figure 3-3. The deck is 7.5 in. thick and 10 ft – 10 in. wide. The transverse reinforcement consisted of No. 5 bars spaced at 7 in. alternating top and bottom bars with truss bars with dimensions shown in Figure 3-4. Furthermore, the longitudinal reinforcement was No. 4 bars at 7 in. Extra reinforcement was added near the ends to provide extra support where possible lift points were added in order to move the bridge after the completion of testing. The deck concrete was specified to be 4 ksi concrete.

The punching shear was calculated to verify that the deck could withstand the applied test loads using ACI 318-11 Section 11.11.2, which includes the same equations as AASHTO just with different units. The loads were applied to the deck with 10 in. by 20 in. neoprene pads, with a ratio of the longer dimension to the shorter dimension, β, of 2. ACI equation 11-31 ($V_c = (2 + \frac{4}{\beta})\lambda\sqrt{f_c'}b_o d$) and ACI equation 11-33 ($V_c = 4\lambda\sqrt{f_c'}b_o d$) yielded the same result for punching shear strength, 99.7 kips. This value is adequate for the maximum test applied patch load of 37.2 kips. (ACI, 2011)

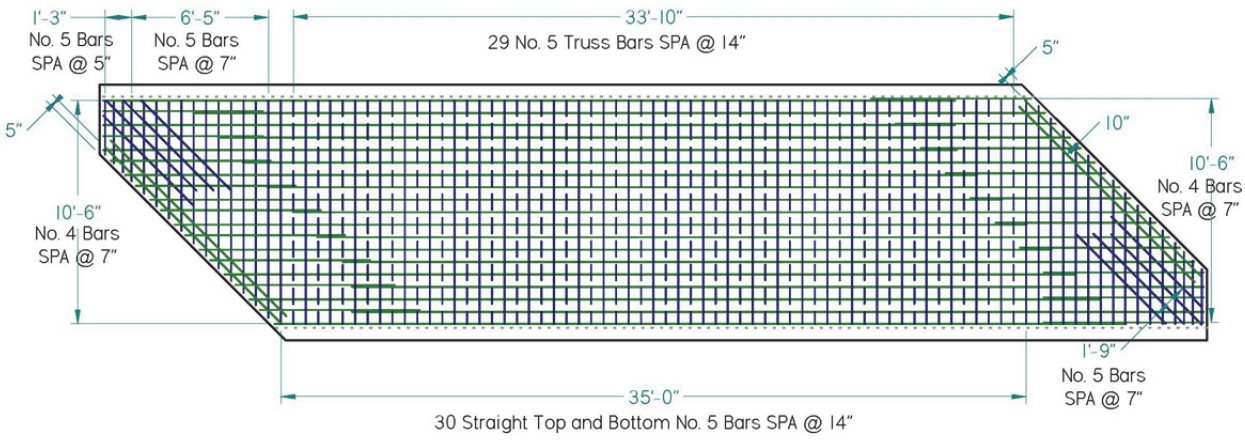

Figure 3-3: Deck Reinforcement Layout

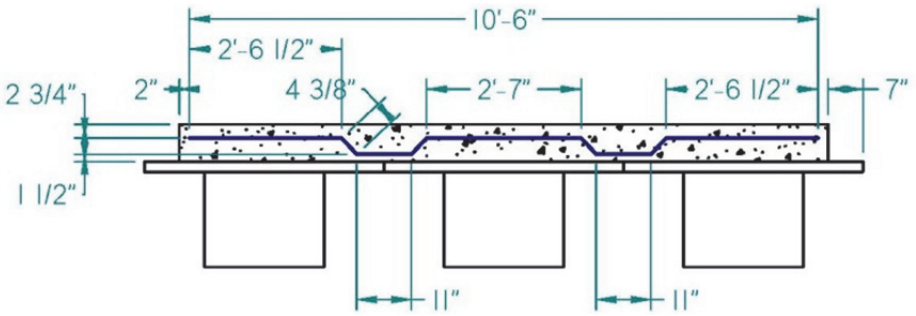

Figure 3-4: Truss Bar Dimensions

CHAPTER 4: LABORATORY BRIDGE AND TEST SETUP

4.1 Setup Prior to Testing

4.1.1 Individual Beams

Three HCB's were delivered to the lab with the lids unattached and the concrete arch not yet placed. This was so testing of the individual beams could be done before and after concrete placement. This testing and the results are presented in Ahsan (2012) and are not discussed in this thesis.

To simulate the bridge layout in the field, simulated skewed bridge abutments were created by rigidly connecting two 17 ft W36x182 to the strong floor through floor beams. Figure 4-1 below shows the layout of the abutments along with the floor beams that ran along the length of the testing bays. (Ahsan, 2012)

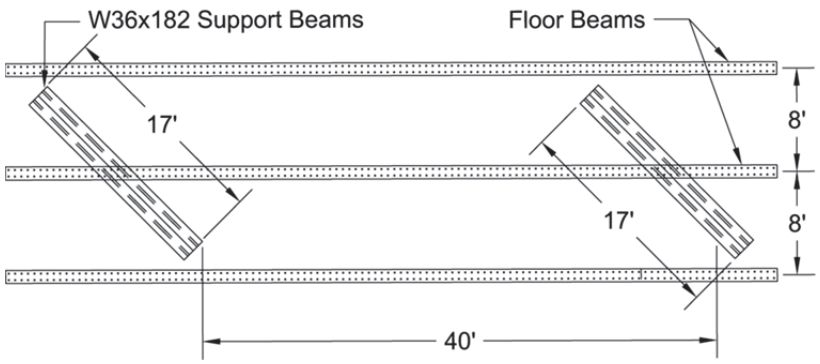

Figure 4-1: Floor Layout (Ahsan, 2012) Used under fair use, 2013

The HCBs were placed on pin and roller supports. The pins and rollers were placed perpendicular to the length of the beams and 6 in. from the ends of the beams, creating a 43 ft span length which is the same as the Tide Mill Bridge. The lids were glued on using an epoxy adhesive and allowed to set. Then, Phase I of Ahsan's testing took place in order to gain more understanding of the properties of the HCBs before the concrete was placed.

After Ahsan's Phase I testing was completed, horizontal shear reinforcement to develop composite action with the deck, consisting of 50 stirrups placed at 45 degrees in pre-drilled holes, was placed and tied. The stirrups protruded 4 in. above the top of the HCB's. Also, the reinforcement to tie the HCB's and diaphragms together which consisted of No. 4 bars with 90

degree bends was installed at the ends of the beams. Self-consolidating concrete was pumped into the beams to form the arch and was allowed to cure. After the concrete in the beams was fully cured, Phase II of Ahsan's tests took place to study the behavior of the individual HCB's.

Concrete was taken from the truck at the beginning and middle of the arch concrete placement to create two batches of concrete test cylinders with a total of 24 cylinders. Segregation of the aggregate and cement was observed, with the first batch having lower aggregate content and higher paste content and the second batch having a higher aggregate to paste ratio. Each time the cylinders were tested, a cylinder was chosen from each batch in order to obtain the average properties. The arch concrete cylinders were cured in an environmental chamber where temperature and humidity were controlled until the day they were tested.

4.1.2 Diaphragms

The diaphragms were designed to mimic the semi-integral backwall used in the Tide Mill Bridge. The abutments used in the Tide Mill Bridge are to be semi-integral abutments. Semi-integral abutments are difficult to create in a lab setting, therefore pin and roller supports were used. The diaphragms were constructed before the deck. The concrete used for the diaphragms was a standard A4 mix used by VDOT in deck designs (Table 4-1).

Table 4-1: A4 Concrete Mix Design (Ahsan, 2012)

Class of Concrete	A4 General
Design Minimum Laboratory Compressive Strength at 28 Days (f'c) (psi)	4,000
Aggregate Size No.	57
Nominal Max. Aggregate Size (in.)	1
Minimum Grade Aggregate	A
Minimum Cement Content (lb./yd3)	635
Maximum Water (lb. water/lb. cement)	0.45
Consistency (in. of slump)	2-4
Air Content (%)	6 ½ ± 1 ½

Because the diaphragms were 16 in. deep where the HCB's were 21 in. deep and the pin and roller supports raised the HCB's, the diaphragm formwork had to be raised above the support beams about 12 in. Once the formwork was constructed, the diaphragm reinforcement was placed. The reinforcement layout for the diaphragms is shown in Figure 4-3 and Figure 4-4 and consisted of longitudinal bars placed at the skew angle and transverse reinforcement of hoops and hooks. The bar bend diagrams are included in Appendix B, which also shows what bar shapes the bar callouts correspond to. Two No. 4 reinforcement bars protrude out of the HCB's on each side of the beam as seen in Figure 4-2. One end of each bar is embedded into the concrete block at the ends of the HCB and then it protrudes out in order to connect the beams to the diaphragms. The reinforcement was bent at a 45˚ angle to match the angle of the end diaphragms.

Figure 4-2: Reinforcement Protruding from HCB

One may observe in Figure 4-3 and Figure 4-4 that the diaphragms have an asymmetrical design. The HCB's are fully restrained by the diaphragms on the east side, but not the west side. This was done so that the behavior of a fully restrained HCB verses the behavior of a partially restrained HCB could be observed.

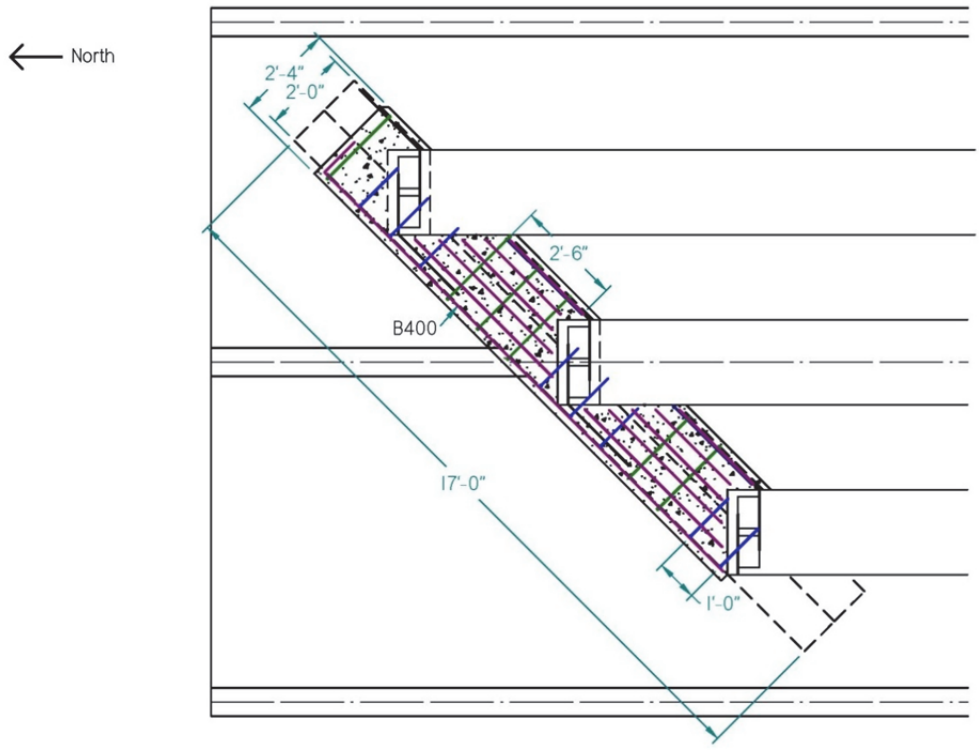

Figure 4-3: End Diaphragm North Side

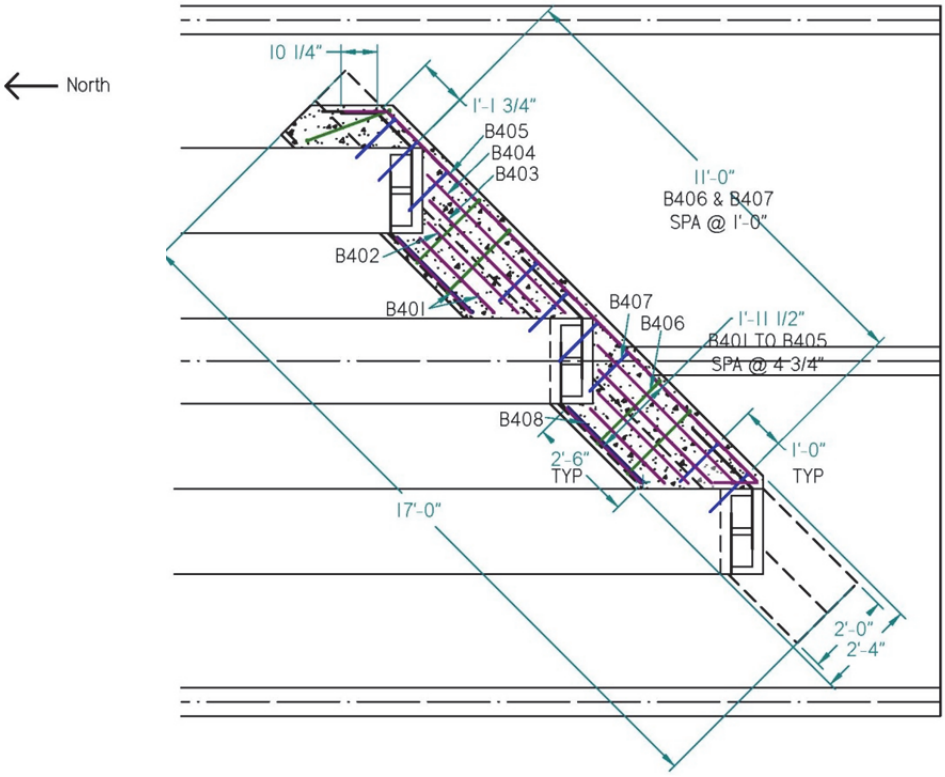

Figure 4-4: End Diaphragm South Side

When the concrete was placed, vibrators were used to help with consolidation. A smooth finish was applied and then a rake was used to roughen the surface in order to improve the interface adhesion between the diaphragm and the not yet placed deck. The diaphragms were moist-cured beneath wet burlap and plastic tarps for seven days.

Concrete was taken from the truck to create 24 concrete cylinders for material testing. The diaphragm concrete cylinders were stored underneath the bridge and were also moist-cured for the same amount of time as the diaphragms in order to create similar conditions to the actual diaphragm concrete during curing.

4.1.3 Deck

The design of the laboratory bridge deck is described in Section 3.1.2. To create the deck, first the formwork had to be designed and constructed. The formwork for the diaphragms was left in place to use as an anchor and support for the deck formwork at the ends of the bridge. Then, 7.5 in. sideforms were placed along the length of the bridge and ends of the bridge as seen in Figure 4-5. Along the length of the bridge, the sideforms were placed 7 in. away from the edge of the HCB's to allow room for a steel angle to be bolted to the top flange as shown below in Figure 4-6. Next the deck reinforcement was put in place.

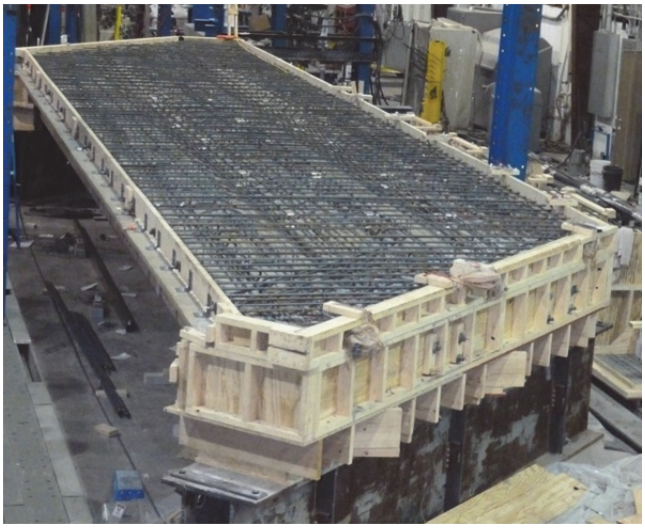

Figure 4-5: Deck Formwork and Reinforcing Steel

Figure 4-6: Deck Formwork Side Walls

To accommodate the amount of concrete required for the deck, two concrete trucks were needed. After the contents of the first truck were placed on the northern half of the bridge, screeding was done, beginning in the middle of the pour and working towards the northern end of the bridge and then screeding proceeded south as seen in Figure 4-7. The deck surface was finished with a bull float and lightly brushed. The second truck arrived abound two hours after the first truck. The concrete near the southern end of the already placed concrete was vibrated to reduce settling and to help prevent a cold joint. Concrete was then placed on the southern half, screeded, and finished. Wet burlap and plastic tarp were placed over the finished deck for a moist cure as seen in Figure 4-8. The burlap was moistened daily for 21 days.

Figure 4-7: Screeding the Deck

Figure 4-8: Covered Deck

Concrete was taken from the truck to create 24 concrete cylinders for each of the two concrete batches for material testing as seen in Figure 4-9. The deck concrete cylinders were stored underneath the bridge and were also moist-cured for the same amount of time as the deck in order to create similar conditions to the actual deck concrete during curing. Three rectangular prisms for shrinkage testing were also created.

Figure 4-9: Deck Concrete Test Cylinders

4.2 Instrumentation

4.2.1 Strain Gages on the Deck Reinforcement

Forty-five 1/8 in. adhesively-bonded strain gages were attached to the reinforcing steel in the deck and covered with a protective coating to prevent damage during the concrete placement

as shown in Figure 4-10. Nine of the gages were placed on the longitudinal bars at the midspan and quarter points of each beam. The remaining thirty-six gages were placed on the transverse bars at the locations with the predicted maximum negative and positive moment. The deck design called for alternating truss bars with top and bottom straight bars. At two locations along the length of the deck, gages were placed on adjacent truss bars along with the top and bottom bars to study the behavior of the truss bars. The gage locations and labels are shown in Figure 4-11.

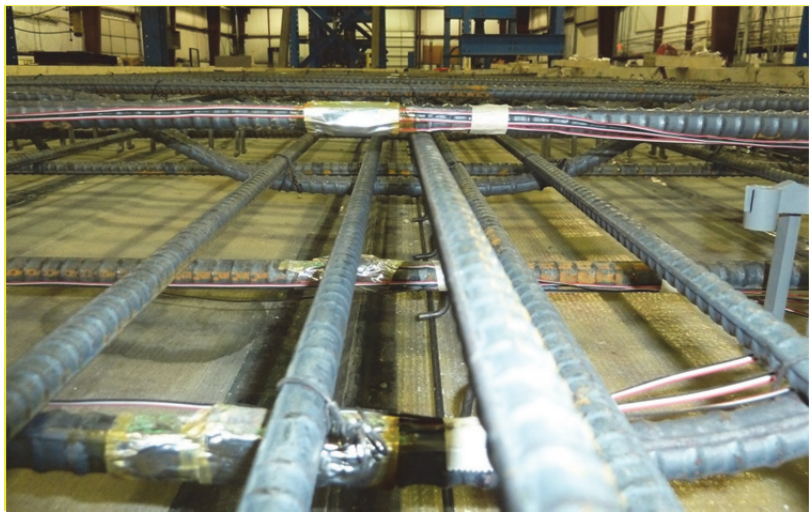

Figure 4-10: Strain Gages and Protective Coating

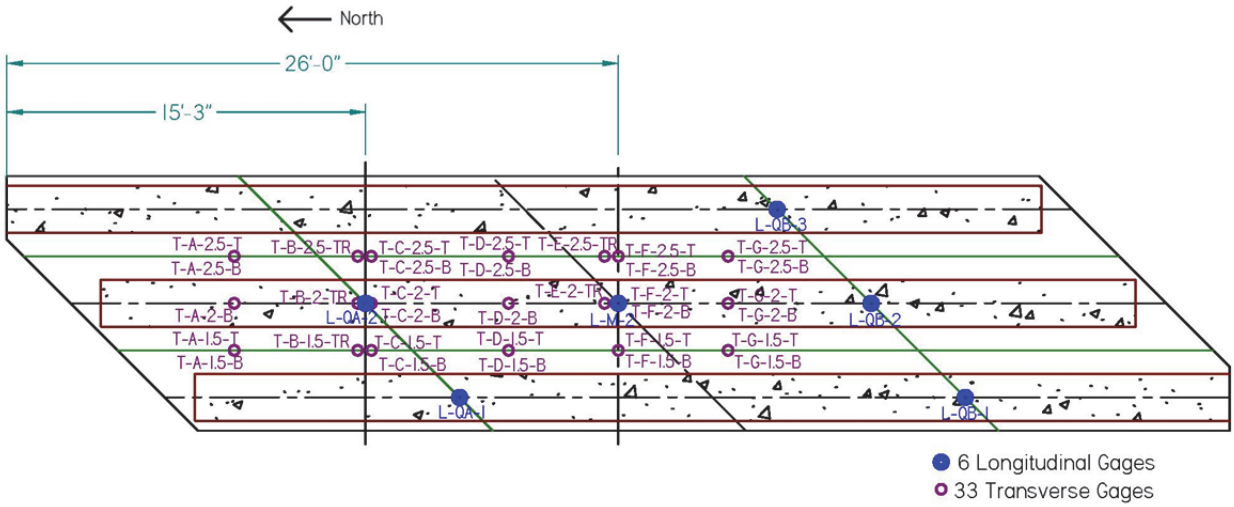

Figure 4-11: Strain Gage Locations

The strain gage nomenclature for the transverse reinforcement has four components. The first letter corresponds to the orientation of the reinforcing bar with T for transverse reinforcement and L for longitudinal. The second letter corresponds to which row the gage is in, ranging from A to G. The third component is the number 2.5, 2, or 1.5. This number depends on which row along the length of the bridge the gage is located. Rows 2.5 and 1.5 were located between two adjacent HCB's, which is the location where the maximum positive moment in the deck is expected to occur. Row 2 is located above the centerline of the middle HCB and is where the maximum negative moment is expected. The final component of the gages name is which type of bar the gage is attached to and the designations are T for top straight bar, B for bottom straight bar, and TR for truss bar. Two examples are shown in Figure 4-12 and Figure 4-13. Figure 4-12 shows the strain gages in Row B, which are located on a truss bar. Figure 4-13 shows the strain gages on the top and bottom bars of Row C.

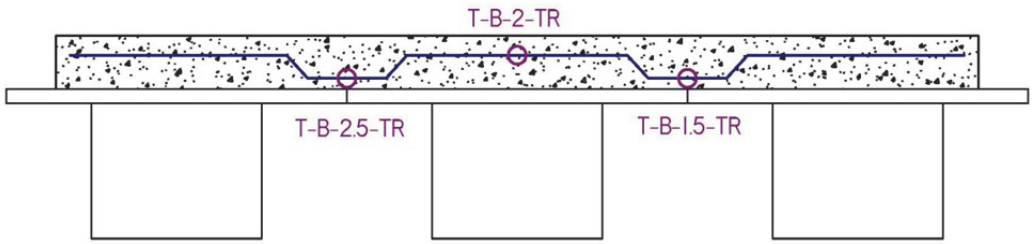

Figure 4-12: Strain Gages on a Truss Bar

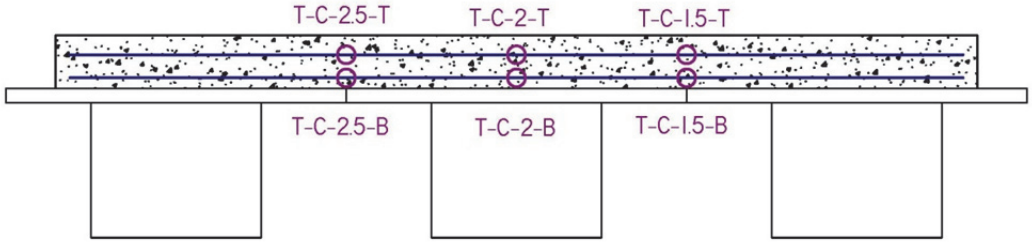

Figure 4-13: Strain Gages on Top and Bottom Straight Bars

For the purpose of making the transverse gage nomenclature easier to understand in the test results section, the row numbers of 2.5, 2, and 1.5 will be replaced with Positive Moment East, Negative Moment Center, and Positive Moment West respectively. This is demonstrated in Figure 4-14.

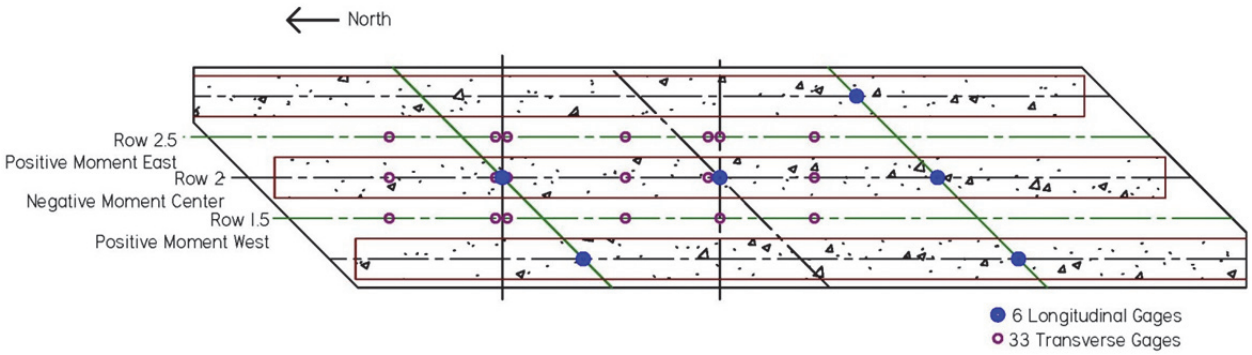

Figure 4-14: New Gage Nomenclature

4.2.2 Potentiometers

Nine potentiometers were used to measure deflections during testing. Three of the potentiometers were placed at the two quarter points and midspan of the center beam and remained there for all eight tests. When the deck was loaded in line with the midspan of the center beam, the six remaining potentiometers were placed in line with the midspan of the center beam with two on the outer flanges, two centered below the exterior beams, and two in the deck in between the interior flanges. When the deck was loaded in line with the quarter point of the center beam, the six remaining potentiometers were placed in line with the quarter point of the center beam with two on the outer flanges, two centered below the exterior beams, and two in the deck in between the interior flanges. The potentiometer layouts are presented in Figure 4-15, Figure 4-16, and Figure 4-19.

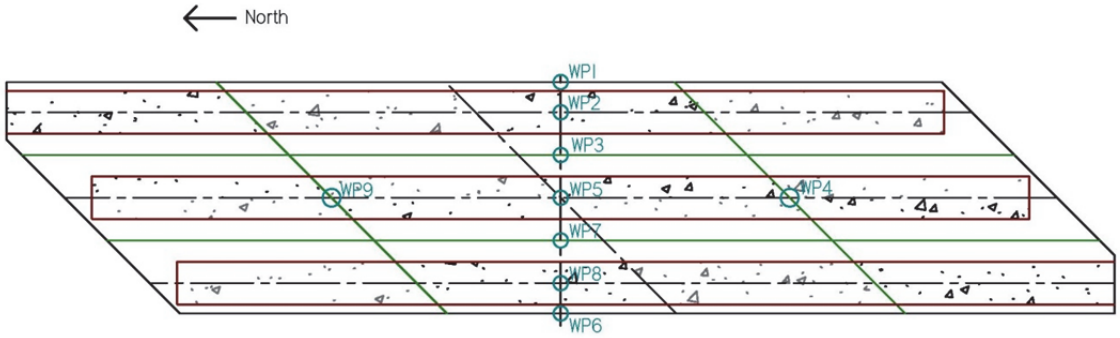

Figure 4-15: Potentiometer Locations for Tests 1 to 4

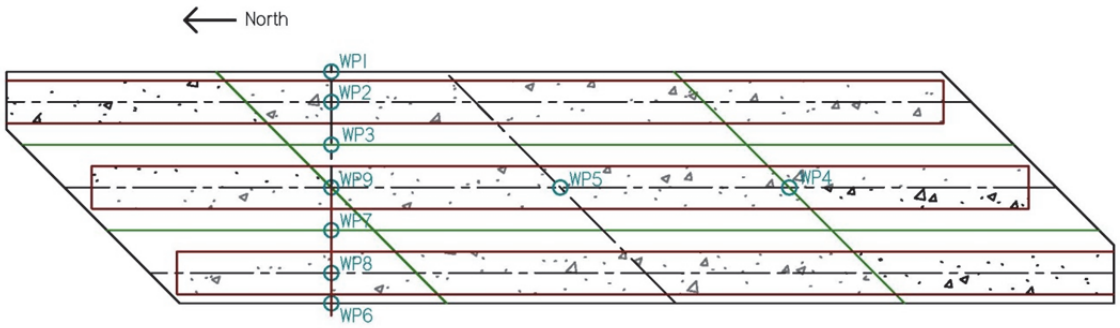

Figure 4-16: Potentiometer Locations for Tests 5 to 8

Figure 4-17: Potentiometers

The potentiometers' wires were connected to the bridge with nylon string as seen in Figure 4-17. Potentiometers WP3 and WP7 as shown in Figure 4-15 and Figure 4-16 were attached to the deck by drilling a 3 in. concrete screw into the deck and attaching the nylon string to the screws as seen in Figure 4-18. The potentiometers were calibrated before testing using a height gage. The potentiometers are accurate to the nearest 0.005 in.

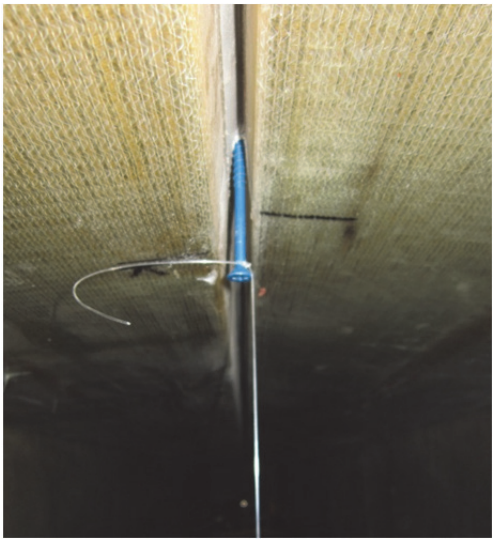

Figure 4-18: Concrete Screw Drilled Into the Deck

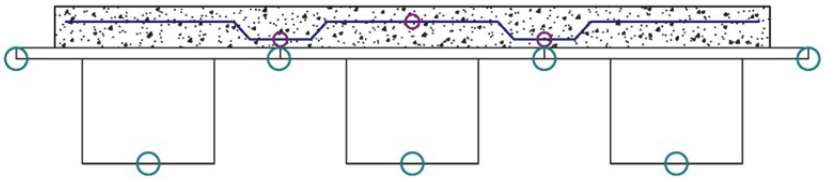

Figure 4-19: Location of Potentiometers

4.3 Deck Testing Setup and Equipment

4.3.1 Load Cell

A 300 kip load cell was placed between the actuator and load frame, which measured the applied force from the actuator (Figure 4-20).

Figure 4-20: Load Cell on Top of the Actuator

4.3.2 Data Acquisition System

A Vishay System 5000 multi-channel data acquisition system was used during testing. The strain gages, potentiometers, and load cell were attached to it.

CHAPTER 5: DECK TESTING AND RESULTS

5.1 Overview

Lab testing of the skewed Hybrid Composite Beam (HCB) test bridge was performed to investigate the behavior of the deck and to assist with validating a design for the Tide Mill Bridge. Testing consisted of load tests on a skewed three-HCB system with a cast-in-place deck and end diaphragms.

The loads were applied to the bridge through 9 in. by 18 in. 70-durometer neoprene bearing pads beneath a stack of ½ in. steel plates that ensured load distribution across the patch. The point load magnitudes for the service load tests were calculated to be 21.3 kips, which was based on a 16 kip HL-93 truck tire load with a 1.33 dynamic load allowance. The point load magnitudes for the strength load tests were calculated to be 37.2 kips, which is obtained by multiplying the service load by 1.75 for strength.

Nine tests were completed on the bridge deck, four at midspan and five at the north quarter point of the bridge. Two single point load tests were done at both midspan and quarter point. The location of the single point load was chosen to maximize the positive moment in the transverse direction by placing the point load between two of the beams, with one test having the load at the east side and one test having the load at the west side. The load on the west side was ¼ in. to the east of the point between the girders because of limitations on the holes available to drill for the overhead beam supporting the actuator. Double point load tests were also done at the midspan and quarter point. The loads were placed in between both beams in order to maximize the negative moment in the transverse direction.

5.2 Concrete Cylinder Material Testing

5.2.1 Cylinder Testing Overview

Concrete material testing was done for the deck, diaphragm, and HCB arch concrete following ASTM testing procedures. Compressive strength tests following ASTM C 39 – 05 (Figure 5-1), splitting tensile strength tests following ASTM C496 – 04 ( ), and elastic modulus

tests following ASTM C496 – 02 (Figure 5-2) were conducted on 4 in. by 8 in. cylinders with sulfur capping.

Figure 5-1: Compression Test and Tensile Tests

Figure 5-2: Elastic Modulus Test Collar

The deck and diaphragm concrete cylinders were stored underneath the bridge in order to create similar conditions to the actual bridge concrete during curing, and the arch concrete cylinders were kept in an environmental chamber with controlled temperature and humidity.

Concrete compressive strength and elastic modulus testing was done at 7, 14, 28, 45, and 206 days and at the start of testing. Splitting tensile strength testing was done at 28 days and at the start of testing. Results for the concrete tests are shown in Table 5-1, Table 5-2, and Table 5-3, and the presented results are the averages for the tested cylinders.

5.2.2 Concrete Cylinder Results

Table 5-1: Deck Concrete Results

		Experimental Results			AASHTO Design Values		
Day	Batch	Compressive Strength (psi)	Tensile Strength (psi)	Modulus of Elasticity (ksi)	Compressive Strength (psi)	Tensile Strength (psi)	Modulus of Elasticity (psi)
7	Batch 1	3460	-	3890	-	-	-
	Batch 2	2690	-	3420	-	-	-
14	Batch 1	4400	-	3650	-	-	-
	Batch 2	3280	-	4010	-	-	-
21	Batch 1	4580	-	4620	-	-	-
	Batch 2	3440	-	4230	-	-	-
28	Batch 1	4480	525	4950	4000	460	3640
	Batch 2	3500	440	4390	4000	460	3640
40	Batch 1	4815	505	4700	-	-	-
	Batch 2	4060	430	6880	-	-	-
134	Batch 1	5477	505	4720	-	-	-
	Batch 2	4100	482	4040	-	-	-

Table 5-2: Diaphragm Concrete Results

	Experimental Results			AASHTO Design Values		
Day	Compressive Strength (psi)	Tensile Strength (psi)	Modulus of Elasticity (ksi)	Compressive Strength (psi)	Tensile Strength (psi)	Modulus of Elasticity (ksi)
7	4180	-	4480	-	-	-
14	4360	-	4680	-	-	-
28	4870	545	5250	4000	460	3640
61	5730	460	4390	-	-	-
155	5250	450	4180	-	-	-

Table 5-3: HCB Arch Concrete Results

	Experimental Results			AASHTO Design Values		
Day	Compressive Strength (psi)	Tensile Strength (psi)	Modulus of Elasticity (ksi)	Compressive Strength (psi)	Tensile Strength (psi)	Modulus of Elasticity (ksi)
7	5120	-	-	-	-	-
14	5360	-	-	-	-	-
28	6190	634	4480	6000	563	4458
45	5680	604	3900	-	-	-
206	5910	518	3820	-	-	-
300	6270	635	3910	-	-	-

The concrete properties used for calculations and the Abaqus models are as follows. The average compressive strength, splitting tensile strength and modulus of elasticity of the deck concrete are 4,790 psi, 490 psi, and 4,380 ksi respectively. For the concrete arch, the modulus of elasticity used was 3,910 ksi.

5.3 Test 1: Midspan Service Test with a Single Point Load on East Side

5.3.1 Test 1 Setup

The first test was a point load at the midspan on the east side of the bridge as seen in Figure 5-3. The test's maximum load was a service load of 21.3 kips.

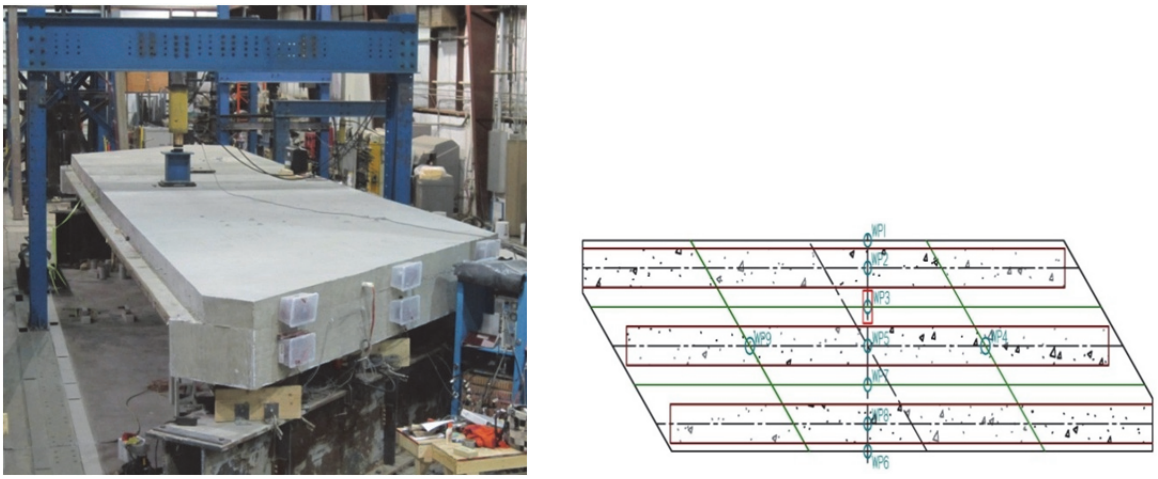

Figure 5-3: Test 1 Setup

5.3.2 Test 1 Results

The maximum deflection was 0.24 in. at potentiometers WP1 and WP3 at the load of 21.3 kips. The deflections measured by the potentiometers are shown in Figure 5-4. Strain gage T-F-15-T did not start at zero, so its values were normalized.

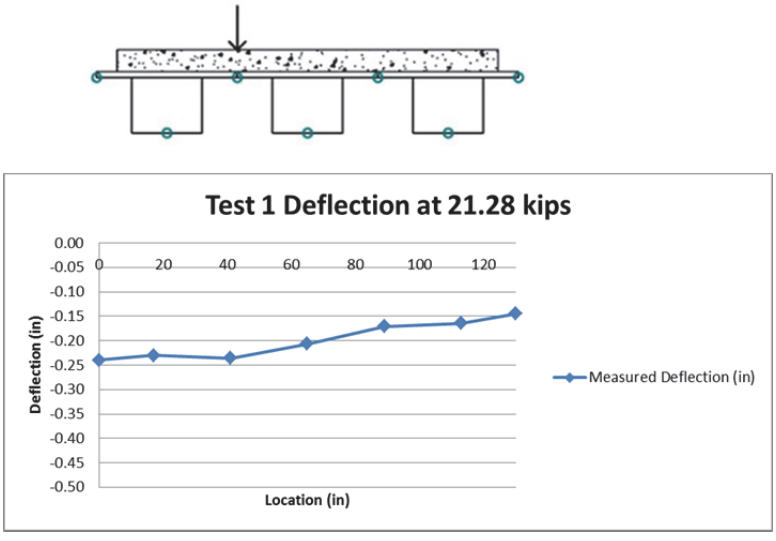

Figure 5-4: Test 1 Deflections

Shown in Figure 5-5 are the strain gage values across the width of the bridge underneath the applied load at midspan, which is also where the maximum strains were recorded. Figure 5-5 shows the strains in the top and bottom bars on the left and the strains in the truss bars on the right. The maximum strain was a tension strain of 217με, which was on the strain gage on the bottom straight bar underneath the load. Also, the truss-type bar only has tension strains. In all graphs, the positive strains are tensile.

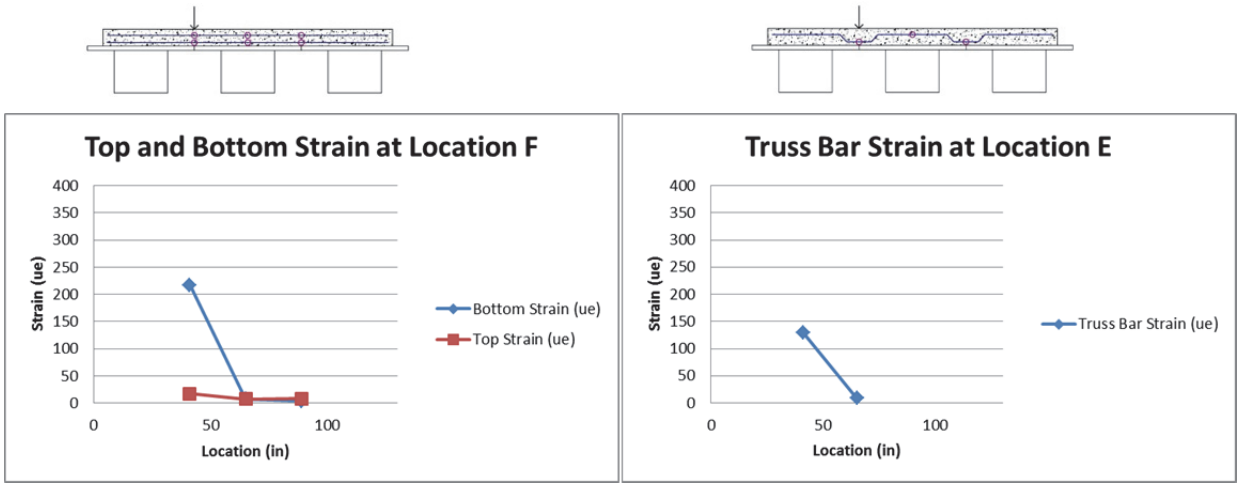

Figure 5-5: Test 1 Strain in Top and Bottom Bars at Midspan and Truss Bar at Midspan

The three graphs in Figure 5-6, Figure 5-7, and Figure 5-8 are the transverse strains along the length of the bridge. The graphs demonstrate that the highest strain occurs along row M+ East which passes through the loading point. The other two lines do not have significant strain. The trend of the maximum strain occurring in the row across the length of the bridge that runs under the load and the rest of the row not showing much load was observed in all of the tests. Therefore, the graphs of the strains across the length of the bridge for the rest of the tests are not shown here, but are included in Appendix D.

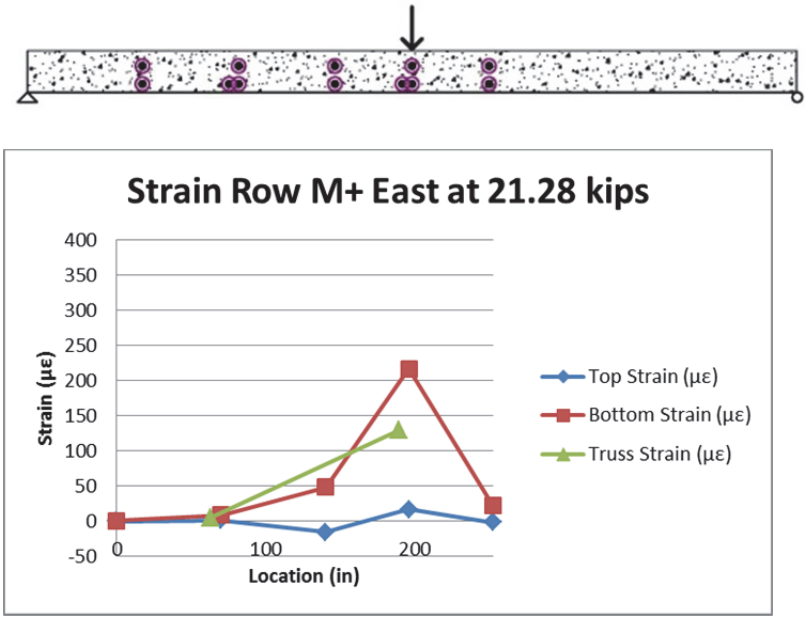

Figure 5-6: Strain Along Row M+ East

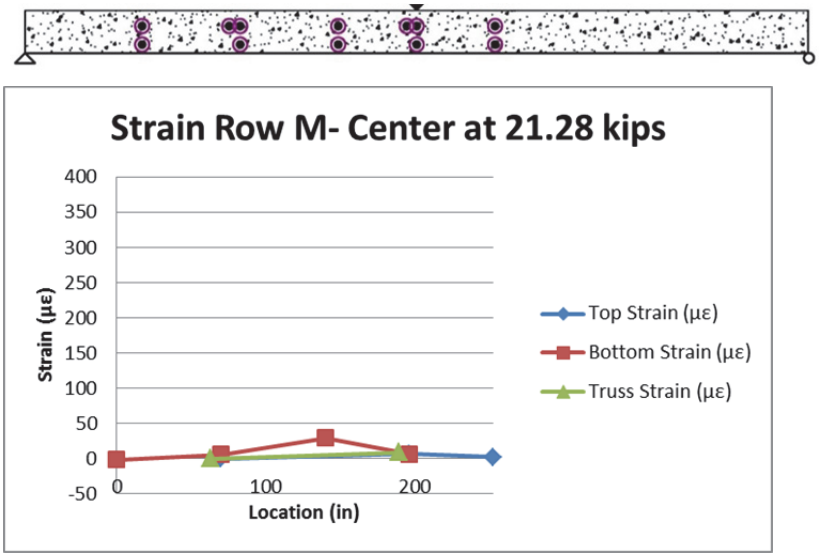

Figure 5-7: Strain Along Row M- Center

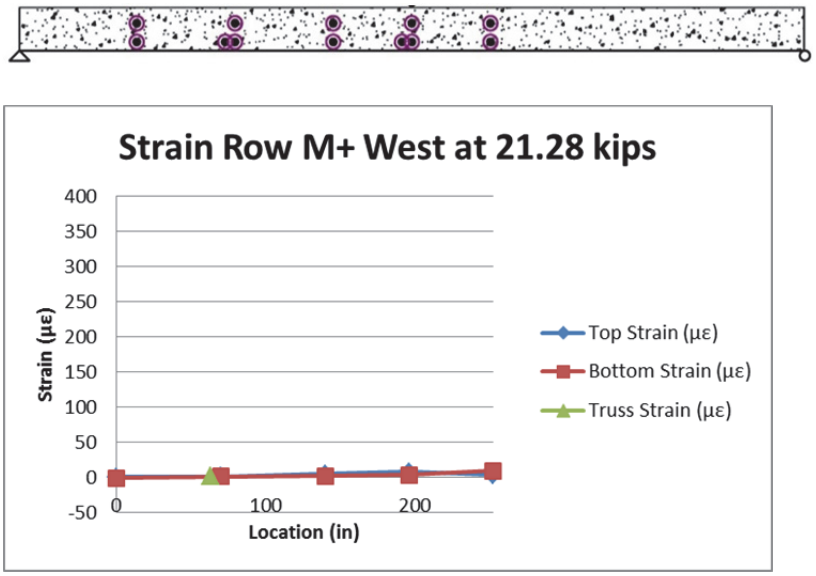

Figure 5-8: Transverse Strains Along the Length of the Bridge

5.4 Test 2: Midspan Service Test with a Single Point Load on West Side

5.4.1 Test 2 Setup

The second test was a point load at the midspan on the west side of the bridge as seen in Figure 5-9. The test's maximum load was a service load of 21.3 kips.

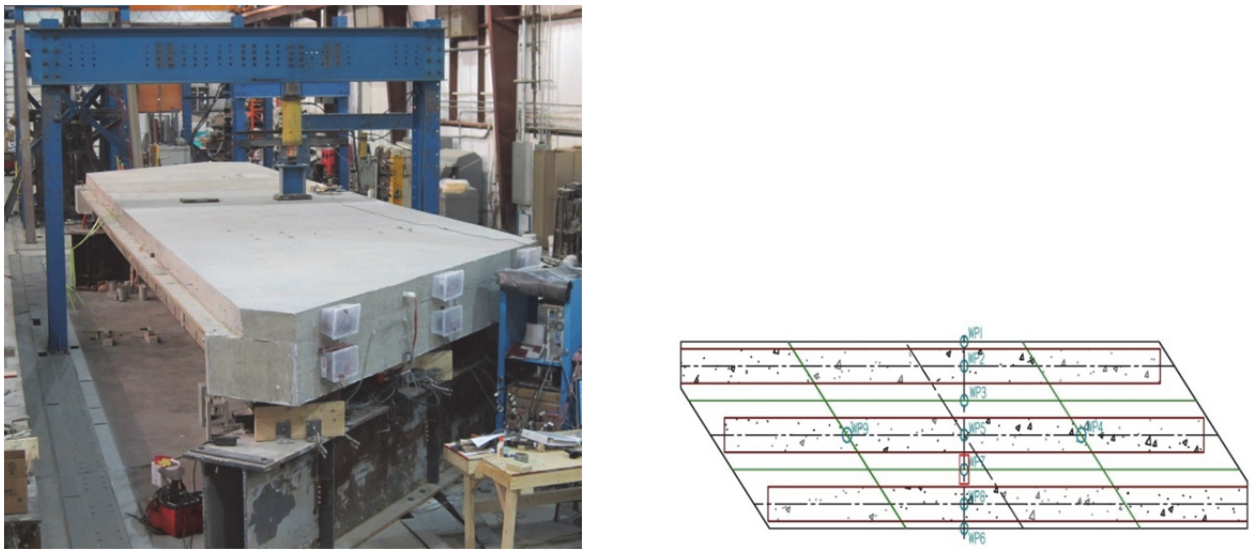

Figure 5-9: Test 2 Setup

5.4.2 Test 2 Results

The maximum deflection was 0.27 in. at potentiometer WP6 at the load of 21.3 kips. The deflections measured by the potentiometers are shown in Figure 5-10.

Shown in Figure 5-11 are the strain gage values across the width of the bridge underneath the applied load at midspan which is also where the maximum strains were recorded. The maximum strain was 305με, which was on the strain gage on the bottom straight bar underneath the load.

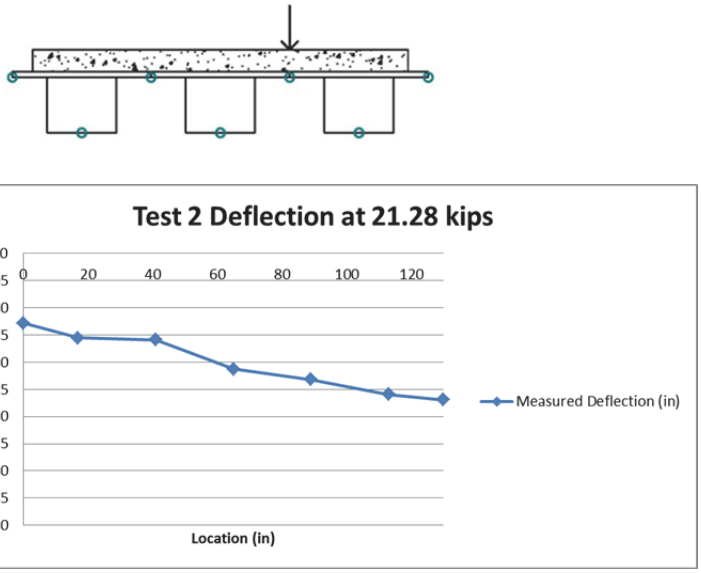

Figure 5-10: Test 2 Deflections

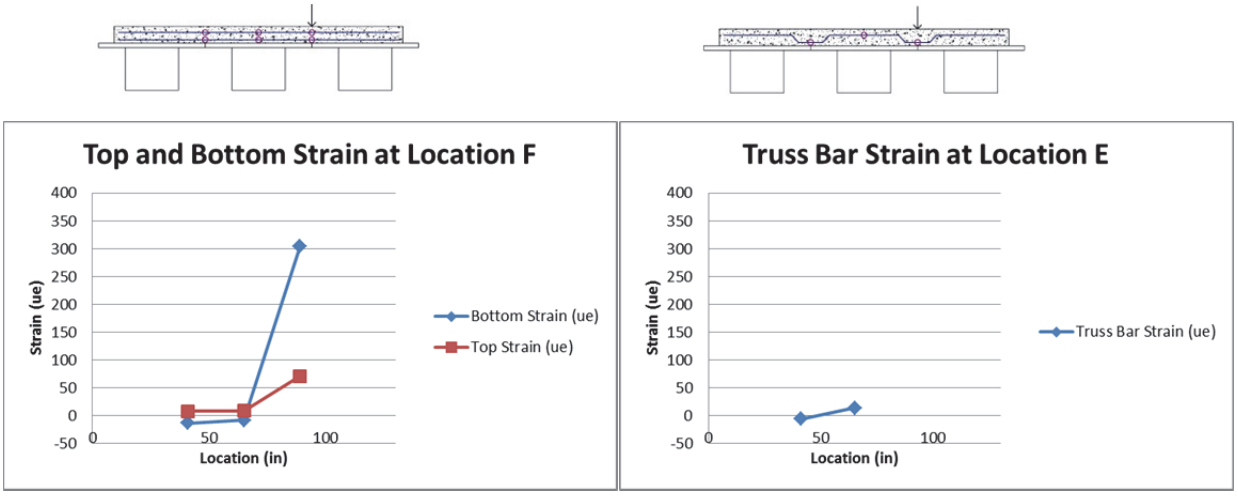

Figure 5-11: Test 2 Strain in Top and Bottom Bars at Midspan and Truss Bar at Midspan

5.5 Test 3: Midspan Service Test with Two Point Loads

5.5.1 Test 3 Setup

The third test was two point loads at the midspan of the bridge as seen in Figure 5-12. The test's maximum load was a service load of 21.3 kips for each patch with a total load of 42.6 kips.

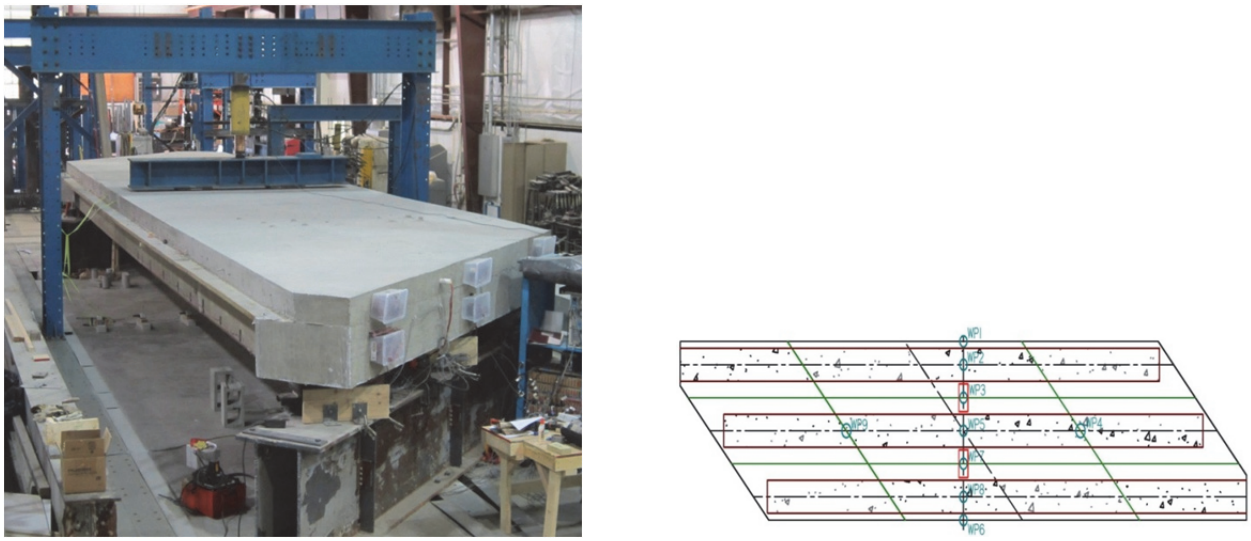

Figure 5-12: Test 3 Setup

5.5.2 Test 3 Results

The maximum deflection was 0.46 in. at potentiometer WP8 at the load of 42.6 kips. The deflections measured by the potentiometers are shown in Figure 5-13.

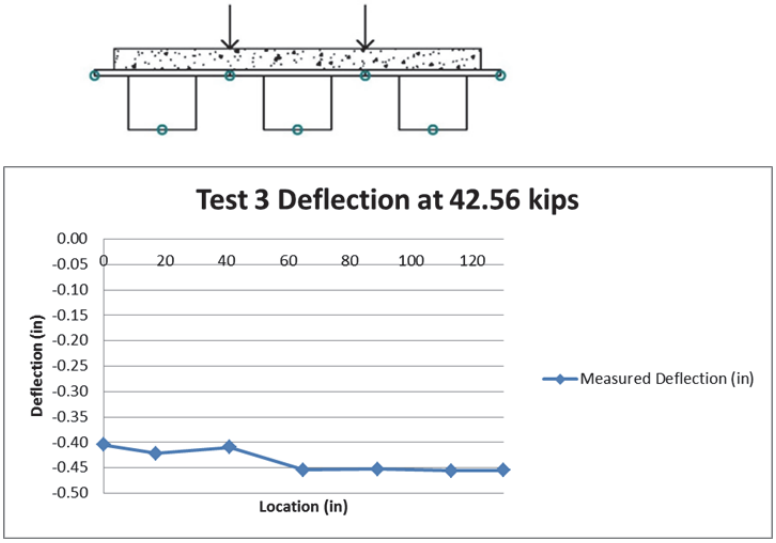

Figure 5-13: Test 3 Deflections

Shown in Figure 5-14 are the strain gage values across the width of the bridge underneath the applied load at midspan which is also where the maximum strains were recorded. The maximum strain was 347με, which was on the strain gage on the bottom straight bar underneath the load.

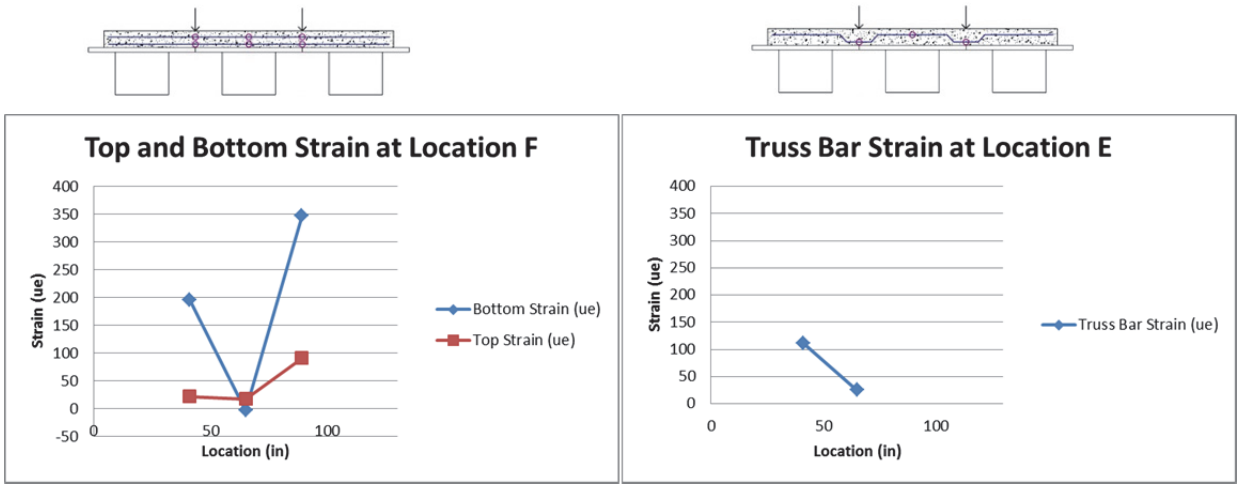

Figure 5-14: Test 3 Strain in Top and Bottom Bars at Midspan and Truss Bar at Midspan

5.6 Test 4: Midspan Strength Test with Two Point Loads

5.6.1 Test 4 Setup

The fourth test was two point loads at the midspan of the bridge with the same test setup as Test 3. The test's maximum load was a strength load of 37.2 kips for each patch with a total load of 74.48 kips.

Following the completion of this test, the loading frame was moved from the midspan to the quarter point of the bridge on the north side. Also, after this test, strain gages T-F-25-B and T-F-15-B stopped working properly.

5.6.2 Test 4 Results

Test 4 had both the highest deflections and strains out of all the tests. The maximum deflection was 0.89 in. at potentiometer WP6 at the load of 74.48 kips. The deflections measured by the potentiometers are shown in Figure 5-15. The maximum strain was 597 με at strain gage T-F-1.5-B, which is the strain gage underneath the load on the bottom bar. This maximum strain is well below the yielding strain.

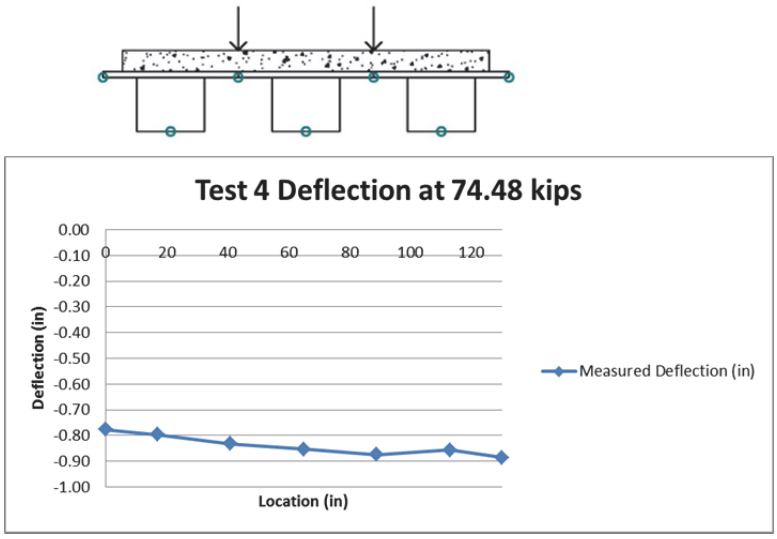

Figure 5-15: Test 4 Deflections

Shown in Figure 5-16 are the strain gage values across the width of the bridge underneath the applied load at midspan which is also where the maximum strains were recorded.

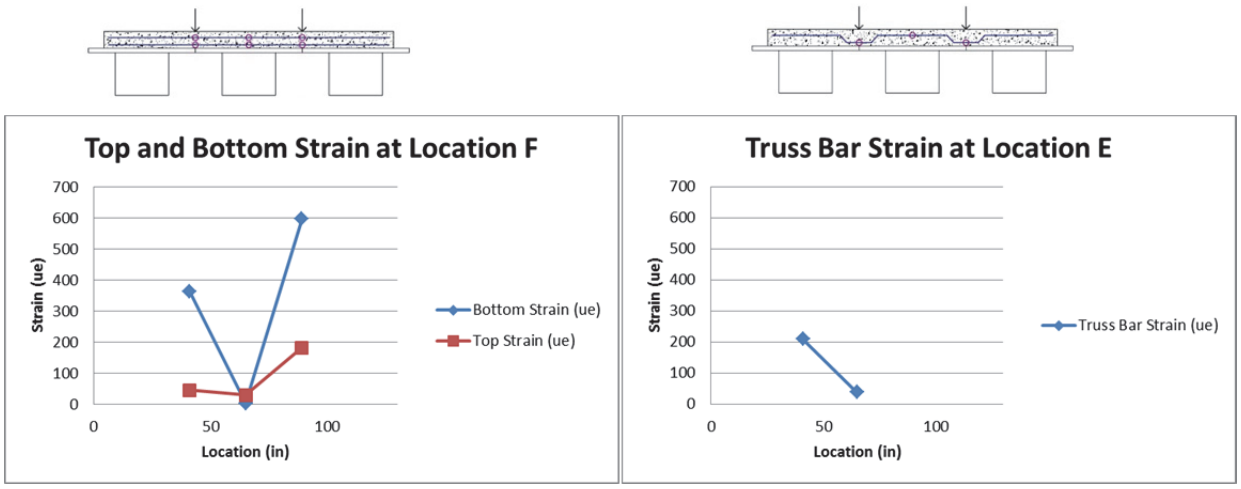

Figure 5-16: Test 4 Strain in Top and Bottom Bars at Midspan and Truss Bar at Midspan

The three graphs in Figure 5-17, Figure 5-18, and Figure 5-19 are the transverse strains along the length of the bridge. The graphs demonstrate that the highest strains occur along Rows M+ East and M+ West which pass through the two loading points. The middle line does not have as much strain.

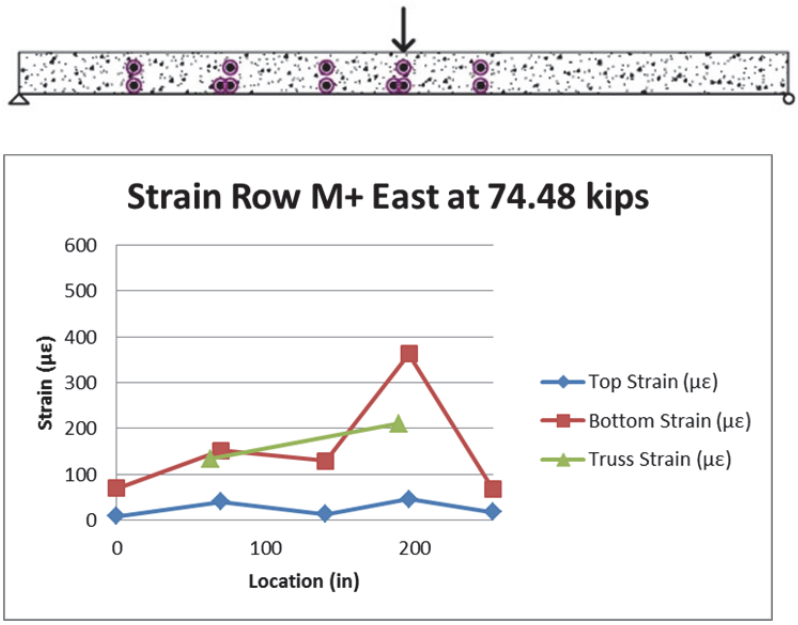

Figure 5-17: Strain Along Row M+ East

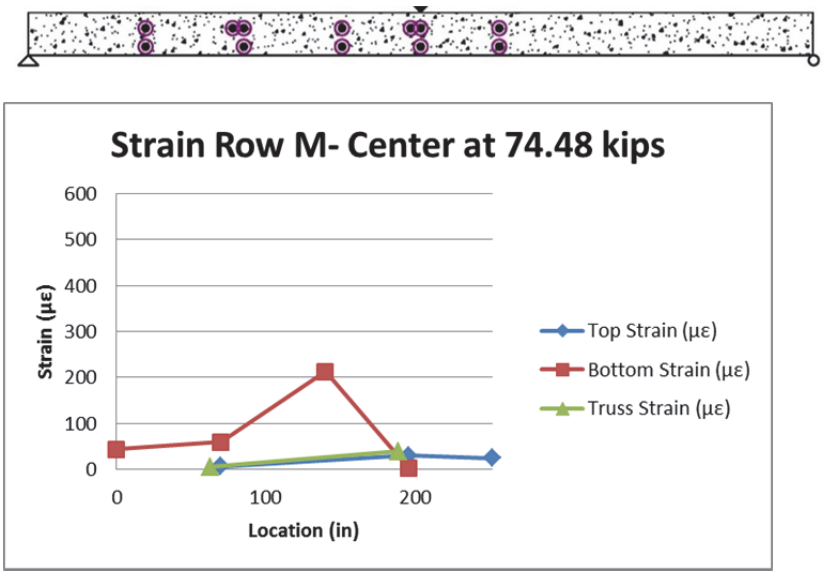

Figure 5-18: Strain Along Row M- Center

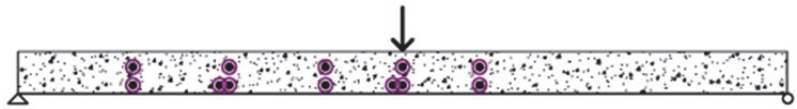

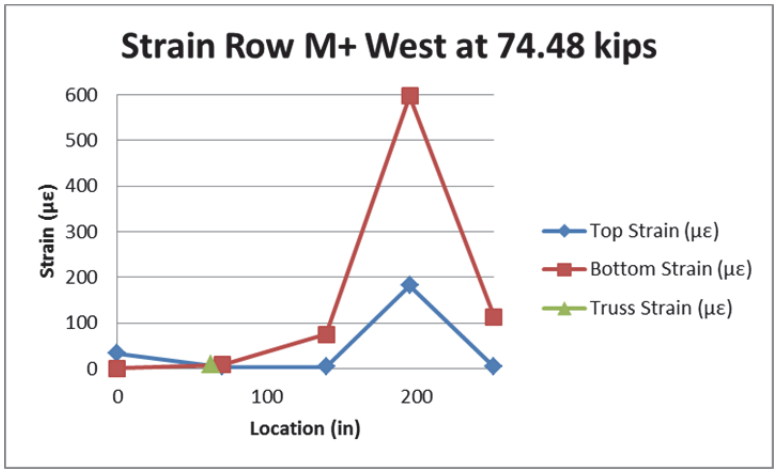

Figure 5-19: Strain Along Row M+ West

5.7 Test 5: Quarter Point Service Test with a Single Point Load on East Side

5.7.1 Test 5 Setup

The fifth test was a point load at the quarter point on the east side of the bridge as seen in Figure 5-20. The test's maximum load was a service load of 21.3 kips.

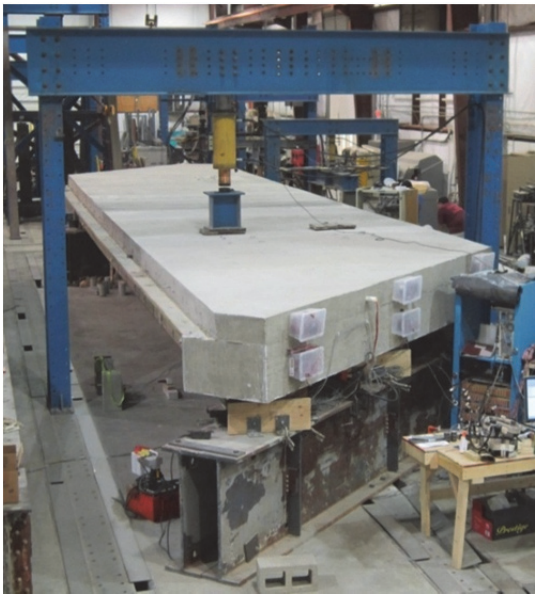

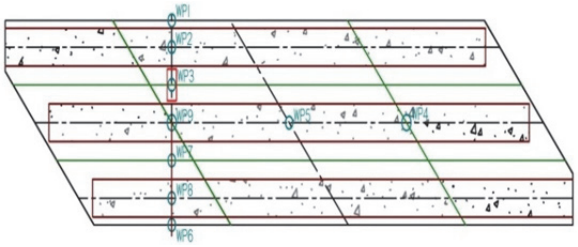

Figure 5-20: Test 5 Setup

5.7.2 Test 5 Results

The maximum deflection was 0.22 in. at potentiometer 1 at the load of 21.3 kips. The deflections measured by the potentiometers are shown in Figure 5-21.

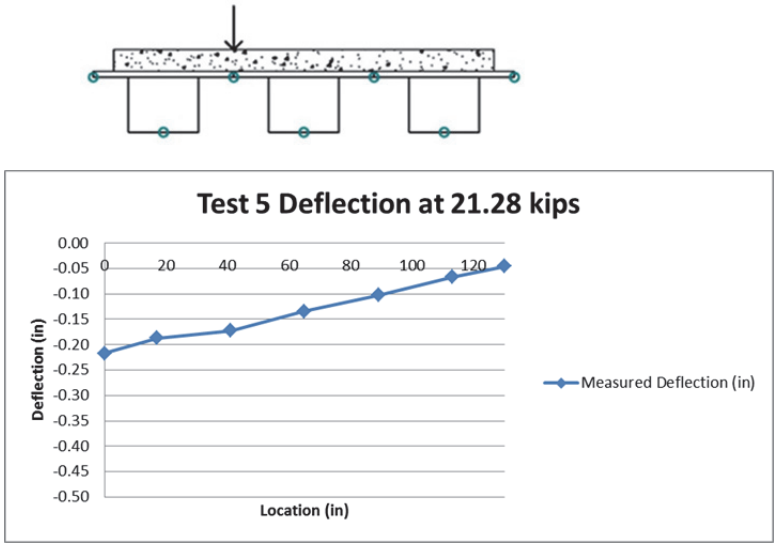

Figure 5-21: Test 5 Deflections

Shown in Figure 5-22 are the strain gage values across the width of the bridge underneath the applied load at midspan which is also where the maximum strains were recorded. The maximum strain was 174 με, which was on the strain gage on the bottom straight bar underneath the load.

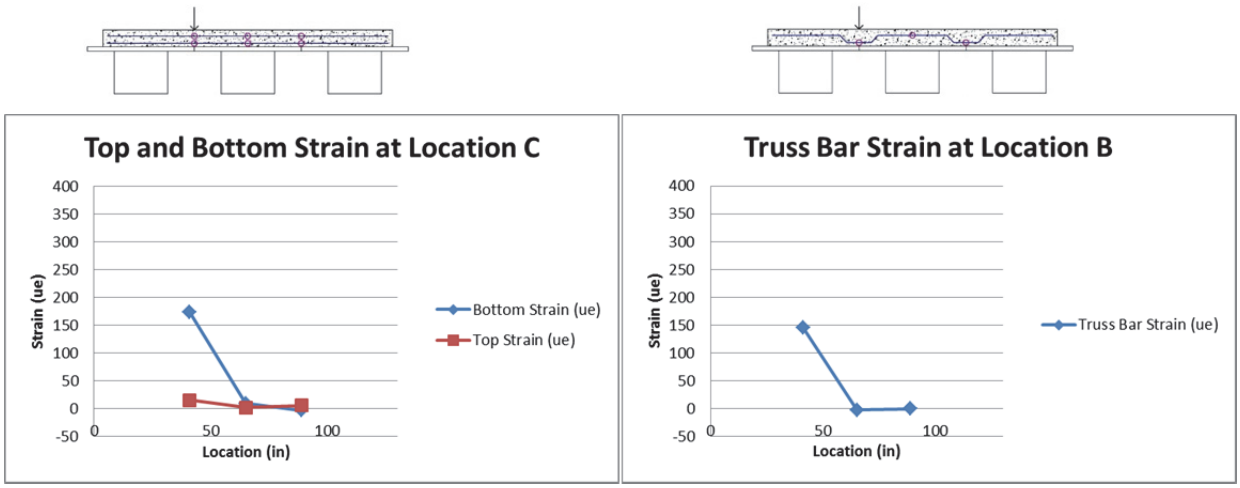

Figure 5-22: Test 5 Strain in Top and Bottom Bars at Midspan and Truss Bar at Midspan

5.8 Test 6: Quarter Point Service Test with a Single Point Load on West Side

5.8.1 Test 6 Setup

The sixth test was a point load at the quarter point on the west side of the bridge as seen in Figure 5-23. The test's maximum load was a service load of 21.3 kips.

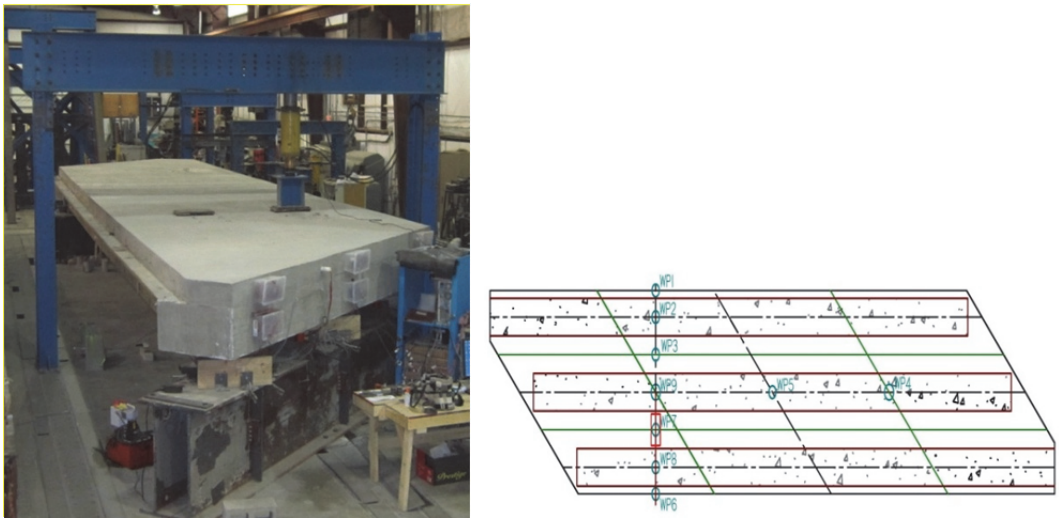

Figure 5-23: Test 6 Setup

5.8.2 Test 6 Results

The maximum deflection was 0.09 in. at potentiometers 2 and 8 at the load of 21.3 kips. The deflections measured by the potentiometers are shown in Figure 5-24.

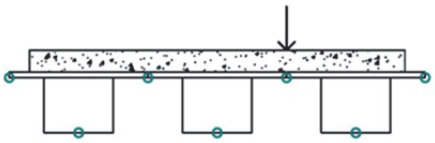

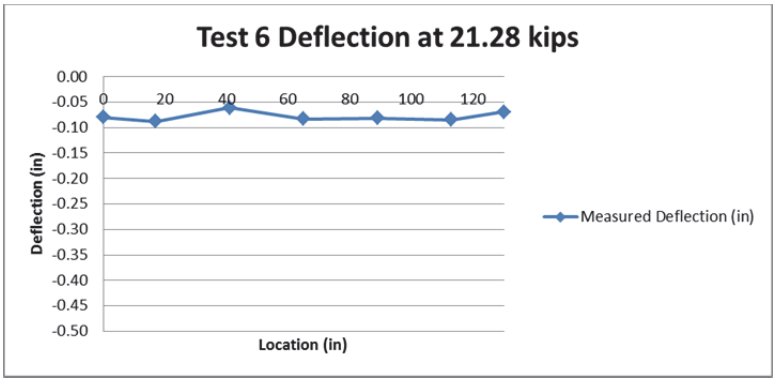

Figure 5-24: Test 6 Deflections

Shown in Figure 5-25 are the strain gage values across the width of the bridge underneath the applied load at midspan which is also where the maximum strains were recorded. The maximum strain was 43 με, which was on the strain gage on the bottom straight bar underneath the load.

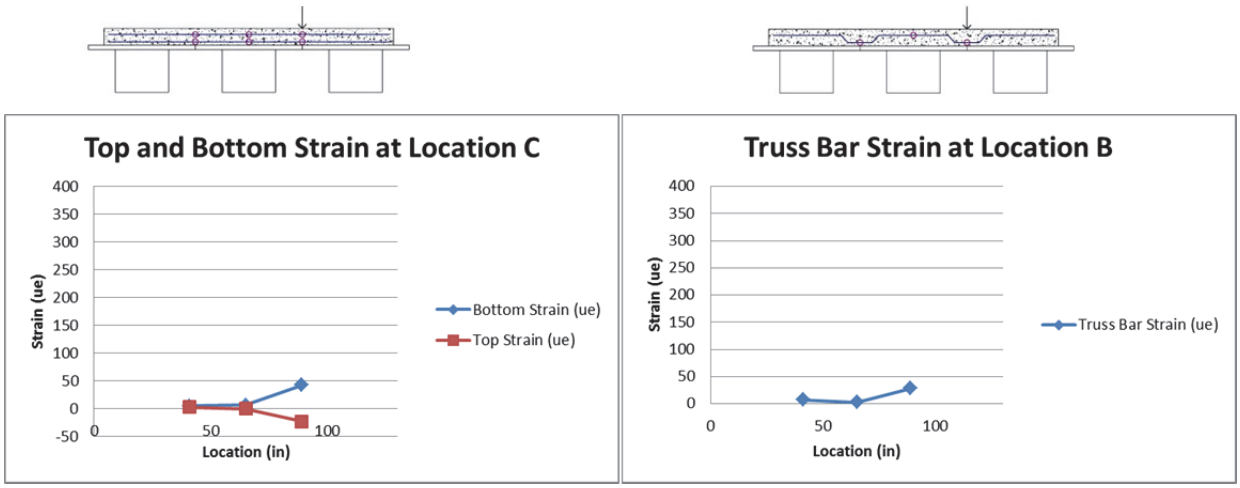

Figure 5-25: Test 6 Strain in Top and Bottom Bars at Midspan and Truss Bar at Midspan

5.9 Test 7: Quarter Point Service Test with Two Point Loads

5.9.1 Test 7 Setup

The seventh test was two point loads at the quarter point of the bridge as seen in Figure 5-26. The test's maximum load was a service load of 21.3 kips for each patch with a total load of 42.6 kips.

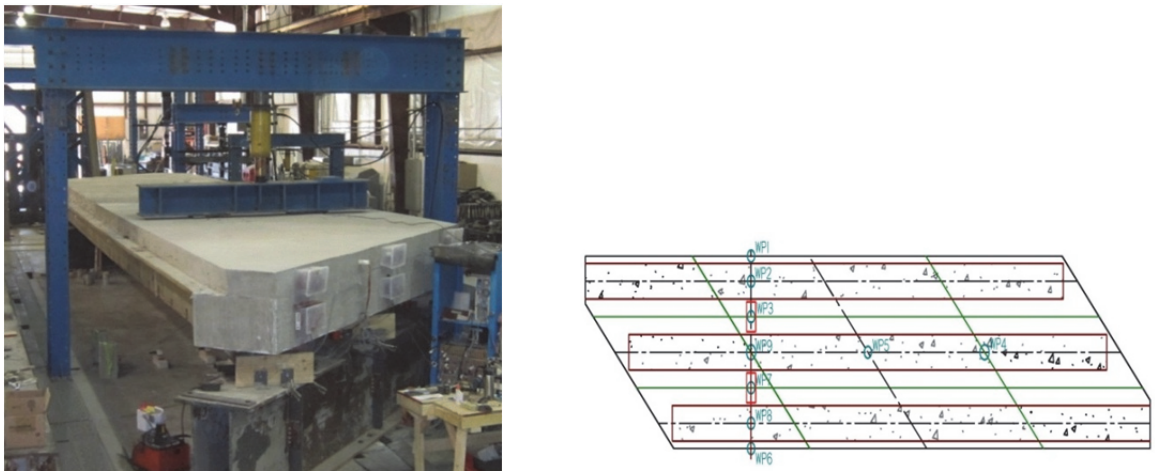

Figure 5-26: Test 7 Setup

5.9.2 Test 7 Results

The maximum deflection was 0.34 in. at potentiometer 1 at the load of 42.6 kips. The deflections measured by the potentiometers are shown in Figure 5-27.

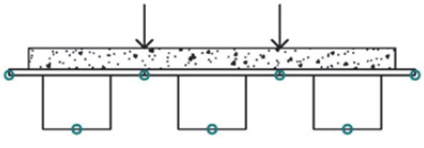

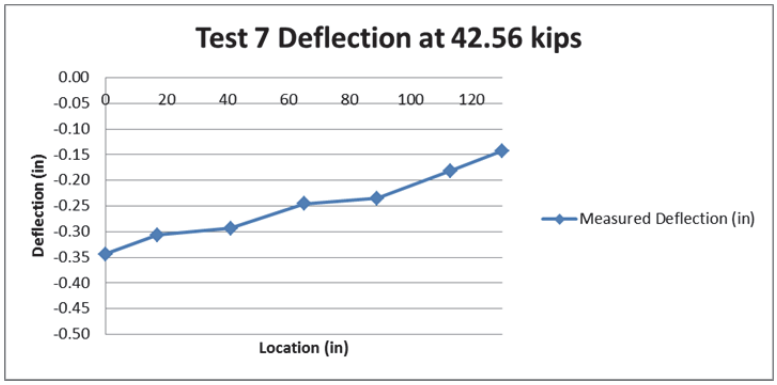

Figure 5-27: Test 7 Deflections

Shown in Figure 5-28 are the strain gage values across the width of the bridge underneath the applied load at midspan which is also where the maximum strains were recorded. The maximum strain was 201 με, which was on the strain gage on the bottom straight bar underneath the load.

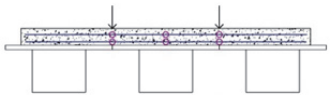

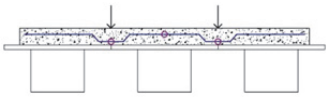

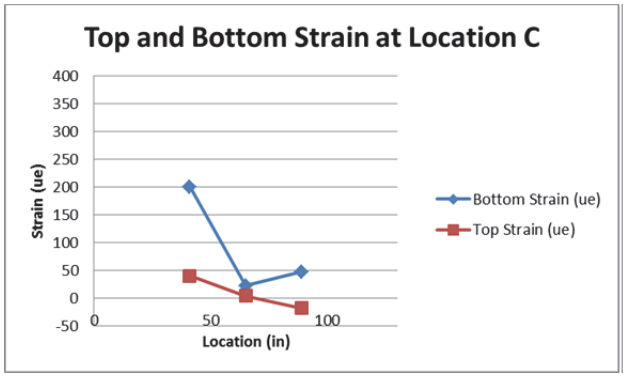

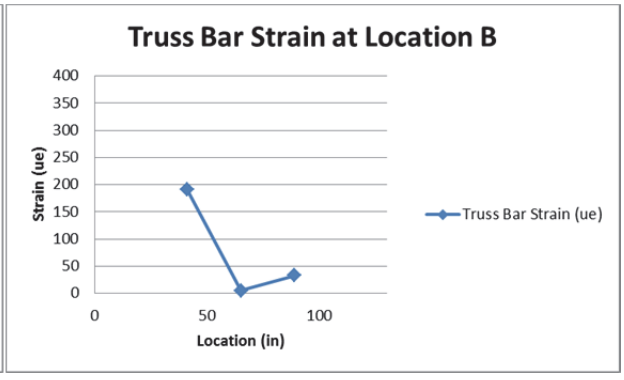

Figure 5-28: Test 7 Strain in Top and Bottom Bars at Midspan and Truss Bar at Midspan

5.10 Test 8: Quarter Point Strength Test with Two Point Loads

5.10.1 Test 8 Setup

The eighth test was two point loads at the midspan of the bridge with the same test setup as Test 7. The test's maximum load was a strength load of 37.2 kips for each patch with a total load of 74.48 kips.

5.10.2 Test 8 Results

Strain gage T-C-1.5-B gave nonlinear results as shown below in Figure 5-29 which did not return to zero. Therefore, the test was repeated and the results were shown in Test 9. The maximum deflection was 0.61 in. at potentiometer 1 at the load of 74.48 kips. The deflections measured by the potentiometers are shown in Figure 5-30.

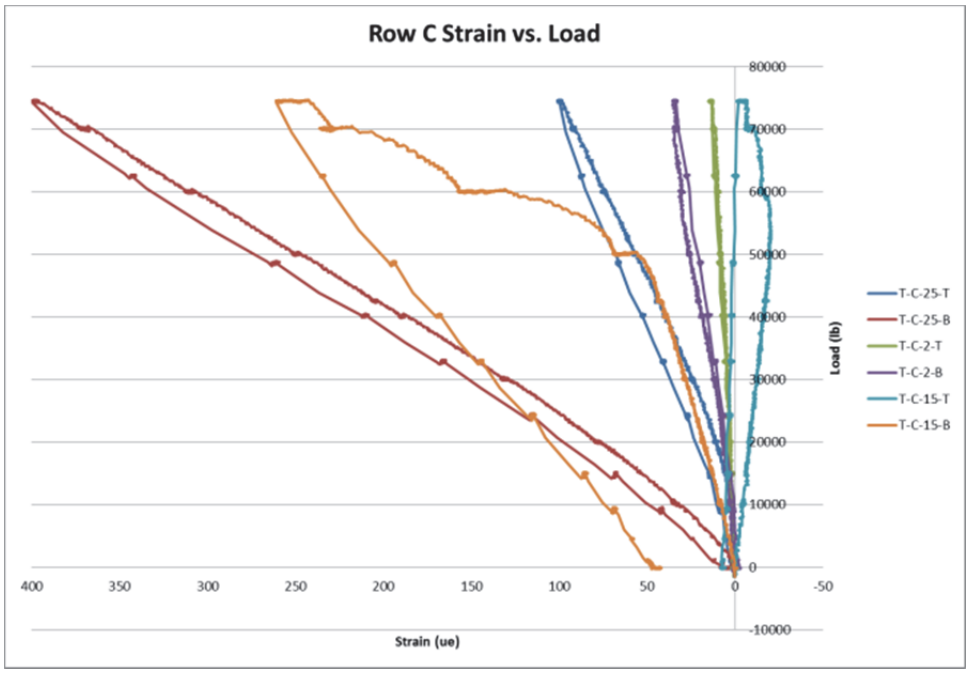

Figure 5-29: Strain Gage Data for Row C

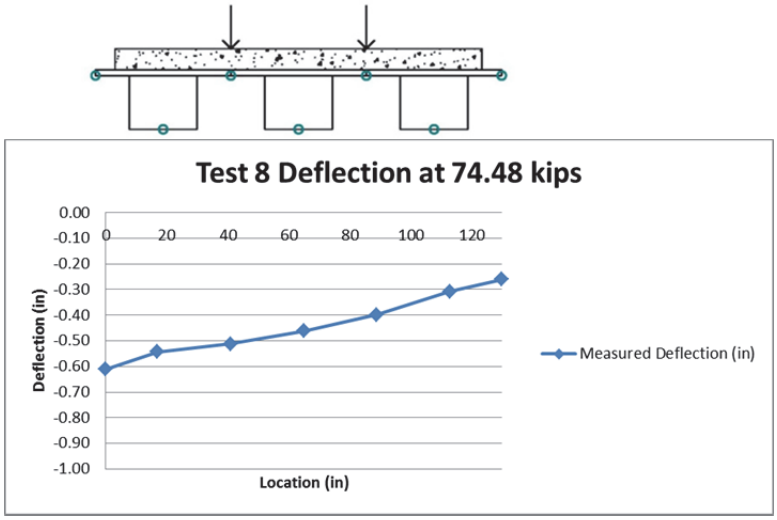

Figure 5-30: Test 8 Deflections

Shown in Figure 5-31 are the strain gage values across the width of the bridge underneath the applied load at midspan which is also where the maximum strains were recorded. The maximum strain was 399 με, which was on the strain gage on the bottom straight bar underneath the load.

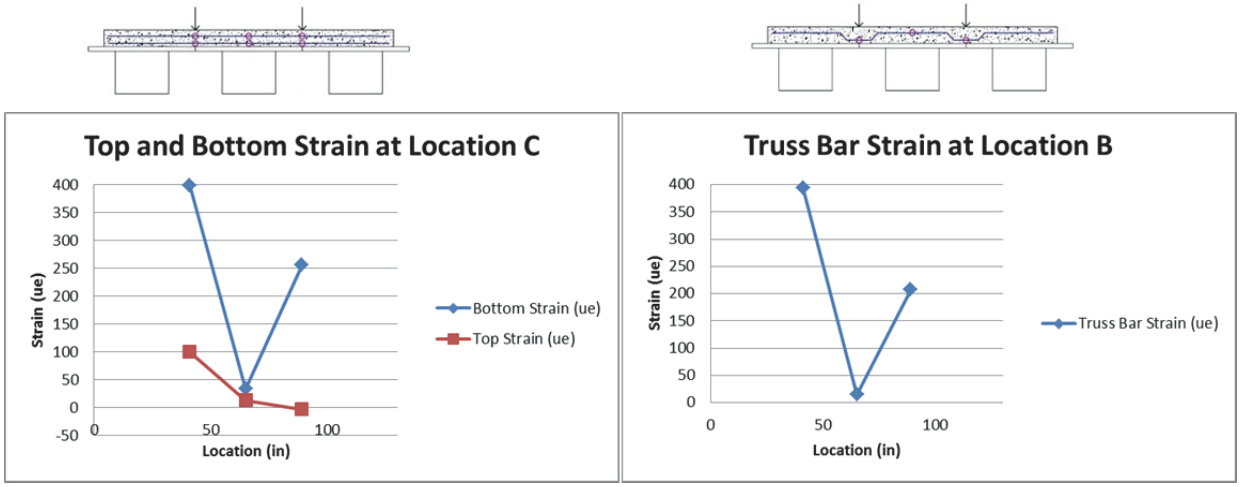

Figure 5-31: Test 8 Strain in Top and Bottom Bars at Midspan and Truss Bar at Midspan

5.11 Test 9: Quarter Point Strength Test with Two Point Loads Redone

5.11.1 Test 9 Setup

The eighth test was redone a second time due to some curious results from strain gage T-C-1.5-B. The test was redone to see if there was any damage done to the deck during the eighth test.

5.11.2 Test 9 Results

This time strain gage T-C-1.5-B showed linear results as shown in Figure 5-32. The non-linear data in Test 8 could be caused by an error by the old data acquisition system. The rest of the data was very similar to Test 8, showing that the test is repeatable. The maximum deflection was 0.58 in. at potentiometer 1 at the load of 74.48 kips. The deflections measured by the potentiometers are shown in Figure 5-33.

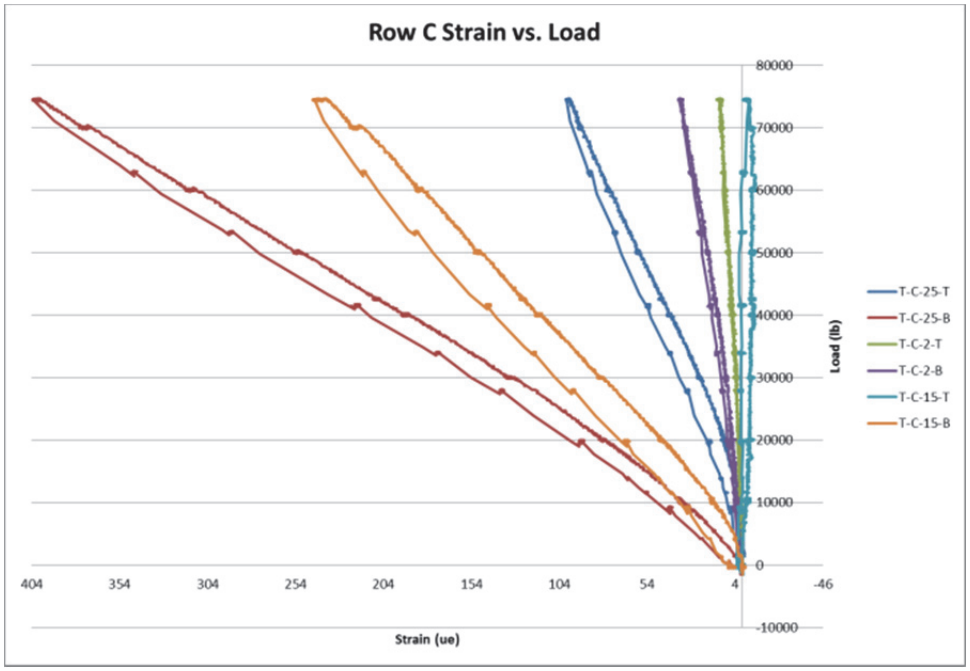

Figure 5-32: Strain Gage Data for Row C

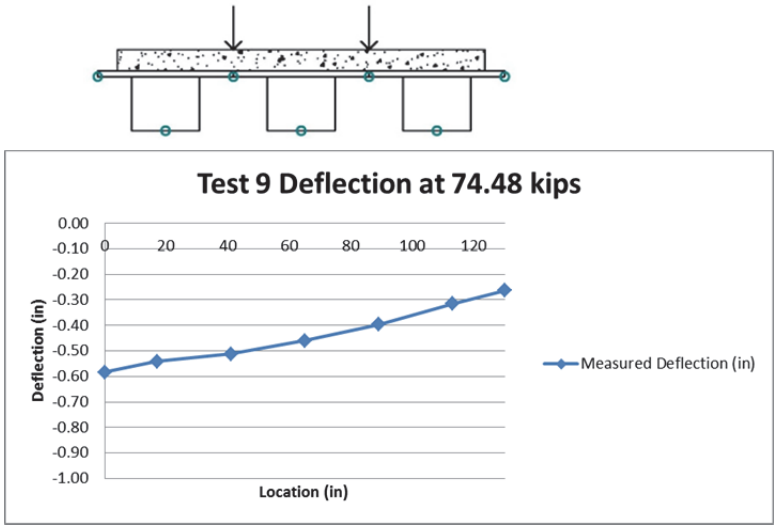

Figure 5-33: Test 9 Deflections

Shown in Figure 5-34 are the strain gage values across the width of the bridge underneath the applied load at midspan which is also where the maximum strains were recorded. The maximum strain was 402 με, which was on the strain gage on the bottom straight bar underneath the load.

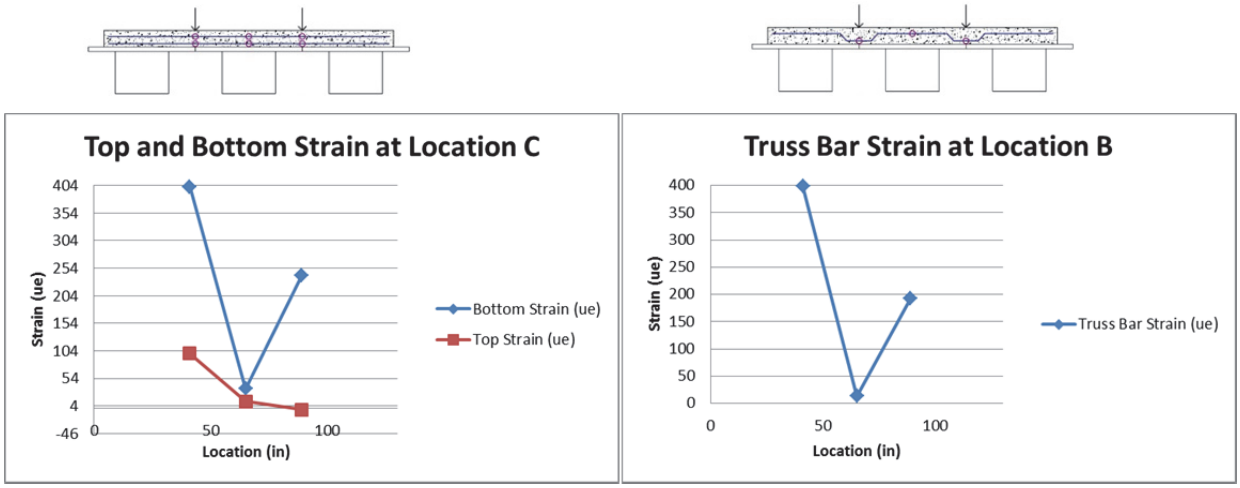

Figure 5-34: Test 9 Strain in Top and Bottom Bars at Midspan and Truss Bar at Midspan

5.12 Testing Summary

The system behavior of the three-HCB bridge test specimen was studied to provide a basis for predicting behavior of the Tide Mill Bridge. No cracks were observed in the deck during testing. Also, the maximum strain in all of the tests was observed in Test 4 and was 597 με

which is well below yielding strain of the reinforcing bars. However, the concrete cracking strain from the cylinder tests was determined to be 112 με, so there may be undetected microcracks.

5.12.1 Load-Deflection Behavior

Linear behavior was observed in the load-deflection behavior of the deck. The deflections returned near zero for all potentiometers except WP3 which is suspect. All of the other potentiometer returning to near zero indicates that permanent deformation did not occur. The maximum deflection and the location are shown in Table 5-4.

Table 5-4: Summary of Maximum Measured Deflection

Test Number	Max Deflection (in.)	Wire Pot
1 Service	-0.24	WP1 & WP 3
2 Service	-0.27	WP 6
3 Service	-0.46	WP 8
4 Strength	-0.89	WP 6
5 Service	-0.22	WP 1
6 Service	-0.10	WP 5
7 Service	-0.34	WP 1
8 Strength	-0.61	WP 1
9 Strength	-0.58	WP 1

5.12.2 Strain

The maximum strain in the top and bottom mat transverse reinforcement and the location of the maximum strain for each test is shown in Table 5-5. The graph demonstrates that the strain in the bottom mat of reinforcement is much greater than the top mat of reinforcement with an average percent difference of 87%. Table 5-6 shows the maximum strain in the longitudinal reinforcement for each test. Figure 4-11 in Section 4.2.1 shows the locations and names of all of the strain gages. Positive values correspond to tension strains and negative values correspond to compression strains.

Table 5-5: Summary of Maximum Transverse Measured Strain in the Top and Bottom Bars

	Bottom Reinforcement		Top Reinforcement	
Test Number	**Strain (με)**	**Gage**	**Strain (με)**	**Gage**
1 Service	217	Bottom 2.5 F	17	Top 2.5 F
2 Service	305	Bottom 1.5 F	72	Top 1.5 F
3 Service	347	Bottom 1.5 F	92	Top 1.5 F
4 Strength	597	Bottom 1.5 F	182	Top 1.5 F
5 Service	174	Bottom 2.5 C	16	Top 2.5 C
6 Service	43	Bottom 1.5 C	-23	Top 1.5 C
7 Service	201	Bottom 2.5 C	41	Top 2.5 C
8 Strength	399	Bottom 2.5 C	100	Top 2.5 C
9 Strength	402	Bottom 2.5 C	99	Top 2.5 C

Table 5-6: Summary of Largest Compressive Longitudinal Measured Strain

Test Number	Strain (με)	Gage
1 Service	-35	L-QB-1
2 Service	-91	L-M-2
3 Service	-162	L-M-2
4 Strength	-259	L-M-2
5 Service	-70	L-QA-2
6 Service	-39	L-QA-2
7 Service	-135	L-QA-2
8 Strength	-225	L-QA-2
9 Strength	-224	L-QA-2

CHAPTER 6: ABAQUS MODEL

6.1 Overview of the Model

In order to gain a better understanding of the bridge behavior, an Abaqus model was created of the test bridge. The first model used beam elements to represent the HCB's, however it did not follow the observed results from testing so another model was created. The second model used shell elements to model the different components of the HCB's and the deflections from the Abaqus model better matched the results from testing.

6.2 First Abaqus Model

6.2.1 Overview of the Model

The first iteration of the Abaqus bridge model consisted of a bridge deck modeled with shell elements, the HCB's modeled with beams elements, and the end diaphragms modeled with beam elements. The element sizes were 0.5625 in. in the longitudinal direction with 1000 elements in total, and the element size was 0.5 in. in the transverse direction with 260 elements in total.

Figure 6-1: Beam Elements

The beam elements of the HCB are shown in Figure 6-1 and used an average value for the entire beam as the beam properties in order to simplify the bridge model. The beam elements were placed so that they would be at the location of the center of the real beams. The model was run twice with two different values for the EI of the beams, one with the values for a beam with an undamaged arch, 27,000,000 kip-in^2, and one with the values as if the arch had cracked in tension and there was no arch, 12,000,000 kip-in^2. The reason for the two tests was that at the conclusion of Ahsan's tests, it was unclear whether or not the concrete arch had been cracked. Therefore, the actual value for the experimental testing should fall between the results from the

two models. Two models were created for each test loading, one with the properties for an intact arch and one with the properties for no arch.

The results from the experimental testing, however, did not correlate well with either model. Therefore, a new approach was taken for modeling the HCB's, which is shown in the next section.

6.3 Final Abaqus Model

6.3.1 Overview of the Model

The final iteration of the Abaqus bridge model consisted of a bridge deck modeled with shell elements, the HCB's modeled with shell elements, and the diaphragm modeled with beam elements connecting to the bottoms of the HCB's. Shell elements were used to represent the deck because the deck slab was connected to the girders with shear connectors, which creates a composite response with member forces in the slab. Shell elements are able to demonstrate this behavior because in-plane stress is developed in shell elements, producing more realistic moment in the deck. (Tangwongchai, Anwar, & Chucheepsakul, 2011) A cross section of the model showing the deck and HCB's in black, the diaphragms in green, and the connections in blue is shown in Figure 6-2.

Figure 6-2: Cross Section of Model

The concrete deck was modeled with an elastic modulus of 4380 ksi which was the value obtained from the concrete cylinder material testing at the time of testing. The deck shell elements were set to be 7.5 in. thick, which is the same as the testing bridge. The mesh of the deck is shown in Figure 6-3. The deck has two different mesh patterns, one for the middle section and one used for both the two exterior sections with the cut off ends. The elements in the middle section are all an identical diagonal shape. For the exterior sections, the shapes of the elements change because one side of the section is straight and the other section is on an angle.

Figure 6-4 shows two zoomed in sections with one on each end of the deck where the exterior section connects to the interior section and how the shapes of the elements change. While this change of element shapes allows for the deck to be meshed, it makes it difficult to obtain the transverse moments.

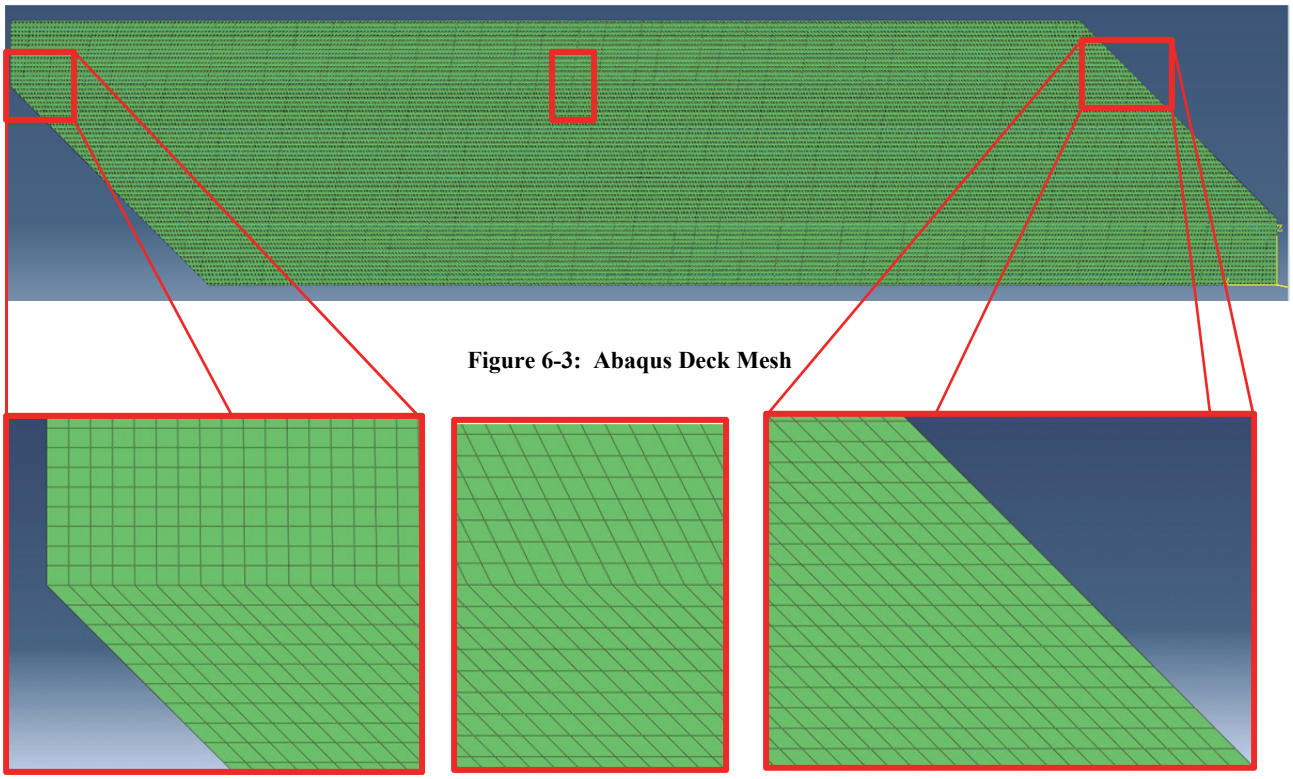

Figure 6-3: Abaqus Deck Mesh

Figure 6-4: Zoomed in Deck Mesh

The modeled HCB's consisted of GFRP shell elements for the sides and top with an elastic modulus of 3100 ksi and a thickness of 0.11 in. The bottom GFRP shell elements included the transformed area of the steel prestressing strands running along the bottom of the beams so the thickness was 1.49 in. The concrete arch was modeled by 4 in. thick horizontal shell elements located at the average elevation of the concrete arch with an elastic modulus of 3910 ksi. The vertical concrete fin was also modeled by shell elements with the same properties and was connected to the middle of the horizontal arch shell elements.

The concrete arch was connected to the deck through the vertical concrete fin with rigid links. The horizontal portion of the concrete arch was connected to the GFRP side walls with rigid links only for six in. on each end because the concrete arch of the test bridge had foam

between the arch and the GFRP side walls. The GFRP shell connects to the deck with rigid links only at the top outside corners.

6.3.2 Validating Abaqus Model

In this Abaqus model, it is assumed that the concrete arch is completely intact even though the results from Ahsan's tests indicated that the concrete arch may have been cracked. Because the concrete arch is inside the GFRP shell of the HCB, there was no way to visually verify if there were any cracks present and if there were any, how many or what size they were. One reason that it is acceptable to include the capacity of an intact arch is that even though the concrete may have cracks, there were still the two steel strands running through the arch that can transfer the tensile load through the cracks to the intact concrete. Tension stiffening is when the stiffness of cracked concrete does not drop completely to zero because the uncracked concrete between the adjacent cracks still carries some tensile stresses. Two ways that tensile stresses are induced in the concrete between the cracks in flexural members are: stress transfer through the steel-reinforcement-concrete bond (Figure 6-5) and shearing action of the curvature of the flexural member (Figure 6-6). (Ng, Lam, & Kwan, 2010)

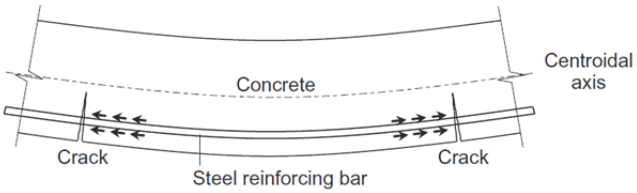

Figure 6-5: Tension Stiffening with Stress through Bond (Ng, Lam, & Kwan, 2010) Used under fair use, 2013

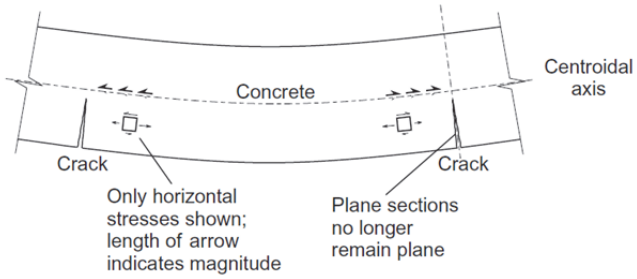

Figure 6-6: Tension Stiffening with Shearing Action of Curvature (Ng, Lam, & Kwan, 2010) Used under fair use, 2013

Another reason that it is acceptable to include the capacity of an intact arch is that when the deck is cast, it compresses the arch, reducing the tensile force in the arch when it is loaded. This

helps keep the stress in the arch below tensile rupture. Using a three hinged arch, the weight of adding the concrete deck induces a compressive force of 105 kips.

To further validate this Abaqus model, it was compared to the experimental results from a load configuration from one of Ahsan's tests because he had data for the stress in the GFRP shell of the HCB's. Ahsan's experimental testing was done on the same testing bridge as used in this research so the bridge setup and geometry are the same. Ahsan's Test 3 load configuration as shown in Figure 6-7 was run with the Abaqus model. Each wheel load was modeled as a distributed load over a rectangle with a length of 20 in. and a width of 10 in. The load magnitude for each rectangle patch could not be made to be exactly 21.3 kips because of the diagonal elements being used. However, care was taken to make it as close as possible.

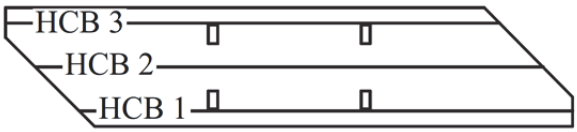

Figure 6-7: Ahsan's Test 3 Load Configuration (Ahsan, 2012) Used under fair use, 2013

The stresses in the GFRP shell at the midpan and quarter point of HCB 2 of the Abaqus model were compared to the values Ahsan observed. Strain profiles for the composite section were created by using the strain gages on the GFRP box, the strain gage on the longitudinal reinforcement in the deck, and the strain values at the same locations provided by the Abaqus model. In general, the experimental data agreed well with the Abaqus results.

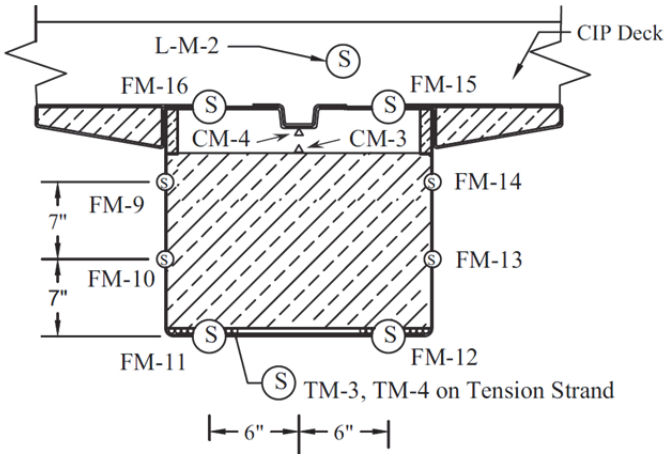

Figure 6-8: Gage Locations for HCB 2 at Midspan (Ahsan, 2012) Used under fair use, 2013

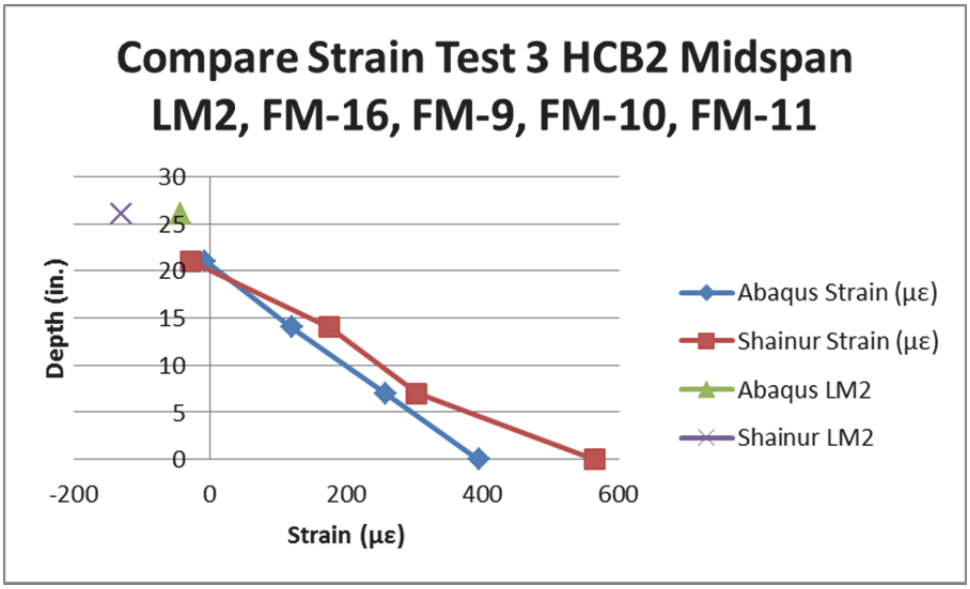

Figure 6-9: HCB 2 Midspan Strain Profile East Side

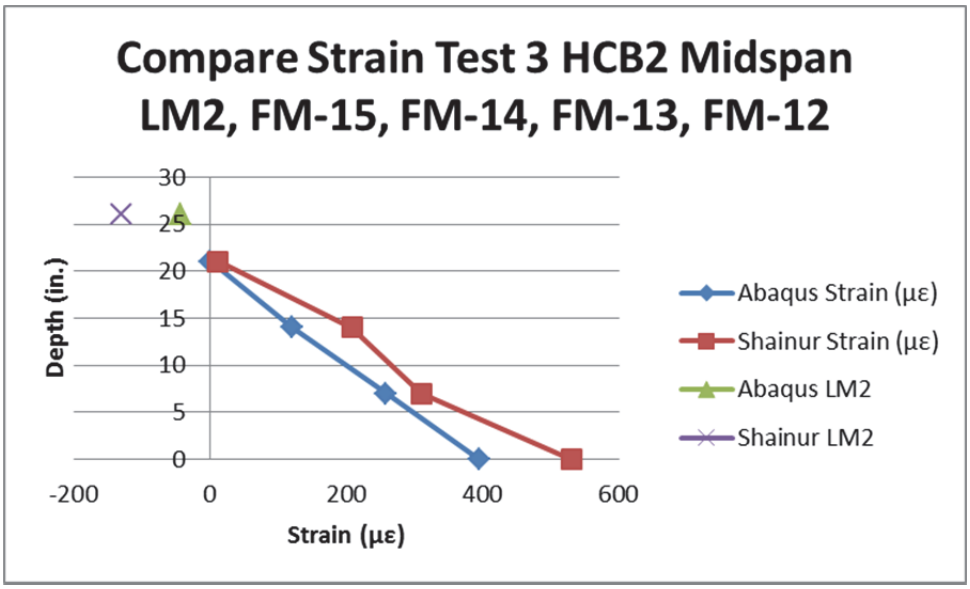

Figure 6-10: HCB 2 Midspan Strain Profile West Side

The gage locations at the midspan of HCB 2 are shown in Figure 6-8. Overall, the strain profiles for both Ahsan's test at midspan and the Abaqus model at midspan are linear as seen in Figure 6-9 and Figure 6-10. Also, the gage values on either side of the beam in Ahsan's test and the Abaqus model were in good agreement.

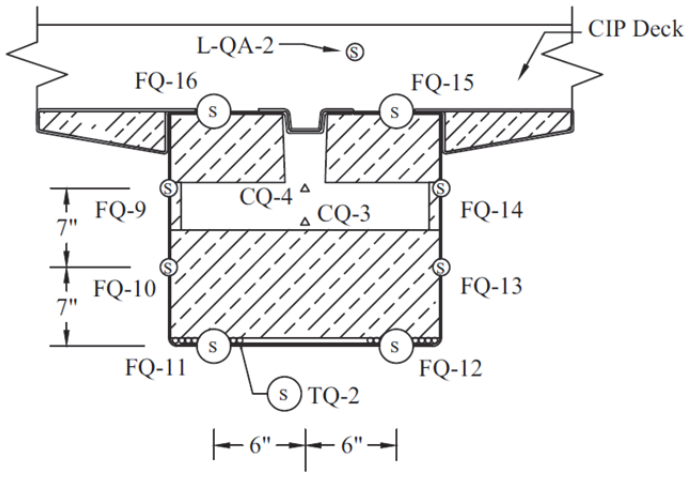

Figure 6-11: Gage Locations for HCB 2 at Quarter Point (Ahsan, 2012) Used under fair use, 2013

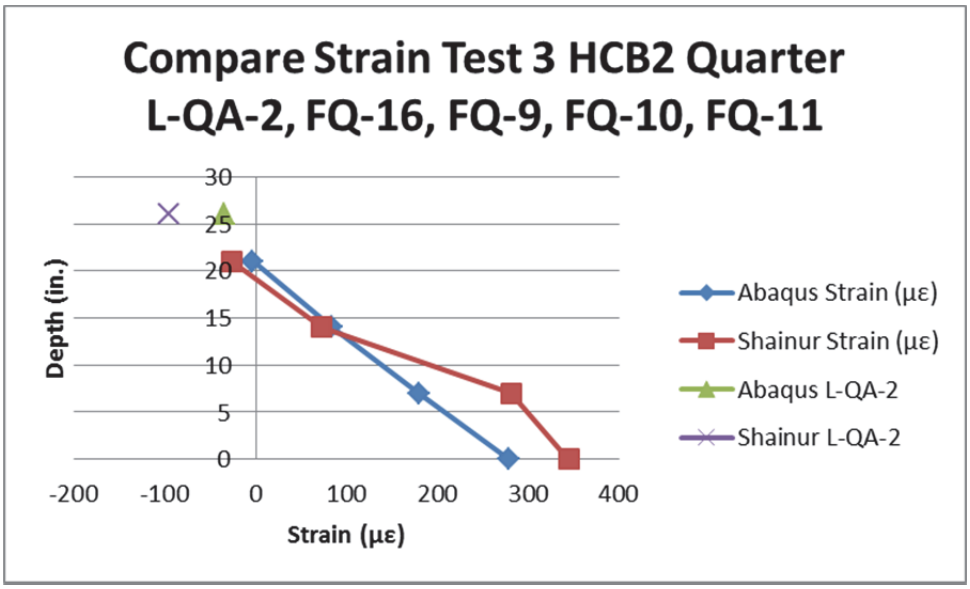

Figure 6-12: HCB 2 Quarter Point Strain Profile East Side

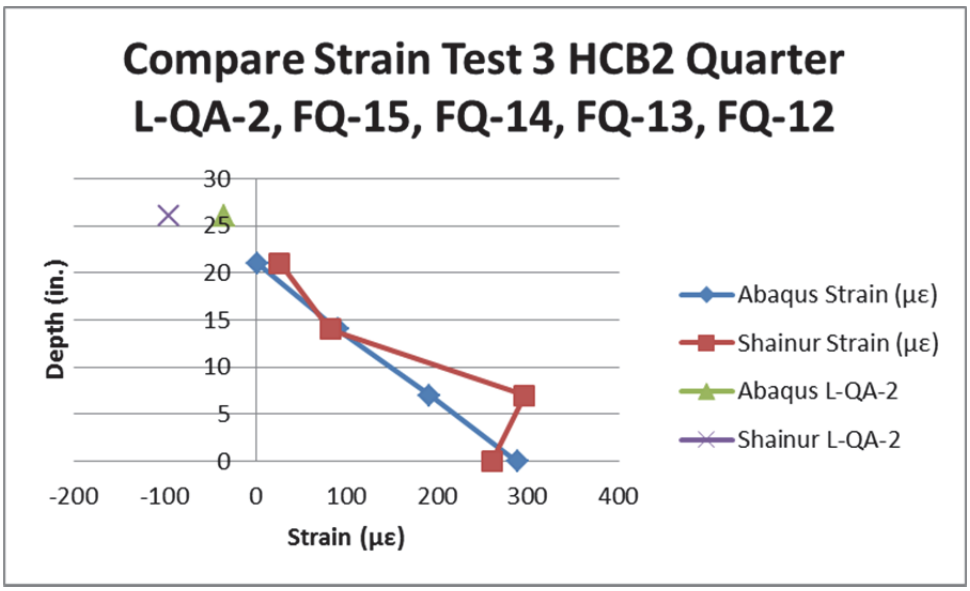

Figure 6-13: HCB 2 Quarter Point Strain Profile West Side

The gage locations at the quarter point of HCB 2 are shown in Figure 6-11. Overall, the strain profile for both Ahsan's test at the quarter point and the Abaqus model at the quarter point are linear for the east side of the beam as seen in Figure 6-12. However, for the west side seen in Figure 6-13, the strain profile for Ahsan's test was not linear, where the Abaqus model was linear. Ahsan accounts for this discrepancy by stating that the FG-12 gage consistently registered less strain than FQ-11 (Ahsan, 2012).

Only the GFRP shell and the deck gage values could be compared between the Abaqus model and Ahsan's data because the steel strand was transformed into the bottom GFRP shell for the Abaqus model and the concrete arch in the Abaqus model is set to an average depth. Therefore, comparing those values would not be appropriate. The strain profiles for the Abaqus model and Ahsan's data show similar trends and values. The biggest difference occurred in the values for the strain in the bottom of the GFRP. Differences in the values could be because the Abaqus model does not take into account the direction of the GFRP fibers.

Equilibrium in the vertical direction was also verified. The sum of the total reaction forces for each girder was equal to 84.40 kips, which is very close to the total applied load of 85.12 kips. The difference in values can be attributed to the difficulty of the load application. The load

applied to the model was in the form of a pressure distributed load and the area the load was applied to was made up of diagonal elements which made it difficult to obtain the correct area.

Finally, the stiffness of the Abaqus model was comparable to the stiffness of the test bridge. This is demonstrated in the next section which shows the comparison between the deflections given by Abaqus and the deflection measured by the potentiometers during testing.

6.4 Comparing Abaqus Results to Measured Data

One advantage of creating an Abaqus model for each of the experiment tests is that the Abaqus model provides many more data points then the number of strain gages on the testing bridge. The maximum strains for the experimental tests usually occurred right underneath the loading point. The problem with this is that it is unclear how much of that maximum strain is due to localized effects of having the load right above the strain gage. The Abaqus model is able to show what is happening all around the load.

6.4.1 Deflections

The Abaqus model stiffness was comparable to the measured data and the deflections from Abaqus were similar to the deflections measured by the potentiometers. The deflections for the experimental test compared to the Abaqus model results are shown with the values across the width of the bridge facing south. The figure above each graph shows the load locations shown with an arrow and the potentiometer locations shown with the circles. In each of the tests, the results from potentiometer WP3, which is the third point from the left in the graphs shown, were suspect because it never seemed to follow the trend of the rest of the potentiometers.

The results from Tests 2, 6, and 9 are shown here since they show the tests that had some of the best and worst correlation. Test 2 was loaded at the midspan and Tests 6 and 9 were loaded at the quarter point. The results for all of the tests are shown in Appendix E.

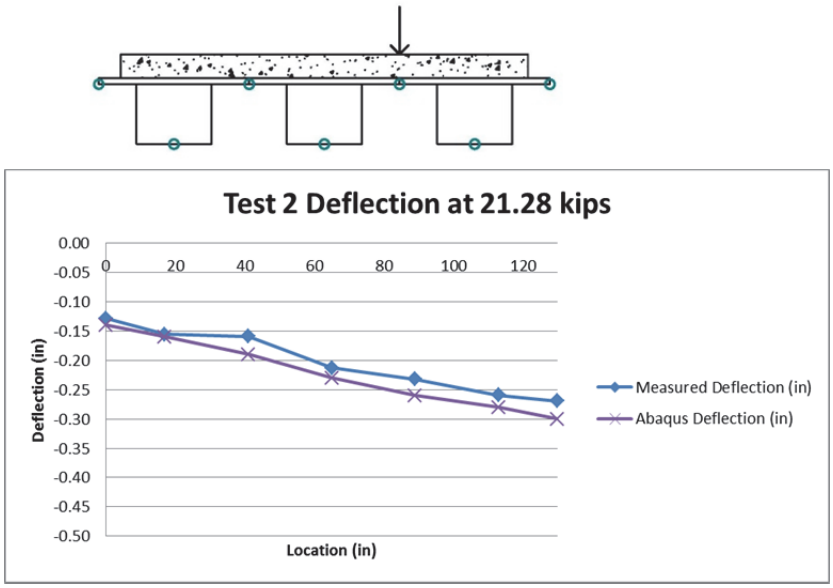

Figure 6-14: Test 2 Maximum Deflection Experimental and Abaqus Values

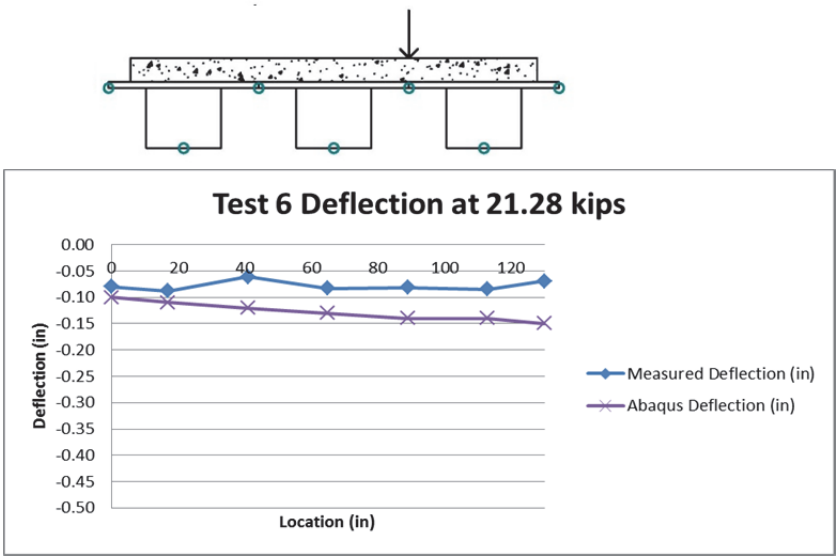

Figure 6-15: Test 6 Maximum Deflection Experimental and Abaqus Values

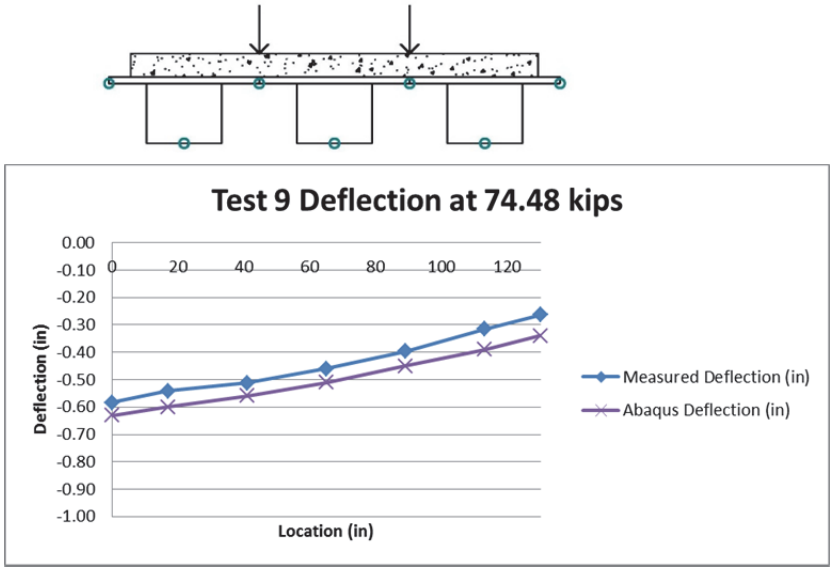

Figure 6-16: Test 9 Maximum Deflection Experimental and Abaqus Values

With the exception of the results from potentiometer WP3, both the results from the laboratory tests and the Abaqus model show the deck as deflecting as one gentle curve. This does not support the idea that the girders be treated as rigid supports in design because if that was the case, the deck would be deflecting in waves over the beams and it is not.

6.4.2 Strains

The strains from the laboratory tests were compared to the strains from the Abaqus model. Three graphs were made for each test along the three rows of strain gages along the length of the bridge. Those three rows were: M+ East (the row of strain gages between the beams on the east side of the bridge), M- Center (the row of strain gages over the center of the middle beam), and M+ West (the row of strain gages between the beams on the west side of the bridge). The measured strains from the laboratory tests are shown with solid lines and the Abaqus strains are shown with dashed lines. The figure above each set of graphs shows the locations of the gages and the loads.

Results for Tests 1, 4, and 6 are show here since they include both a single point load test at the quart point and midspan, and a double point load test. The results for all of the tests are shown in Appendix D.

6.4.2.1. Test 1 Strains: Midspan Service Single Point Load on East Side

Test 1 had a point load at the midspan on the east side of the bridge. Figure 6-17 shows the strains along the length of the bridge that passed under that point load. As can be observed in the figure, the Abaqus strain values were consistently lower than the observed values, especially right underneath the load. The difference right underneath the load can be attributed to localized effects of the load being applied right below the strain gage. The Abaqus model did follow the pattern of behavior of the measured data, except right underneath the load. Underneath the load, the strain gage measured a tension strain in the top reinforcing bar, where the Abaqus model predicted a compression strain. In Figure 6-18 and Figure 6-19 the strains along the length of the bridge over the center beam and between the two beams with no load, and they show very little strain in both the test data and the Abaqus model predictions.

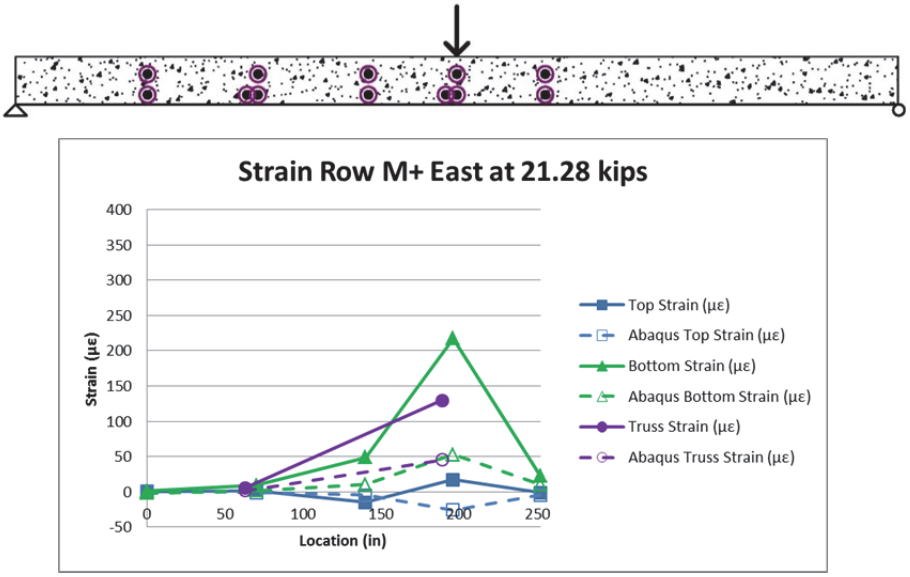

Figure 6-17: Test 1 Strain for Row M+ East

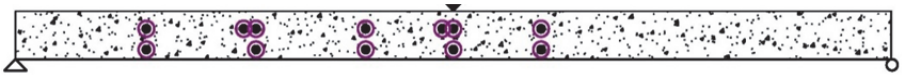

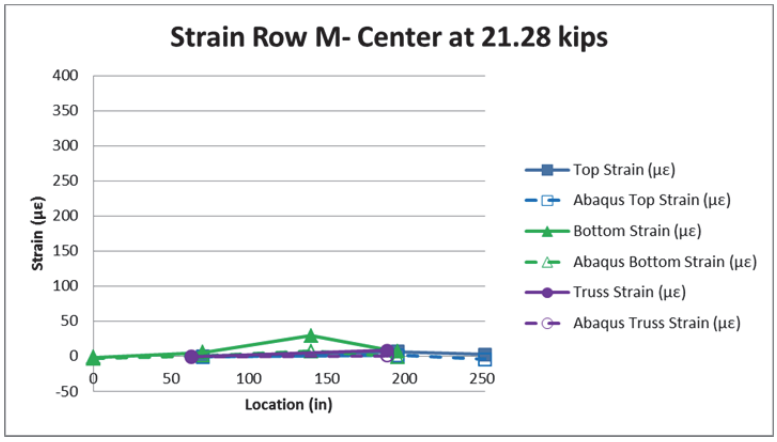

Figure 6-18: Test 1 Strain for Row M- Center

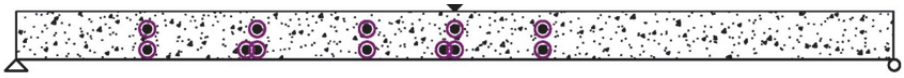

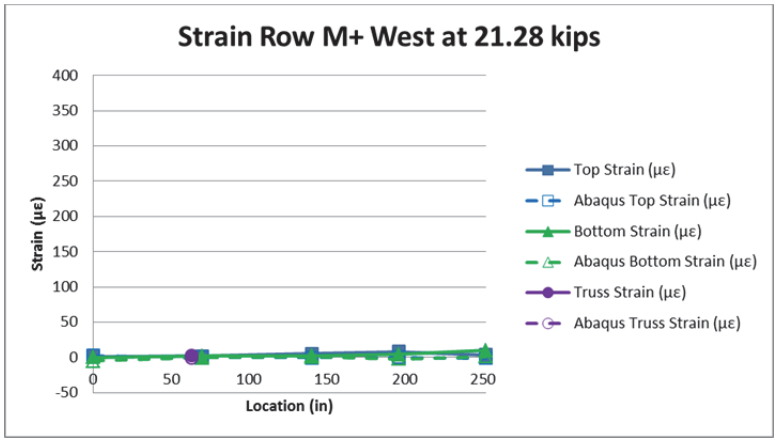

Figure 6-19: Test 1 Strain for Row M+ West

6.4.2.2. Test 4 Strains: Midspan Strength Two Point Loads

Test 4 had two point loads at the midspan on both the east and west sides of the bridge. Figure 6-20 and Figure 6-22 shows the strains along the length of the bridge that passed under the point loads. The Abaqus strain values were once again consistently lower than the observed values, and differed from the measured data directly under the loads by predicting a compression strain when the measured strain was tension. In Figure 6-21, small strains were observed in both the test data and the Abaqus model predictions with one spike in strain from the measured data.

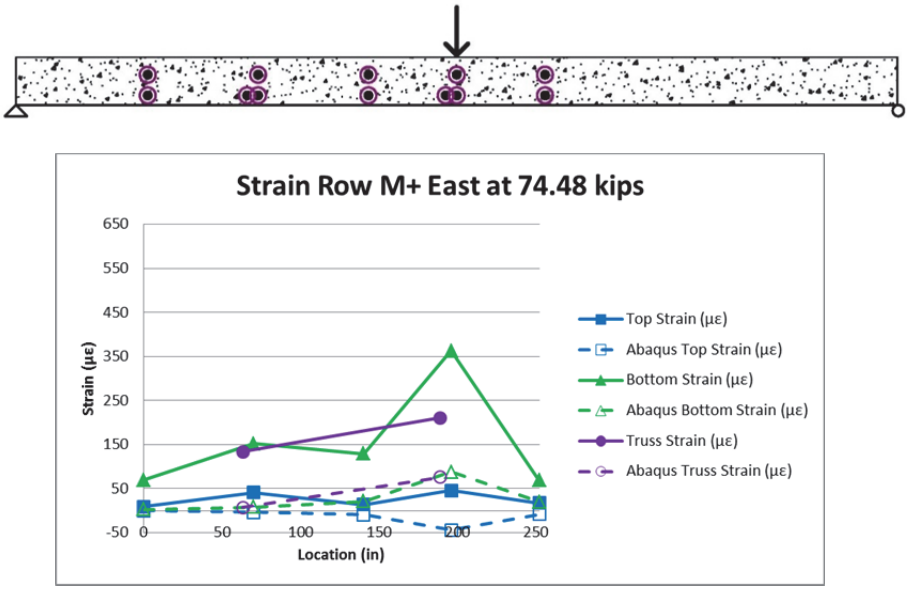

Figure 6-20: Test 4 Strain for Row M+ East

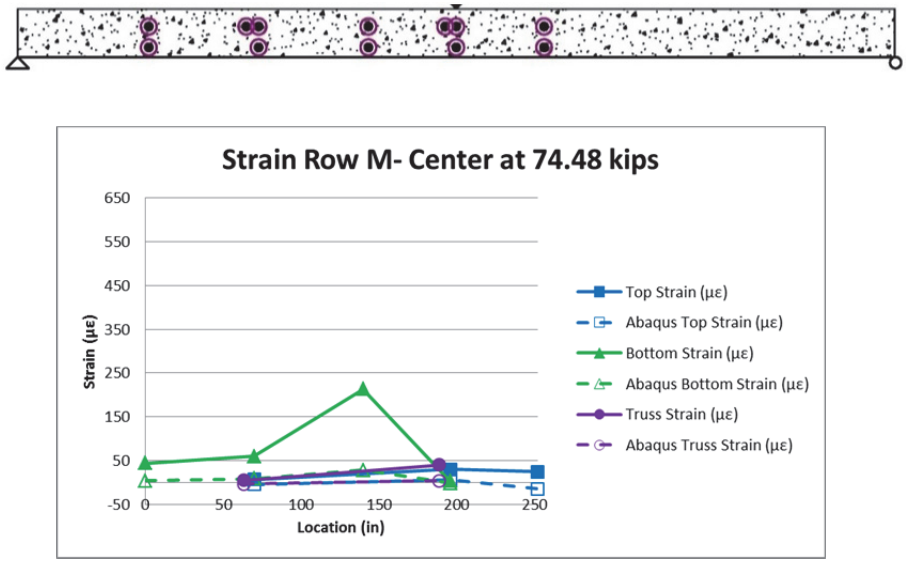

Figure 6-21: Test 4 Strain for Row M- Center

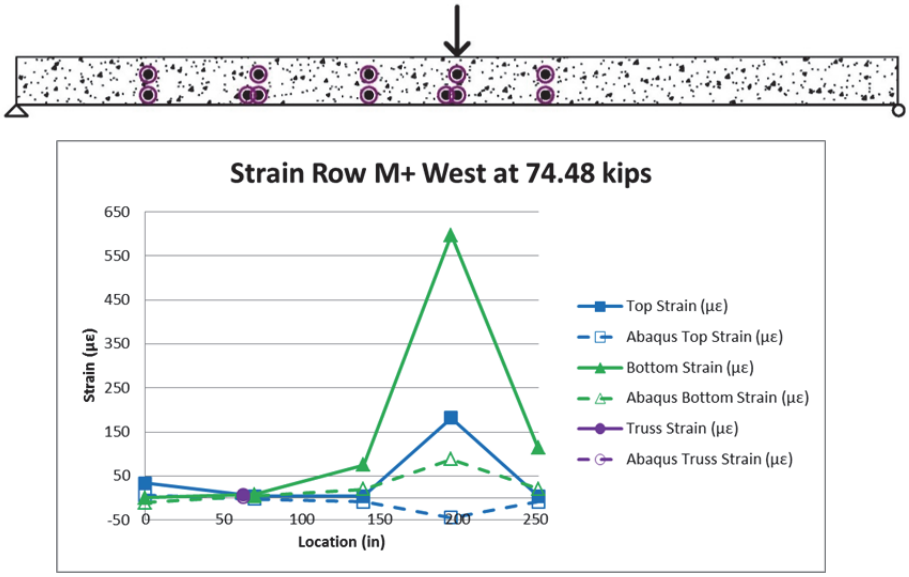

Figure 6-22: Test 4 Strain for Row M+ West

6.4.2.3. *Test 6 Strains: Quarter Point Service Single Point Load on West Side*

Test 6 had a point load at the quarter point on the west side of the bridge. Figure 6-23, Figure 6-24, and Figure 6-25 all show that the measured data and the Abaqus model are in agreement. The maximum strains occur underneath the load point, and the rest of the strains are all small.

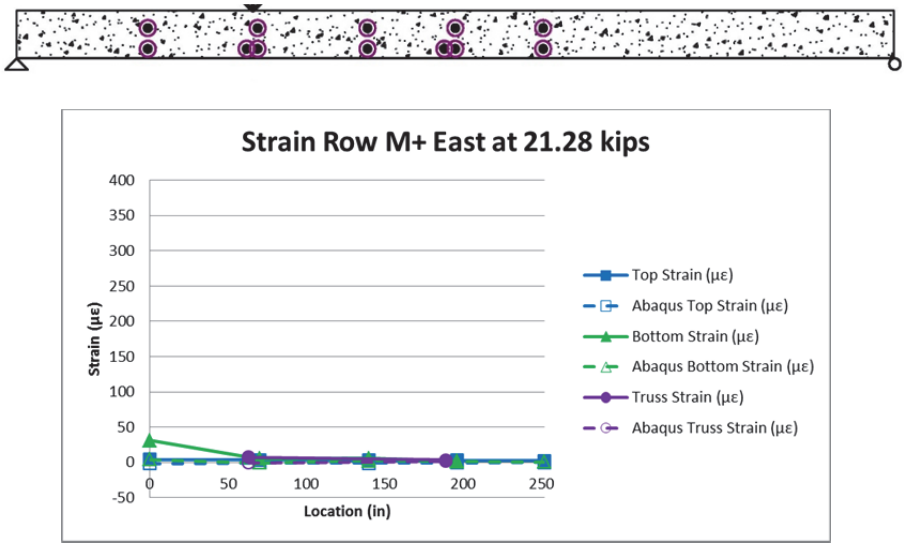

Figure 6-23: Test 6 Strain for Row M+ East

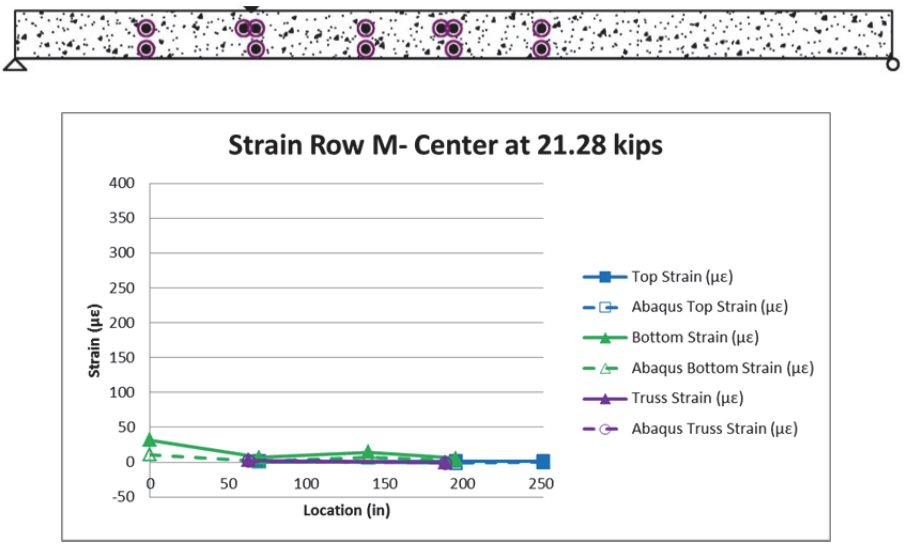

Figure 6-24: Test 6 Strain for Row M- Center

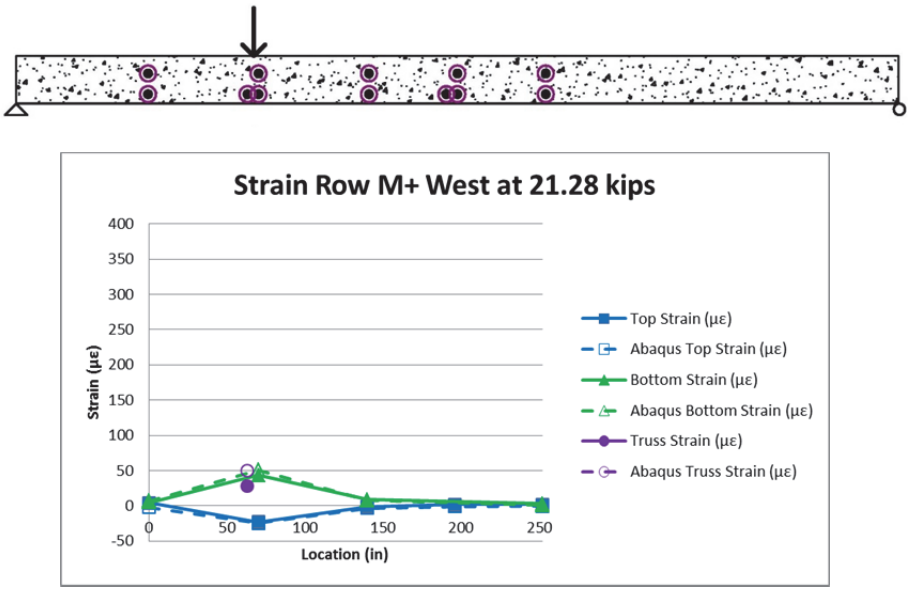

Figure 6-25: Test 6 Strain for Row M+ West

6.5 Further Study with Abaqus Model

6.5.1 Deflections

Because the Abaqus model has more data points than the number of strain gages on the testing bridge, the model can be used to further study the behavior of the bridge. Graphs of the deflections across the width of the bridge were made with data points at every inch. These graphs better show the curvature of the bridge deck under load. The first four sets of graphs in Figure 6-26 are the midspan tests and the second four sets of graphs in Figure 6-27 are the quarter point tests.

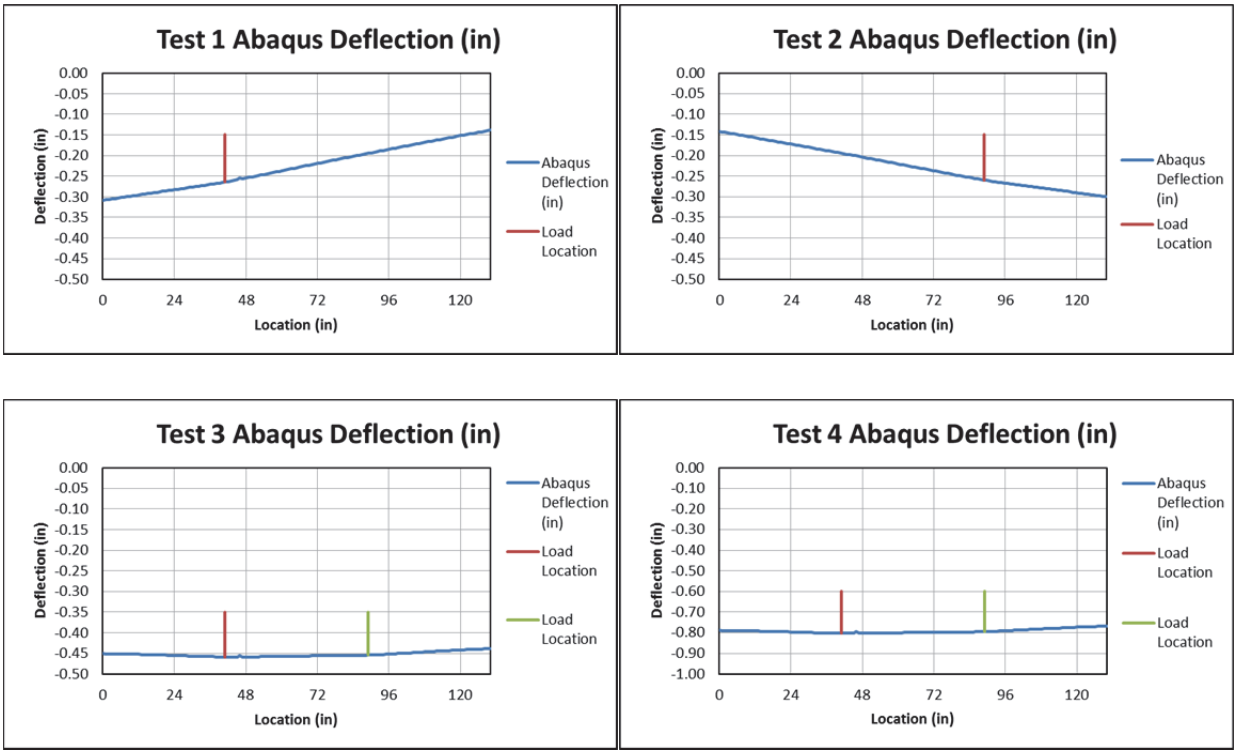

Figure 6-26: Abaqus Deflections for Midspan Tests

The deflections for the tests at the midspan show very little curvature underneath the load and instead show one single gentle curve along the width of the bridge, indicating that at the midspan, the bridge behaves more like a stiffened plate.

Shown in Figure 6-27 are the quarter point tests. Once again one single gentle curve can be seen in the graphs. The deflection in Test 6 shows slightly more curvature underneath the load than the midspan test, which may indicate that the bridge is starting to behave a little more like beams on rigid supports.

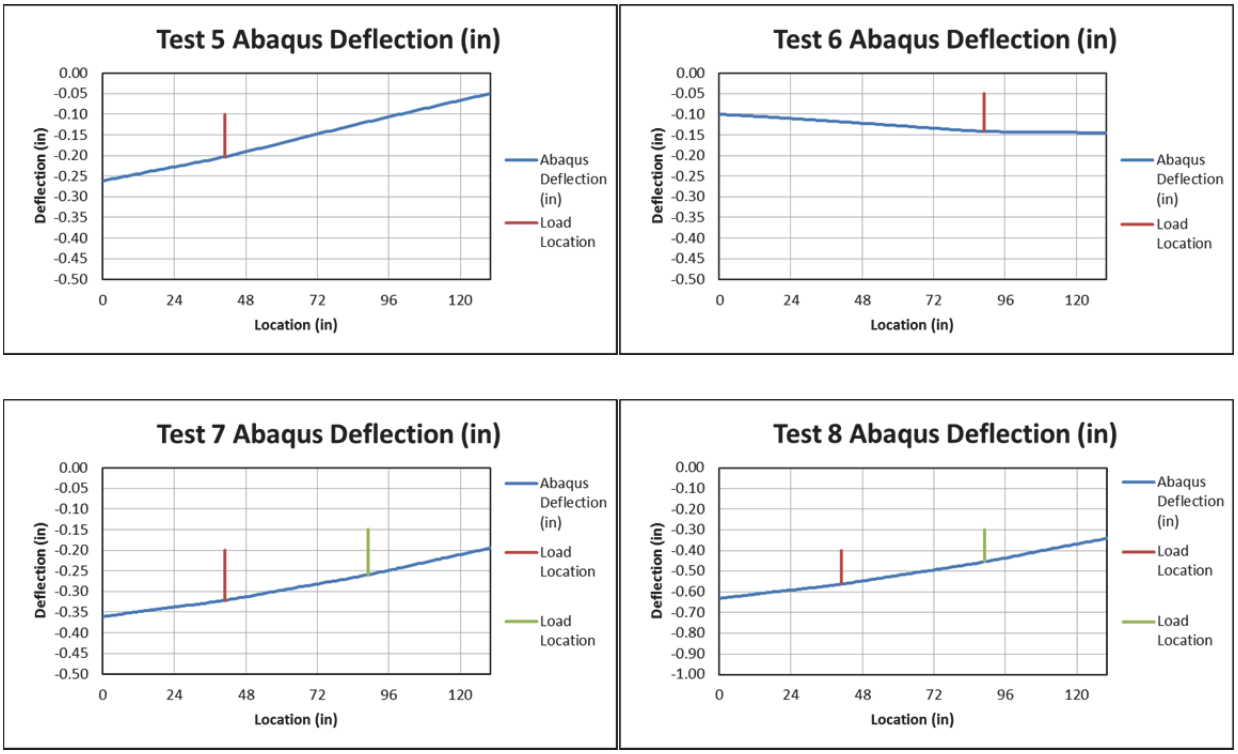

Figure 6-27: Abaqus Deflections for Quarter Point Tests

The Abaqus models for the various load conditions shows that the flexibility of the girders needs to be taken into account when designing the deck. This is because in each graph of the deflection, the deflection is more of one gentle curve along the width of the bridge instead of waves between the girders which would have been seen if the girders were behaving like stiff supports.

6.5.2 Effective Width from Abaqus

To find the effective width, the transverse stresses along the length of the bridge were graphed for both the locations for the top and bottom bars. The points chosen were along Rows M+ East and M+ West that go through the load locations. The area under the graphs for the top and bottom bars were taken and divided by the maximum stress for each to find the effective width. Then the values were averaged and recorded in Table 6-1. The average effective width from all eight tests is 72 in. (6 ft) for positive moment and 173 in. (14 ft) for negative moment. The values for the effective width from AASHTO are 52 in. (4 ft) for positive moment and 60 in. (5 ft) for negative moment with a beam spacing of 4 ft.

Table 6-1: Effective Width for Positive Moment from Abaqus

Test	Effective Width Row M+ East (in.)	Effective Width Row M+ West (in.)
1	70 (5.85 ft)	-
2	-	70 (5.85 ft)
3	79 (6.55 ft)	80 (6.68 ft)
4 Strength	79 (6.55 ft)	80 (6.68 ft)
5	64 (5.30 ft)	-
6	-	67 (5.54 ft)
7	72 (6.03 ft)	68 (5.70 ft)
8 Strength	72 (6.03 ft)	68 (5.70 ft)

Table 6-2: Effective Width for Negative Moment from Abaqus

Test	Effective Width Row M- Center (in.)
1	229 (19.1 ft)
2	212 (17.7 ft)
3	194 (16.2 ft)
4 Strength	194 (16.2 ft)
5	141 (14.3 ft)
6	122 (10.2 ft)
7	144 (12.0 ft)
8 Strength	144 (12.0 ft)

Figure 6-28 and Figure 6-29 are the two graphs used to determine the effective widths for positive moment for Test 4, and Figure 6-30 is the graph used to find the effective width for negative moment for Test 4.

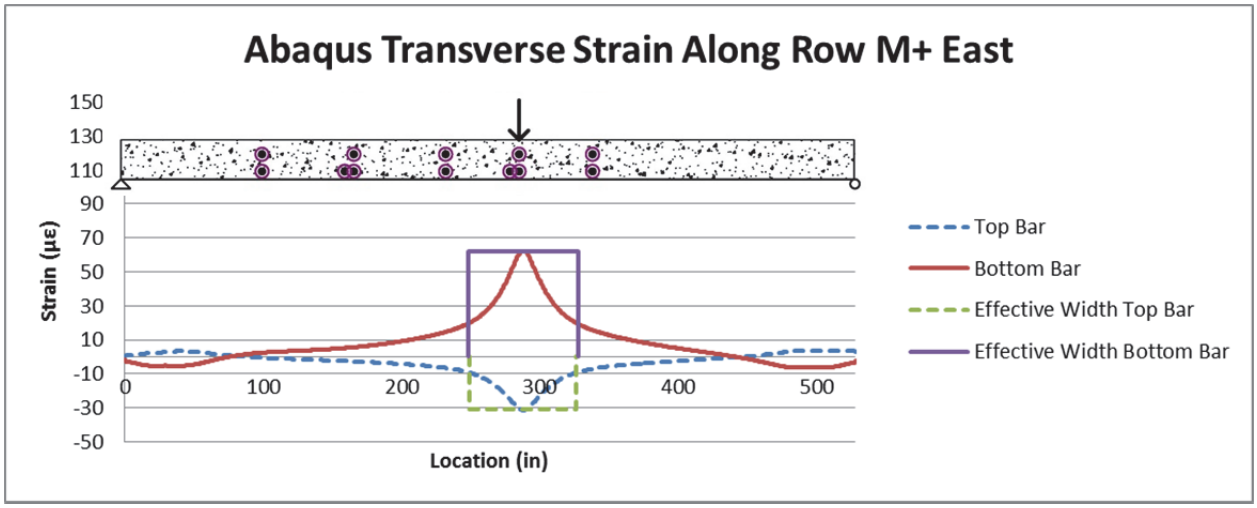

Figure 6-28: Test 4 Effective Width for Row M+ East

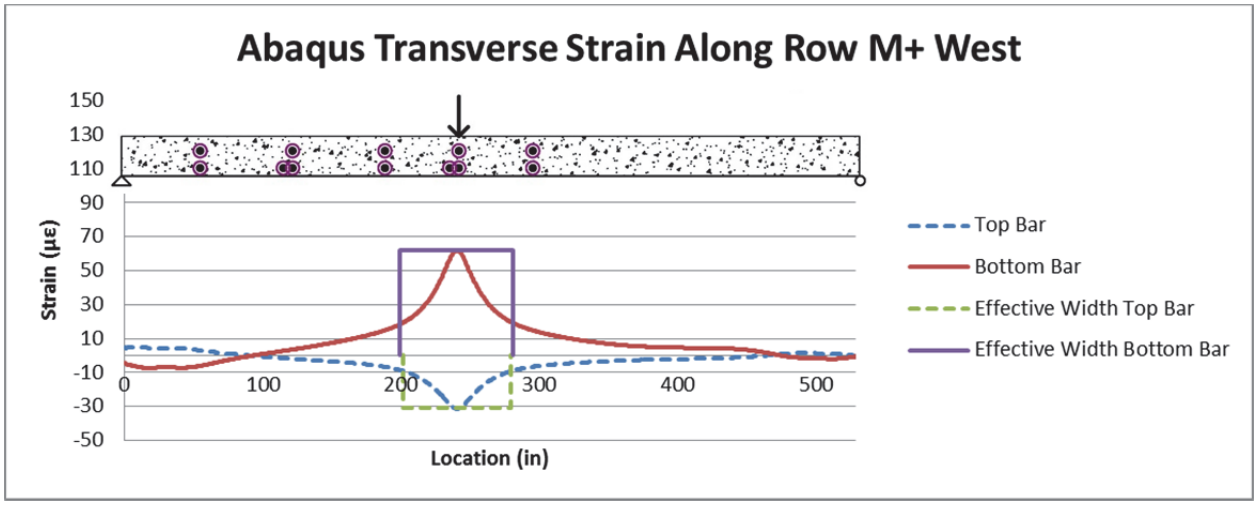

Figure 6-29: Test 4 Effective Width for Row M+ West

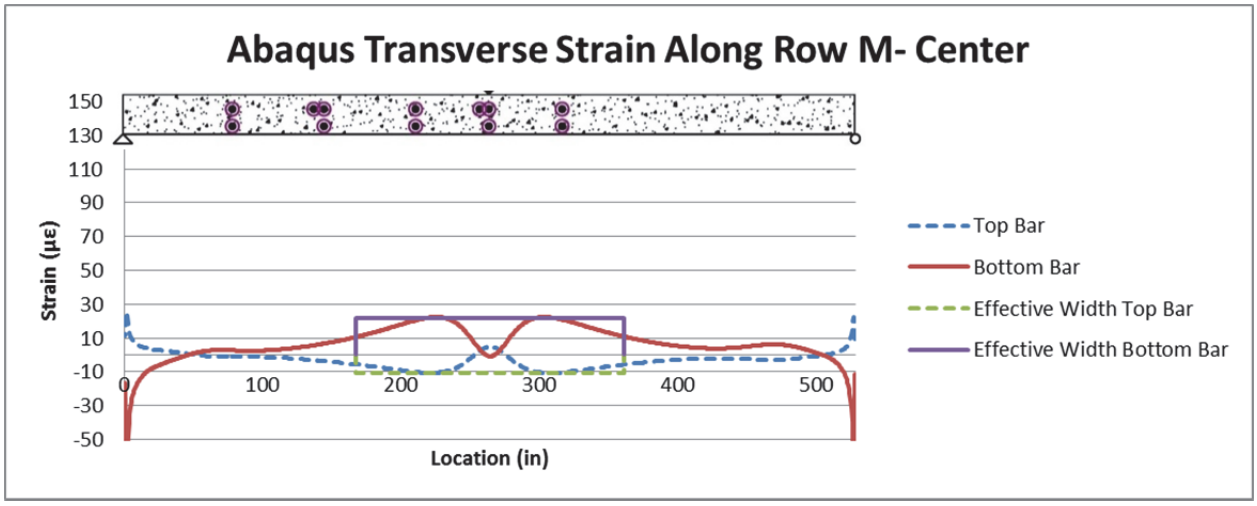

Figure 6-30: Test 4 Effective Width for Row M- Center

6.5.3 Moments from Abaqus

To calculate the transverse moments across the width of the bridge, first the transverse stresses were determined from the Abaqus model. The deck was meshed with diamond shapes, so the stresses given by the Abaqus model were decomposed into the transverse and longitudinal components. Abaqus gives the values for the stresses at the top, middle, and bottom of the deck. Using the assumption that plane sections remain plane, the values of the stresses in the reinforcement at different depths were obtained though linear interpolation.

The moments were determined for 14 in. wide strips along the length of the deck because the transverse reinforcement is spaced at 7 in. and a 14 in. strip would include both a set of top and bottom straight bars and a truss-type bar. Because the truss-type bar is located at the top part of the deck for 75 percent of the width of the deck, the truss bar was treated as another straight bar at the top of the deck in order to make the moment diagrams more continuous. The stress in the concrete deck was calculated using the flexure stress only at the top and bottom of the deck, assuming an uncracked section. The moments were then calculated about the centroid of the section as seen in Figure 6-31.

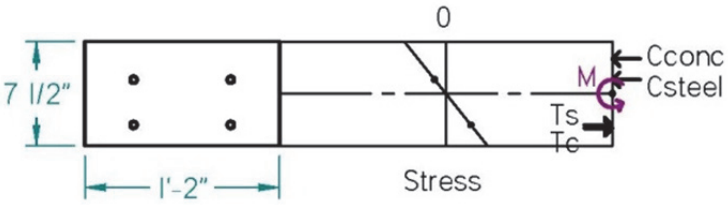

Figure 6-31: Moments

The results from Test 1 and Test 4 are shown here since they include both a single and double point load test. The moment diagrams for all of the tests can be found in Appendix C.

6.5.3.1. Test 1 Moments: Midspan Service Single Point Load on East Side

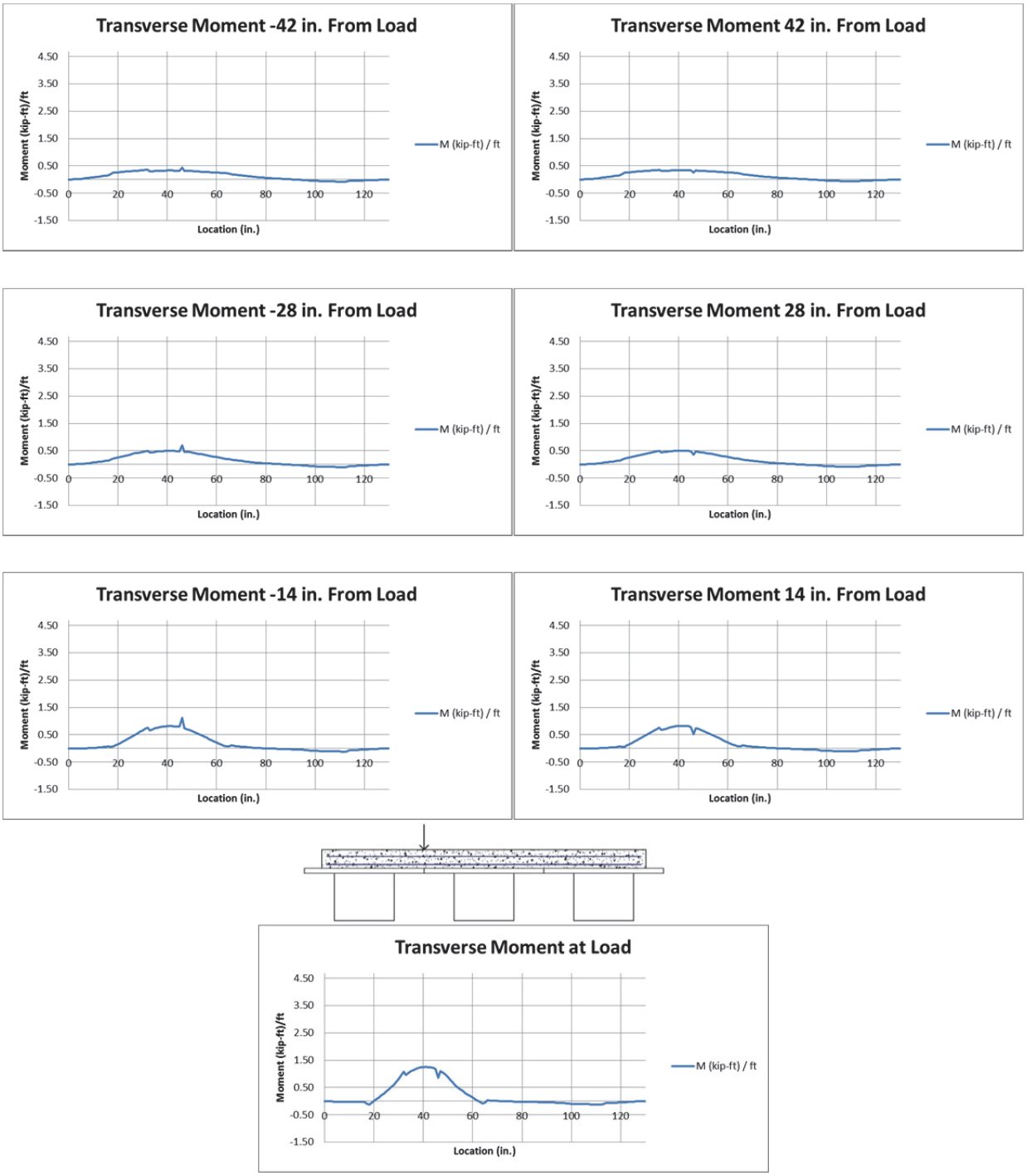

Figure 6-32: Test 1 Transverse Moments at Varying Distances Away from the Load

6.5.3.2. *Test 4 Moments: Midspan Strength Two Point Loads*

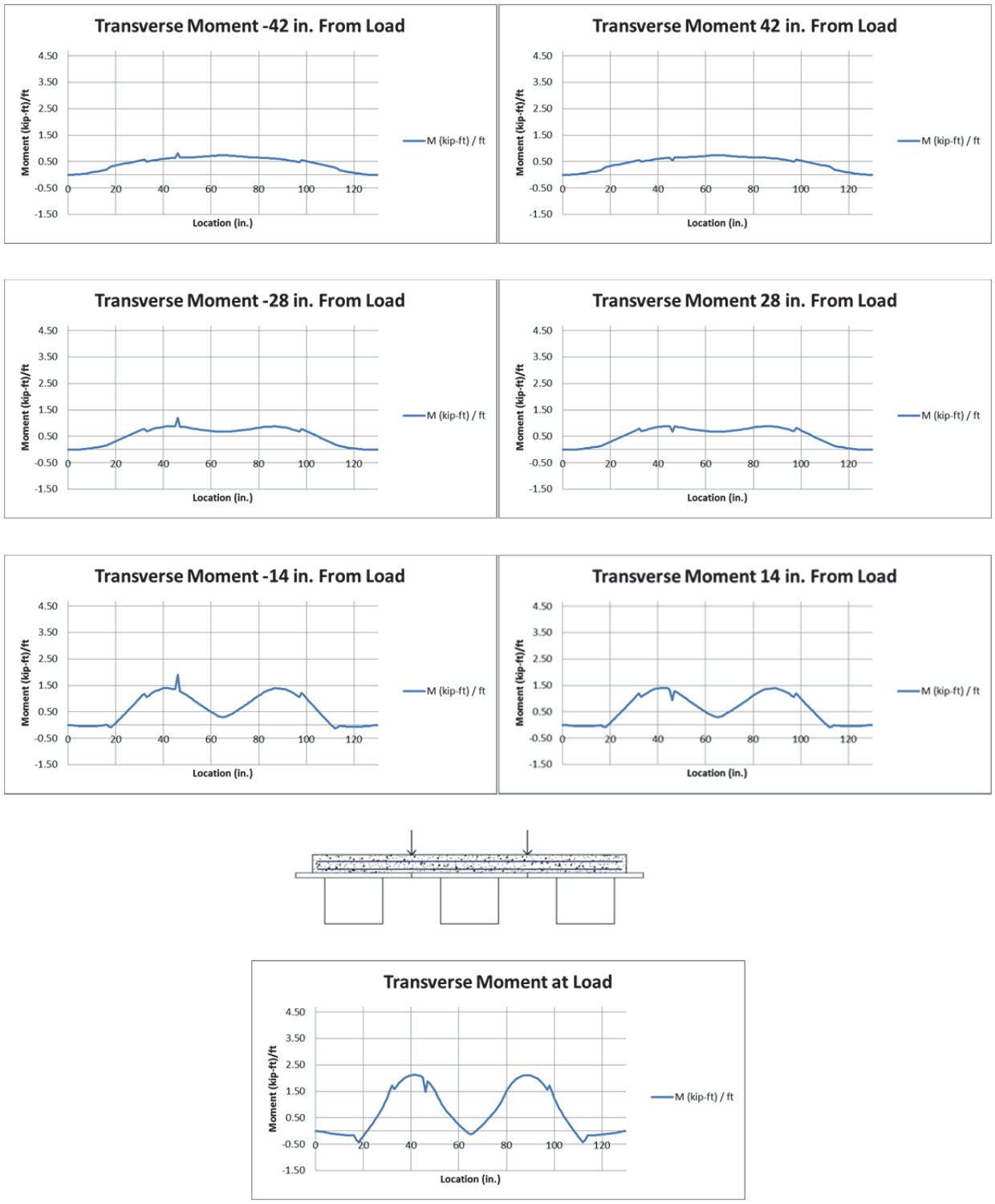

Figure 6-33: Test 4 Transverse Moments at Varying Distances Away from the Load

The maximum positive moment from all of the tests is 2.12 $\frac{kip-ft}{ft}$, and the maximum negative moment over the center beam is -0.17 $\frac{kip-ft}{ft}$. These moments are smaller than the ones obtained using AASHTO's Table A4-1, which provide a maximum design positive moment for beams spaced at 4 ft of 4.68 $\frac{kip-ft}{ft}$ and a maximum design negative moment, using a critical location for negative moment at the face of the beam per AASHTO Article 4.6.2.1.6, of -1.25 $\frac{kip-ft}{ft}$.

6.6 Conclusions from Abaqus Model

The deflections graphs along the width of the bridge all showed one smooth gentle curve, indicating that the bridge behaves more like a stiffened plate than a beam on rigid supports. The strip method uses the assumption that the girders behave like rigid supports, therefore, this method may not be suitable for bridges using flexible beams such as HCB's. The average effective width was found to be 72 in. (6 ft) for positive moment and 173 in. (14 ft) for negative moment. The largest negative moment over the center beam was very small, with a maximum negative moment of -0.17 $\frac{kip-ft}{ft}$.

CHAPTER 7: SUMMARY & RECOMMENDATIONS

7.1 Summary

During laboratory testing, the maximum measured strain in the transverse reinforcement was 597 με which is well below yielding strain of the reinforcing bars. However, the concrete cracking strain from the cylinder tests was determined to be 112 με, so there may be undetected microcracks. Based on these results, the Tide Mill Bridge deck design seems adequate.

AASHTO's traditional design method using the strip method is based upon the assumption that the bridge deck behaves like a beam on rigid supports. The observed behavior of the bridge deck during testing and from the Abaqus model, however, showed that across the width of the bridge, the deck behaves more like a stiff plate than a beam on rigid supports with the global effect shown in Figure 2-9 in Section 2.4.2 being dominant in the behavior of the deck. Therefore, the strip design method does not seem suitable for bridges using flexible beams such as HCB's. AASHTO's other method of bridge deck design, the empirical method, also cannot be used for a bridge with HCB's because it violates the requirement that the supporting components must be made of concrete or steel.

With both methods being invalidated for use in the deck design of bridges with HCB's, another approach was needed. An Abaqus finite-element model has been developed for the laboratory bridge that matches the test data quite well, and it can be used to predict the behavior of the bridge.

7.2 Design Recommendations

7.2.1 Truss-Type Bars

Truss-type bars are used because they provide reinforcement near the top of the deck over the girders to resist the negative bending moment, and reinforcement near the bottom of the deck between the beams to resist the positive bending moment. A disadvantage of using truss-type bars is that they can be difficult to manufacture and make the placement of the deck reinforcement more challenging. This can take more time and cost more money.

From the experimental testing done during this research project, it was found that the strains measured in the truss bars for each test at the truss bar location closest to the applied load were almost all in tension, and when a compression strain was observed, it was quite small. In order to warrant the use of truss bars, a change from positive to negative moment regions across the width of the bridge that would be expected, but this was not observed. Therefore, truss-type bars are not as appropriate for use in decks with flexible girders such as HCB's.

7.2.2 Transverse Reinforcement Design

Near the supports, the beams can be considered stiffer because their deformations are restricted and therefore the assumption of the beams being rigid supports is feasible. An example of this behavior is shown in Figure 7-1 on the left. Therefore, in the areas close to supports, it is recommended to follow the current AASHTO standards for design. However, near the center of the bridge, the beams are flexible and the bridge behaves more like a stiffened plate with more global deflection as shown in Figure 7-1 on the right. Because the results from both the quarter point tests and midspan tests demonstrated more global behavior, the flexible zone may be taken as the area of the bridge deck between the two quarter points.

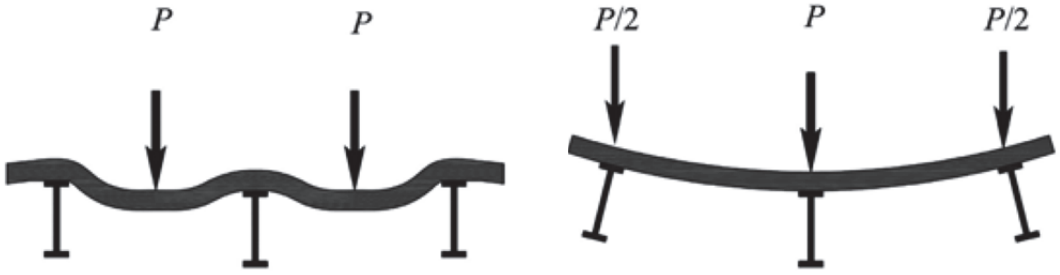

Figure 7-1: Deformation (Tangwongchai, Anwar, & Chucheepsakul, 2011) Used under fair use, 2013

In the flexible zone, the strip method is recommended for determining the live load design moments with some modifications. A modified strip method approach is recommended despite the fact that it uses the assumption that the beams act as rigid supports because the strip method is widely used by and is familiar to engineers for the design of bridge decks. The strip widths for the flexible zone of the Tide Mill Bridge were determined to be 72 in. (6 ft) for positive moment and 173 in. (14.4 ft) for negative moment when taking into account the flexibility of the HCB's. These strip widths are larger than the strip width values obtained when using AASHTO, which are 4.4 ft for positive moment and 5 ft for negative moment. The design section recommended is

at the face of the supporting girder, which was chosen from the closest girder type to HCB's found in AASHTO Article 4.6.2.1.6.

Another modification to traditional deck design is that when determining the design moment of a bridge deck supported by HCB's, the self-weight of the deck may be neglected for the entire deck. The reason for this is that the flanges of the HCB's support the weight of the bridge deck while it is being cast and continue to support the weight of the deck throughout the life of the bridge because they remain in place and are made of a corrosion resistant GFRP material. Therefore, the deck never has to support its own weight.

Table 7-1: Compare Tide Mill Bridge Designs

Original Tide Mill Bridge Design using Traditional AASHTO Method	**New Tide Mill Bridge Design in the Flexible Zone**
Strip Method used to determine live load moments	Strip Method used to determine live load moments
Positive strip width determined from AASHTO: 4.4 ft	Positive strip width determined from Abaqus model: 6 ft
Negative strip width determined from AASHTO: 5 ft	Negative strip width determined from Abaqus model: 14.4 ft
Design section at ¼ of flange	Design section at beam face
Truss-type bars used	No truss-type bars used
Self-weight included in design	Self-weight of deck neglected for entire bridge deck design

A summary of the differences between the original Tide Mill Bridge design method and the recommended design method is shown in Table 7-1. Using the above recommendations and strip widths, the required reinforcement for the Tide Mill Bridge in the flexible zone was calculated in Appendix F. The required reinforcement for the Tide Mill Bridge would be straight No. 4 bars spaced at 7 in. for the bottom mat of reinforcement and straight No. 4 bars spaced at 11 in. for the top mat of reinforcement. These spacings satisfy the minimum requirements for crack control and temperature and shrinkage. The original design required No. 5 bars top and

bottom spaced at 14 in. with truss-type bars placed in between the rows of top and bottom straight bars also spaced at 14 in. Therefore, the design using the new strip widths requires 30 percent less steel reinforcement. The reduction in transverse reinforcement not only saves money in materials and placement, it also increases the longevity of a bridge deck because the reduced steel area is less likely to cause popouts and spalling of the deck's wearing surface. (Fang, J. Worley, Burns, & Klingner, 1990) With less steel in the top mat of reinforcement, there are also fewer locations in the deck susceptible to chlorine attacks. (Cao, 1996)

7.3 Recommendations for Future Work

Further study using finite-element models is recommended to determine simplified equations for designing bridges using HCB's that take into account the flexibility of the beams. Because the testing bridge only had three HCB's due to restrictions on space in the laboratory, it is recommended that the actual Tide Mill Bridge with its eight HCB's be monitored in the field. A study to see if the maximum negative moment in an eight girder system is higher than the three girder system is also recommended. A new Abaqus model should be created with eight HCB's to compare to the completed Tide Mill Bridge. Exploring new and more efficient ways to mesh the deck in Abaqus is recommended in order to make calculations easier.

REFERENCES

(AASHTO), American Association of State Highway and Transportation Officials. (2012). *AASHTO LRFD Bridge Design Specifications.*

(TXDOT), Texas Department of Transportation. (2010, 07). *Slab Design Example*. Retrieved from http://ftp.dot.state.tx.us/pub/txdot-info/library/pubs/bus/bridge/slab_example.pdf

(VDOT), Virginia Department of Transportation. (2011). Tide Mill Interim Plans.

Ahsan, S. (2012). *Evaluation of Hybrid-Composite Beam for Use in Tide Mill Bridge.* Blacksburg: Virginia Polytechnic Institute and State University.

American Concrete Institute (ACI). (2011). *Building Code Requirements for Structural Concrete ACI 318-11.*

Barker, R. M., & Puckett, J. A. (2007). *Design of Highway Bridges* (2nd ed.). Hoboken, New Jersey: John Wiley & Sons, Inc.

Bettigole, N. H., & Robinson, R. (1997). *Bridge Decks: Design, Construction, Rehabilitation, Replacement.* ASCE.

Cao, L. (1996). Behavior of RC Bridge Decks With Flexible Girders. *Journal of Structural Engineering, 122*(1), 11-19. Retrieved 12 24, 2012

Fang, I. K., J. Worley, Burns, N. H., & Klingner, R. E. (1990). Behavior of Isotropic R/C Bridge Decks on Steel Girders. *Journal of Structural Engineering, 116*(3), 659-678.

Gupta, A., & Dhir, S. (n.d.). *Grillage Method of Analysis for Designing a Beam and Slab Type Deck*. Retrieved 01 16, 2013, from Internet Knowledge Base: http://paniit.iitd.ac.in/webiit/bridge/Superexp/staadfra.htm

Hambly, E. C. (1991). *Bridge Deck Behavior* (2 ed.). New York: E & FN SPON.

Hillman, J. R. (n.d.). *Product Information*. Retrieved 11 11, 2012, from http://www.hcbridge.com

Marx, H. J., Khachaturian, N., & Gamble, W. L. (1986). *Development of Design Criteria for Simply Supported Skew Slab-and-Girder Bridge.* Urbana: University of Illinois at Urbana-Champaign.

Menn, C. (1990). *Prestressed Concrete Bridges.* Boston.

Mondorf, P. E. (2006). *Concrete Bridges.* New York: Taylor & Francis.

Newmark, N. M. (1938). *A Distribution Procedure for the Analysis of Slabs Continuous Over Flexible Beams.* Urbana: University of Illinois.

Ng, P. L., Lam, J., & Kwan, A. (2010). Tension stiffening in concrete beams. Part 1: FE analysis. *Proceedings of the Institution of Civil Engineers. Structures and Buildings, 163*(1), 19-18.

Nilson, A. H., Darwin, D., & Dolan, C. W. (2004). *Design of Concrete Structures* (13th ed.). New York: McGraw-Hill.

O'Brien, E. J., & Keogh, D. L. (1999). *Bridge Deck Analysis.* New York: Routledge.

Park, R., & Gamble, W. L. (2000). *Reinforced Concrete Slabs.* New York: John Wiley & Sons, Inc.

PCI. (n.d.). *Curved and Skewed Bridges.* Retrieved 11 11, 2012, from PCI Bridge Design Manual: http://www.pci.org/pdf/find/knowledge_bank/active/MNL-133-97_ch12.pdf

POPSCI. (2011). *Knickerbocker Bridge.* Retrieved December 14, 2012, from Popular Science: http://www.popsci.com/bown/2011/product/knickerbocker-bridge

Tangwongchai, S., Anwar, N., & Chucheepsakul, S. (2011). Flexural responses of concrete slab over flexible girders through FEA-based parametric evaluation. *KSCE Journal of Civil Engineering, 15*(6), 1057 - 1065.

Tonias, D. E., & Zhao, J. J. (2007). *Bridge Engineering* (Second ed.). New York: McGraw-Hill Companies.

VDOT. (n.d.). *Concrete Deck Slab.* Retrieved 11 11, 2012, from VDOT Bridge Manual Volume V - Part 2 Chaper 10: http://www.extranet.vdot.state.va.us/locdes/electronic%20pubs/Bridge%20Manuals/VolumeV-Part2/Chapter10.pdf

Westergaard, H. M. (1930, March). Computation of Stresses in Bridge Slabs Due to Wheel Loads. *Public Roads, 11*(1).

APPENDIX A: VDOT CONCRETE DECK SLAB DESIGN

VDOT Chapter 10 Volume V Part 2 Sheets 1 - 12: Concrete Deck Slab Design

Used with permission of VDOT (2013)

General:

A. Concrete deck slabs on bridges designed in accordance with AASHTO LRFD for HL-93 loading. Design shall be in accordance with LRFD Sections 3, 4, 5, 9, 13, and VDOT Modifications. The empirical design method shall not be used.

Main reinforcement may be designed by use of the tables on File No. 10.01-4. This table is based on the requirements of LRFD Design Specifications and a ratio of $A'_s/A_s = 0.5$. A set of example calculations is provided for a slab design and cantilever design in File Nos. 10.01-6 thru 10.01-9.

Distribution steel is to be designed in accordance with LRFD Article 9.7.3.2 and office modifications. A set of example calculations is provided in File Nos. 10.01-10 thru 10.01-11.

B. Unless circumstances require other thicknesses, the following shall be used for deck slabs supported by stringers, according to the c-c stringer spacings shown:

Minimum Slab Thickness	Spacing of Stringers	
	Steel	Concrete
7 1/2"	6'-0" or less	6'-9" or less
8"	over 6'-0" to 7'-0"	over 6'-9" to 7'-9"
8 1/2"	over 7'-0" to 10'-0"	over 7'-9" to 10'-0"
9"	over 10'-0" to 12'-0"	over 10'-0" to 12'-0"

C. Main reinforcing bars shall be detailed as follows for the usual simple spans (long spans, non-parallel beams/girders, etc. may require deviation from this) LRFD Article 9.7.1.3:

1. For skew angles from 0° to 20°, main reinforcement shall be placed parallel to ends of slab(s) with truss-type slab bars alternating with straight bars top and bottom.

2. For skews over 20°, all main reinforcement shall be placed perpendicular to centerline of bridge. Main reinforcement in the end sections shall be detailed as straight bars top and bottom. Section of slab requiring full-length main bars shall be detailed with truss-type bars alternating with straight bars top and bottom. Consideration should be given to reinforcing the ends of the slab by placing additional slab bars in the vicinity of and parallel to end diaphragms.

3. Main reinforcement bars shall be #5, distribution bars shall be #4, and reinforcing bars in negative moment regions over piers shall typically not be greater than a #6 bar.

4. Longitudinal bars may be detailed using a series of 40' bars with one bar at the end to make up the remaining length.

D. For deck slabs cast in a single pour wider than 60' to 80', a longitudinal or construction joint should be considered. For deck slabs cast in a single pour wider then 80', a longitudinal joint shall be provided.

E. Deck reinforcement shall typically be detailed as straight bars without hooks unless there is insufficient length for development (top bars only).

CONCRETE DECK SLAB DECK SLAB DESIGN – LRFD GENERAL	VOL. V - PART 2 DATE: 01Jul2011 SHEET 1 of 12 FILE NO. 10.01-1

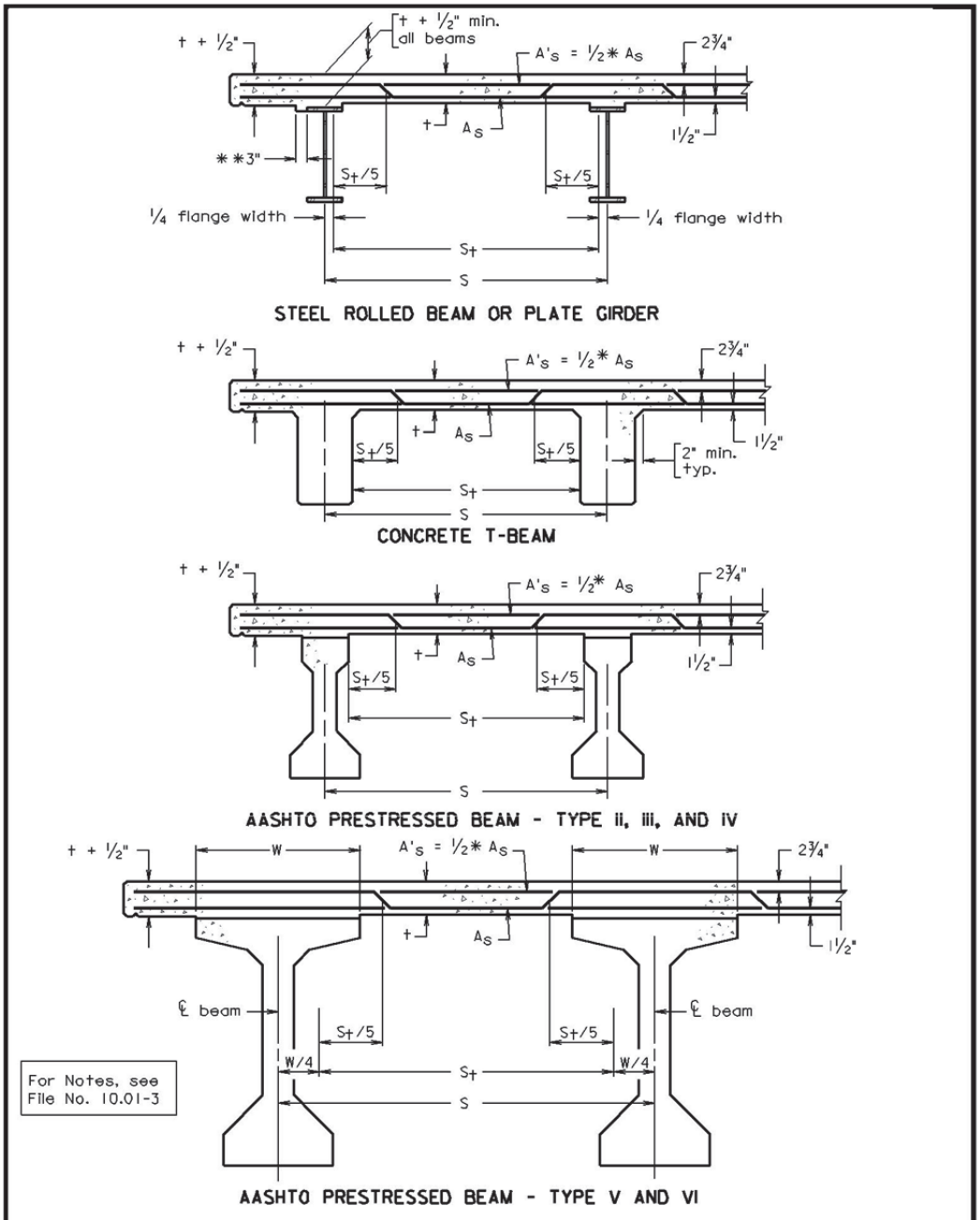

CONCRETE DECK SLAB
DECK SLAB DESIGN – LRFD
PART TRANSVERSE SECTIONS

VOL. V - PART 2
DATE: 17Dec2008
SHEET 2 of 12
FILE NO. 10.01-2

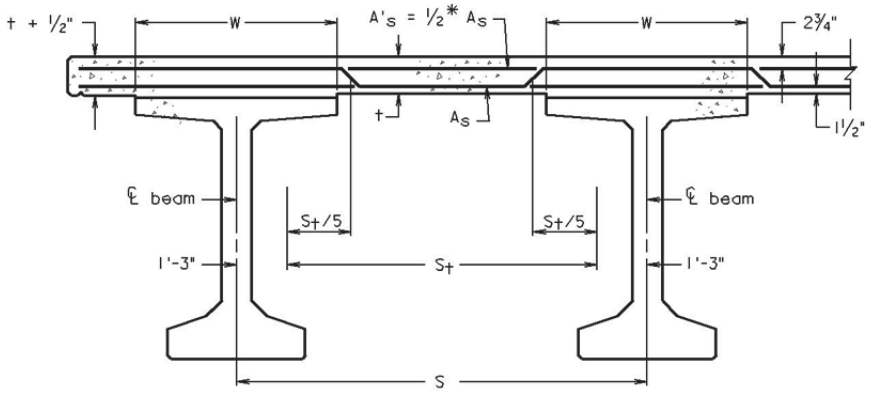

PRESTRESSED BULB-T

Notes:

S = span Length to be used in Deck Design Table File No. 10.01-4.

S_t = span length to determine geometry of truss bar.

t Includes 1/2" monolithic wearing surface

Dimensions are to centers of bars.

* Normally - see Note C, File No. 10.01-1, for other requirements.

** Outside of fascia of steel beams/girders and at outside of steel beams/girders each side of an open joint.

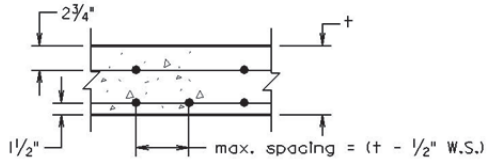

LONGITUDINAL SECTION TAKEN BETWEEN STRINGERS

Longitudinal bars not shown for clarity

CONCRETE DECK SLAB DECK SLAB DESIGN – LRFD PART TRANSVERSE SECTIONS	VOL. V - PART 2 DATE: 17Dec2008 SHEET 3 of 12 FILE NO. 10.01-3

DECK DESIGN TABLE

Span Length (S) (ft.)	Reinforcement Steel Required					
	Steel Beams/Girders			Prestressed Conc. Beams		
	Deck Thickness (t) (in.)	Area ($in.^2$)	Bar Spacing	Deck Thickness (t) (in.)	Area ($in.^2$)	Bar Spacing
4.00	7 1/2"	0.53	#5 @ 7" *	7 1/2"	0.53	#5 @ 7" *
4.25		0.53	#5 @ 7" *		0.53	#5 @ 7" *
4.50		0.53	#5 @ 7" *		0.53	#5 @ 7" *
4.75		0.53	#5 @ 7" *		0.53	#5 @ 7" *
5.00		0.53	#5 @ 7" *		0.53	#5 @ 7" *
5.25		0.53	#5 @ 7" *		0.53	#5 @ 7" *
5.50		0.53	#5 @ 7" *		0.53	#5 @ 7" *
5.75		0.53	#5 @ 7" *		0.53	# 5 @ 7" *
6.00		0.53	#5 @ 7" *		0.53	#5 @ 7" *
6.25	8"	0.50	#5 @ 7 1/2" *		0.53	#5 @ 7" *
6.50		0.50	#5 @ 7 1/2" *		0.53	#5 @ 7" *
6.75		0.50	#5 @ 7 1/2" *		0.53	#5 @ 7" *
7.00		0.50	#5 @ 7 1/2" *	8"	0.50	#5 @ 7 1/2" *
7.25	8 1/2"	0.47	#5 @ 8" *		0.50	#5 @ 7 1/2" *
7.50		0.47	# 5@ 8" *		0.50	#5 @ 7 1/2" *
7.75		0.47	#5 @ 8" *		0.50	#5 @ 7 1/2" *
8.00		0.47	#5 @ 8"	8 1/2"	0.47	#5 @ 8" *
8.25		0.47	#5 @ 8"		0.47	#5 @ 8" *
8.50		0.47	#5 @ 8"		0.47	#5 @ 8" *
8.75		0.50	#5 @ 7 1/2"		0.47	#5 @ 8" *
9.00		0.50	#5 @ 7 1/2"		0.47	#5 @ 8" *
9.25		0.50	#5 @ 7 1/2"		0.47	#5 @ 8"
9.50		0.53	#5 @ 7"		0.47	#5 @ 8"
9.75		0.57	#5 @ 6 1/2"		0.50	#5 @ 7 1/2"
10.00		0.62	#5 @ 6"		0.50	#5 @ 7 1/2"
10.25	9"	0.57	#5 @ 6 1/2"	9"	0.47	#5 @ 8"
10.50		0.62	#5 @ 6"		0.50	#5 @ 7 1/2"
10.75		0.62	# 5 @ 6"		0.50	#5 @ 7 1/2"
11.00		0.68	#5 @ 5 1/2"		0.53	#5 @ 7"
11.25		0.68	#5 @ 5 1/2"		0.53	#5 @ 7"
11.50		0.68	#5 @ 5 1/2"		0.53	#5 @ 7"
11.75		0.74	#5 @ 5"		0.57	#5 @ 6 1/2"
12.00		0.74	#5 @ 5"		0.57	# 5 @ 6 1/2"

Design assumptions:

1. S (Span Length) = center-to-center stringer/girder spacing.
2. Values given in the design table are based on the equivalent strip method. The crack control criterion has been neglected in the design.
3. Design is applicable for decks supported on at least three stringers and having a width of not less than 14 feet between centerlines of exterior stringers.
4. For steel beams/girders, a minimum top flange width of 12 inches is assumed.

* Design controlled by maximum spacing requirement per VDOT Modifications to LRFD.

CANTILEVER DESIGN

The cantilever deck slab shall be designed/detailed with additional #5 bars between the transverse bars in the top layer. The bars shall extend past the exterior beam/girder with the development length extending past the contraflexure point in the slab. No yield-line analysis will be required if all four of the following requirements are met:

beam/girder spacing is less than or equal to 12'-0"

cantilever length is less than or equal to 0.3 x beam/girder spacing

railing/parapet type (if any on the cantilever) is an approved VDOT crash tested system.

No additional loading shall be added to cantilever except for fencing as shown in BPF-series standards. i.e. soundwall, utilities, etc.

For all other cases, the designer will be required to adhere to the yield-line analysis as noted in the LRFD specifications.

Required:
Deck reinforcement for a steel plate girder.

Design Specifications:
AASHTO LRFD Bridge Design Specifications with current Interims and VDOT Modifications.

Data Provided:

Girder spacing	= 10 feet
t	= 8.5 inches
f_c'	= 4 ksi
f_s	= 60 ksi
E_{st}	= 29,000 ksi
Future W.S.	= 15 psf
Min. top flange	= 12 inches

Dead Loads:

$$M = \frac{(w)(S)^2}{10}$$

$$w_{deck} = \frac{(8.5")}{12} \times 0.150 \text{ kcf} = 0.106 \text{ klf}$$

$$w_{w.s.} = 1 \text{ foot} \times 0.015 \text{ ksf} = 0.015 \text{ klf}$$

$$M_{deck} = \frac{(0.106)(10.0)^2}{10} = 1.06 \text{ k-ft/ft}$$

$$M_{w.s.} = \frac{(0.015)(10.0)^2}{10} = 0.15 \text{ k-ft/ft}$$

(Assume these moments act for both positive and negative dead load moments.)

Live Loads:

Use Design Table A4-1 LRFD Specifications to compute moments based on interpolation.
(The table has been reproduced on File No. 10.01-12)

Positive Moment:

S = 10 feet , ∴ Positive moment = 6.89 k-ft/ft

Negative Moment:

Distance from ℄ girder to design section = flange width/4 = 12/4 = 3 inches

∴ Negative moment = 6.99 k-ft/ft

Factored Moments:

Factored moment $= \sum \eta_i \gamma_i M_i$

Strength I, factored moment = 1.25 (DC) + 1.5 (DW) + 1.75 (LL+IM)

η_i = Load modifier = 1.0
γ_i = Load factor = 1.0
DC = Dead load of structural components and nonstructural attachments
DW = Dead load of wearing surface and utilities
LL+IM = Vehicular live load and vehicular dynamic load allowance

Maximum factored (+) moment:

M(+) = 1.25(1.06) + 1.5(0.15) + 1.75(6.89) = 13.6 k-ft/ft

Maximum factored (-) moment:

M(-) = 1.25(1.06) + 1.5(0.15) + 1.75(6.99) = 13.8 k-ft/ft

Design for negative flexure in deck:

Design as singly reinforced section and ignore compression steel.

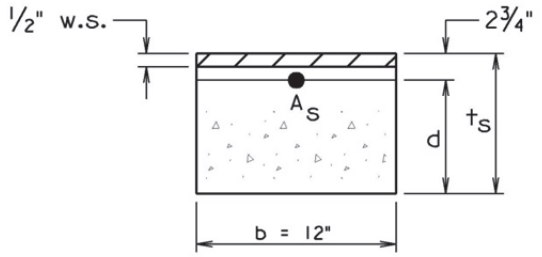

$M_n = A_s f_s (d - a/2)$
$a = (A_s f_s) / (0.85 f_c' b)$

Try #5 with 6 inch spacing

A_s = 0.62 in^2/ft.
b = 12 inches
d = t – cover of top bar = 8.5 – 2.75 = 5.75 inches

$$a = \frac{(0.62 \times 60)}{0.85 \times 4 \times 12} = 0.91 \text{ in.}$$

Design for negative flexure in deck (cont'd):

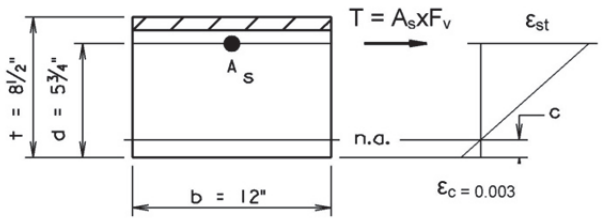

$c = a/\beta_1$

$\beta_1 = 0.85$ for $f'_c = 4$ ksi

$c = 0.91/0.85 = 1.07$ in.

$c/d = 1.07/5.75 = 0.186 < 0.6 \therefore$ OK, strain compatibility check not required, but provided below as an example.

$\varepsilon_{st} = \varepsilon_c (d-c)/c$

$= 0.003 (5.75-1.07)/1.07 = 0.01312$ in/in

$E_{st} \times \varepsilon_{st} = 29{,}000 \times 0.01312 = 380$ ksi > 60 ksi

$M_n = 0.62 \times 60 (5.75 - 0.91/2)/12 = 16.4$ k-ft/ft

$\Phi M_n = 0.90 \times 16.4 = 14.8$ k-ft/ft > 13.8 k-ft/ft $\therefore$ OK

$\therefore$ #5 @ 6" spacing is OK.

Design for positive flexure in deck:

Design as singly reinforced section and ignore compression steel.

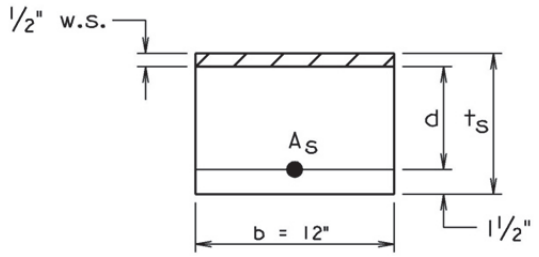

$M_n = A_s f_s (d - a/2)$
$a = (A_s f_s) / (0.85 f_c' b)$

Try #5 with 6 inch spacing

$A_s = 0.62$ in^2/ft.
b = 12 inches
d = t – wearing surface - cover of bottom bar = 8.5 – 0.5 – 1.5 = 6.5 inches

$$a = \frac{(0.62 \times 60)}{0.85 \times 4 \times 12} = 0.91 \text{ in.}$$

$c = a/\beta_1$

$\beta_1 = 0.85$ for $f'_c = 4$ ksi

$c = 0.91/0.85 = 1.07$ in.

c/d = 1.07/5.75 = 0.186 < 0.6 ∴ OK, Strain compatibility check not required.

$M_n = 0.62 \times 60 (6.50 - 0.91/2)/12 = 18.7$ k-ft/ft

$\Phi M_n = 0.90 \times 18.7 = 16.8$ k-ft/ft > 13.8 k-ft/ft ∴ OK

∴ #5 @ 6" spacing is OK.

After the spacing is determined for negative and positive flexure, the smaller spacing shall be used for the transverse reinforcement.

Design distribution reinforcement:

For effective length, use S = 10'-0". Neglect the small deduction in span for the thickness of the web in steel beams. For prestressed beams, subtract the thickness of the web to determine the effective length.

Compute percentage of distribution reinforcement required:

% longitudinal steel required = $220/\sqrt{S} = 220/\sqrt{10} = 70\ \% > 67\ \%$ ∴ Use 67 %

Steel for long. reinforcement = 0.67 x 0.62 = 0.415 in^2/ft

Total long. reinf. in bottom of truss = 0.6 x (10 – 0.5) x 0.415 = 2.37 sq. in.

bars = 2.37 / 0.2 = 12 # 4 bars

Spacing = 0.6 x 9.5 / (12-1) = 0.518 ft. = 6.21"

Spacing everywhere else = 2 x 6.21" = 12.42" or 12 $^1/_2$"

The following PART SECTION shows the typical steel required:

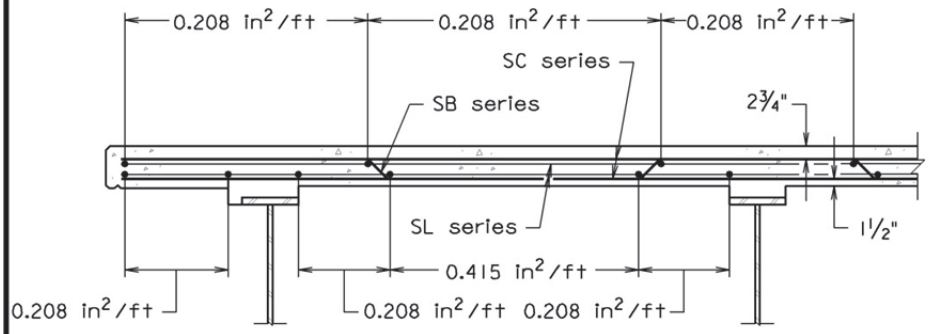

PART SECTION - STEEL REQUIRED

The following typical PART SECTION is shown in the contract plans:

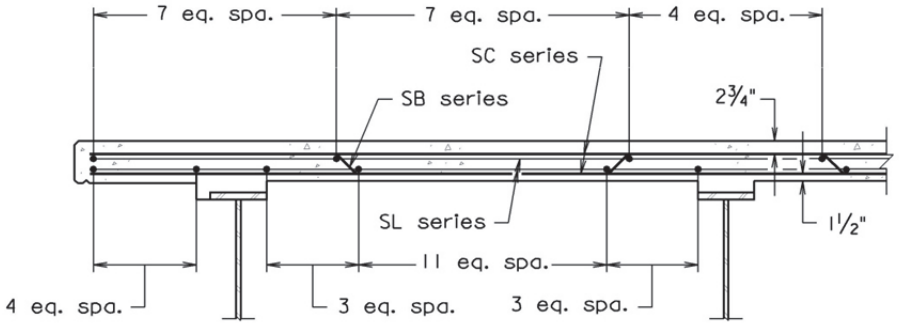

PART SECTION

(Part Section for beams/girders with truss bar shown. Reinforcement for slabs without truss bars similar.)

MAXIMUM LIVE LOAD MOMENT TABLE

S (ft.)	Positive Moment (k-ft/ft)	Negative Moment (k-ft/ft) Distance from centerline stringer/girder to design section						
		0 in.	3 in.	6 in.	9 in.	12 in.	18 in.	24 in.
4.00	4.68	2.68	2.07	1.74	1.60	1.50	1.34	1.25
4.25	4.66	2.73	2.25	1.95	1.74	1.57	1.33	1.20
4.50	4.63	3.00	2.58	2.19	1.90	1.65	1.32	1.18
4.75	4.64	3.38	2.90	2.43	2.07	1.74	1.29	1.20
5.00	4.65	3.74	3.20	2.66	2.24	1.83	1.26	1.12
5.25	4.67	4.06	3.47	2.89	2.41	1.95	1.28	0.98
5.50	4.71	4.36	3.73	3.11	2.58	2.07	1.30	0.99
5.75	4.77	4.63	3.97	3.31	2.73	2.19	1.32	1.02
6.00	4.83	4.88	4.19	3.50	2.88	2.31	1.39	1.07
6.25	4.91	5.10	4.39	3.68	3.02	2.42	1.45	1.13
6.50	5.00	5.31	4.57	3.84	3.15	2.53	1.50	1.20
6.75	5.10	5.50	4.74	3.99	3.27	2.64	1.58	1.28
7.00	5.21	5.98	5.17	4.36	3.56	2.84	1.63	1.37
7.25	5.32	6.13	5.31	4.49	3.68	2.96	1.65	1.51
7.50	5.44	6.26	5.43	4.61	3.78	3.15	1.88	1.72
7.75	5.56	6.38	5.54	4.71	3.88	3.30	2.21	1.94
8.00	5.69	6.48	5.65	4.81	3.98	3.43	2.49	2.16
8.25	5.83	6.58	5.74	4.90	4.06	3.53	2.74	2.37
8.50	5.99	6.66	5.82	4.98	4.14	3.61	2.96	2.58
8.75	6.14	6.74	5.90	5.06	4.22	3.67	3.15	2.79
9.00	6.29	6.81	5.97	5.13	4.28	3.71	3.31	3.00
9.25	6.44	6.87	6.03	5.19	4.40	3.82	3.47	3.20
9.50	6.59	7.15	6.31	5.46	4.66	4.04	3.68	3.39
9.75	6.74	7.51	6.65	5.80	4.94	4.21	3.89	3.58
10.00	6.89	7.85	6.99	6.13	5.26	4.41	4.09	3.77
10.25	7.03	8.19	7.32	6.45	5.58	4.71	4.29	3.96
10.50	7.17	8.52	7.64	6.77	5.89	5.02	4.48	4.15
10.75	7.32	8.83	7.95	7.08	6.20	5.32	4.68	4.34
11.00	7.46	9.14	8.26	7.38	6.50	5.62	4.86	4.52
11.25	7.60	9.44	8.55	7.67	6.79	5.91	5.04	4.70
11.50	7.74	9.72	8.84	7.96	7.07	6.19	5.22	4.87
11.75	7.88	10.01	9.12	8.24	7.36	6.47	5.40	5.05
12.00	8.01	10.28	9.40	8.51	7.63	6.74	5.56	5.21

Data taken from AASHTO *LRFD Bridge Design Specifications 4th edition*, 2007 and 2008 Interim Revisions, Section 4, Appendix A4, Table A4-1 "Maximum Live Load Moments Per Unit Width, k-ft/ft".

APPENDIX B: BAR BENDING DIAGRAMS

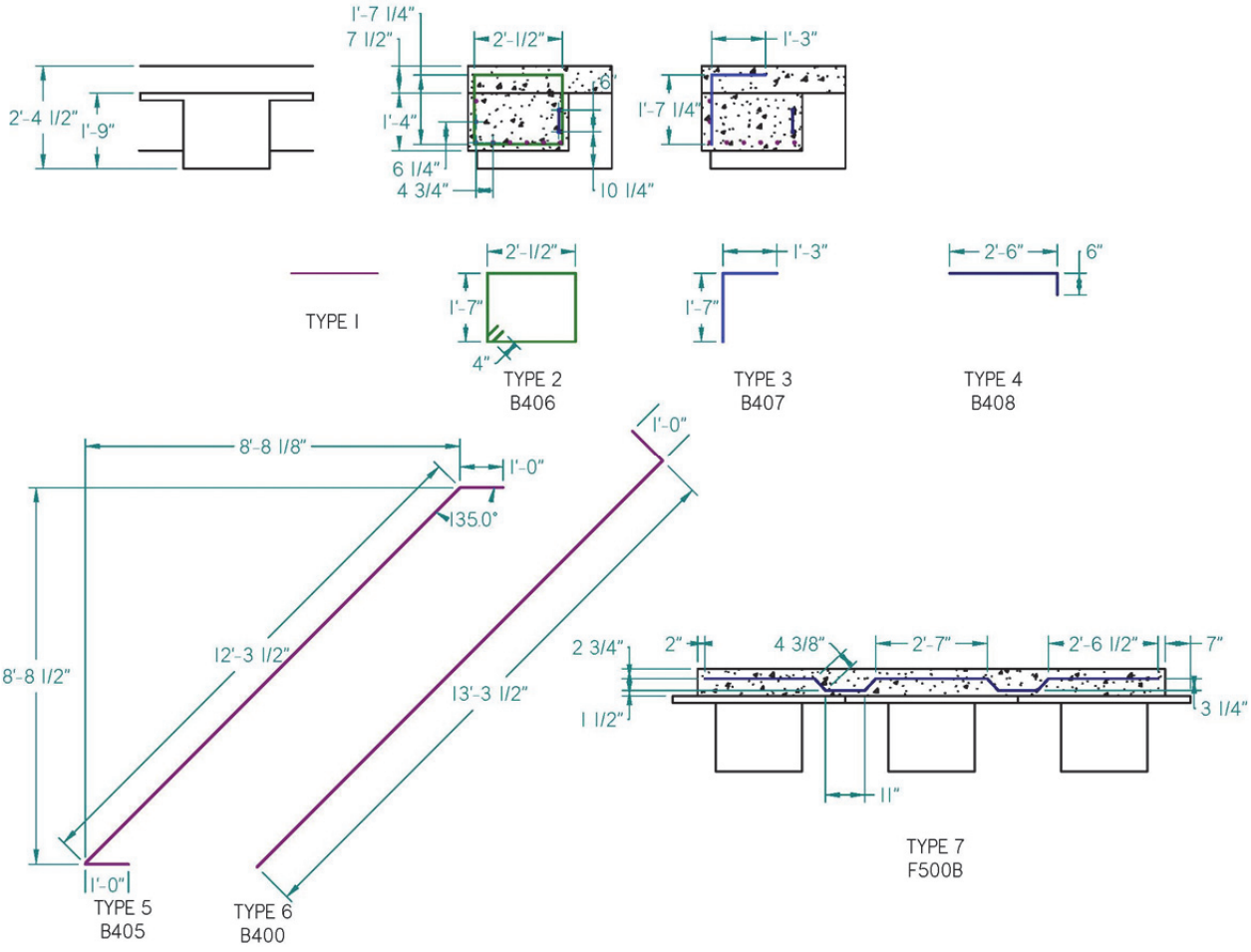

APPENDIX C: MOMENTS FROM ABAQUS

Test 1 Moments: Midspan Service Single Point Load on East Side

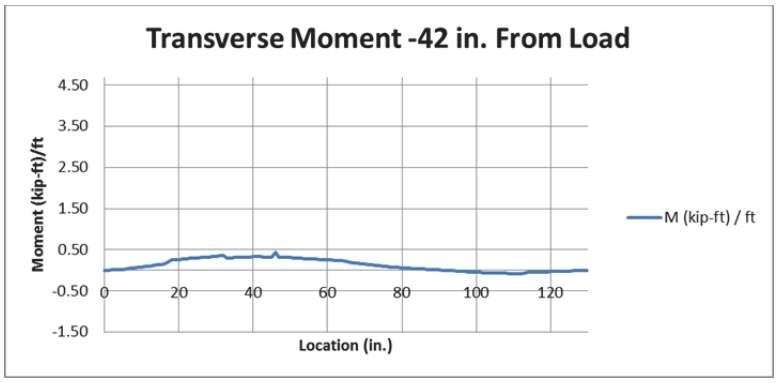

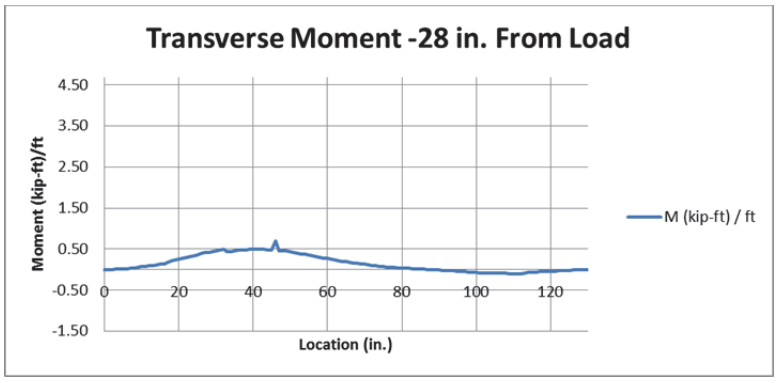

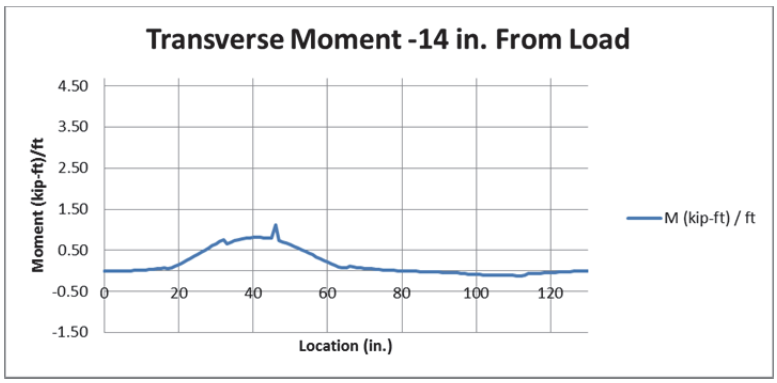

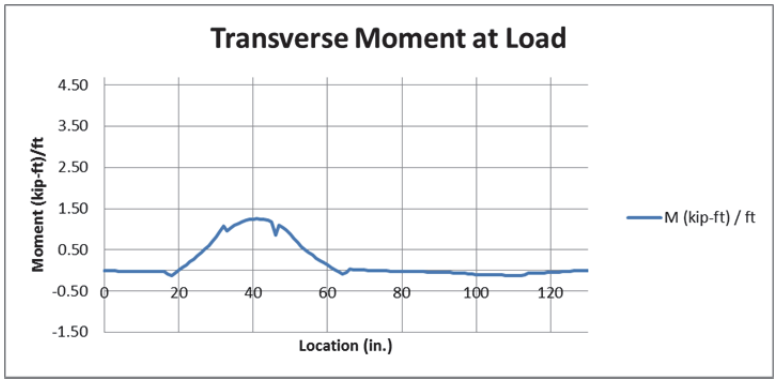
Transverse Moment at Load
Moment (kip-ft)/ft
4.50
3.50
2.50
1.50
0.50
-0.50
-1.50
0
20
40
60
80
100
120
Location (in.)
M (kip-ft) / ft

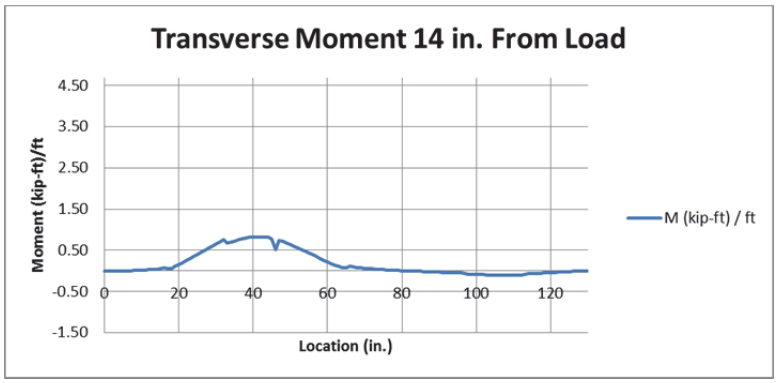
Transverse Moment 14 in. From Load
Moment (kip-ft)/ft
4.50
3.50
2.50
1.50
0.50
-0.50
-1.50
0
20
40
60
80
100
120
Location (in.)
M (kip-ft) / ft

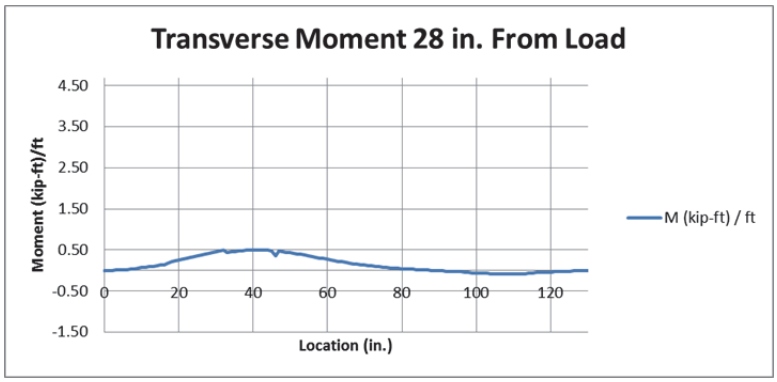
Transverse Moment 28 in. From Load
Moment (kip-ft)/ft
4.50
3.50
2.50
1.50
0.50
-0.50
-1.50
0
20
40
60
80
100
120
Location (in.)
M (kip-ft) / ft

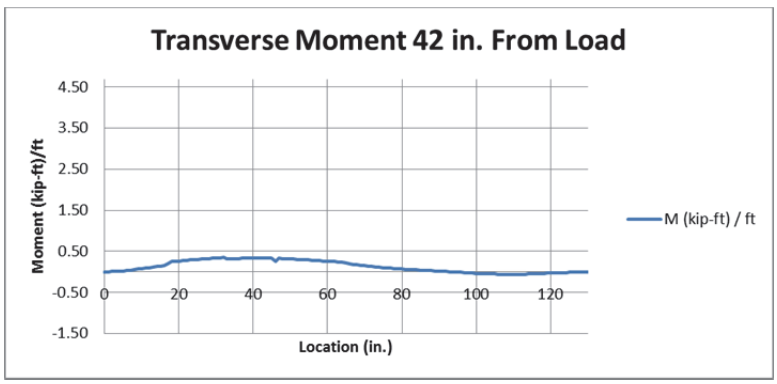
Transverse Moment 42 in. From Load
Moment (kip-ft)/ft
4.50
3.50
2.50
1.50
0.50
-0.50
-1.50
0
20
40
60
80
100
120
Location (in.)
M (kip-ft) / ft

Test 2 Moments: Midspan Service Single Point Load on West Side

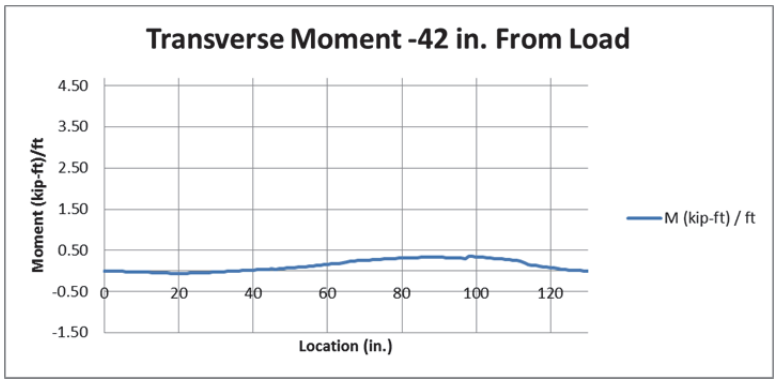

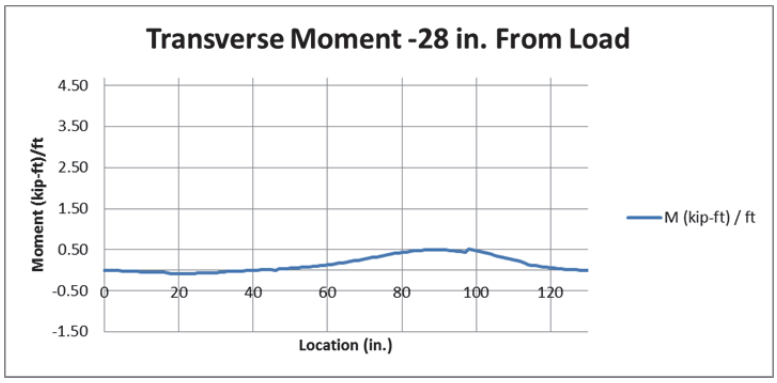

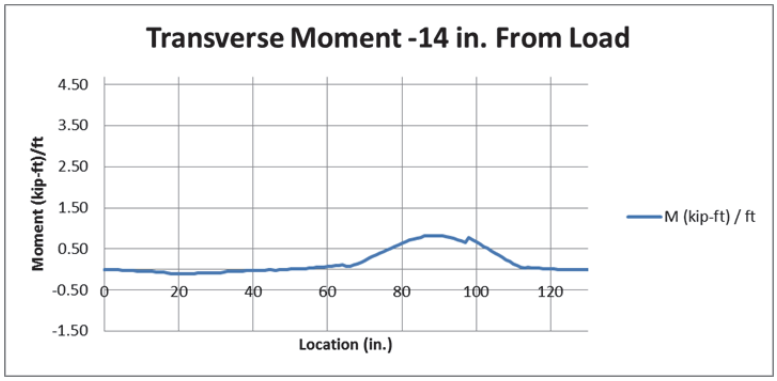

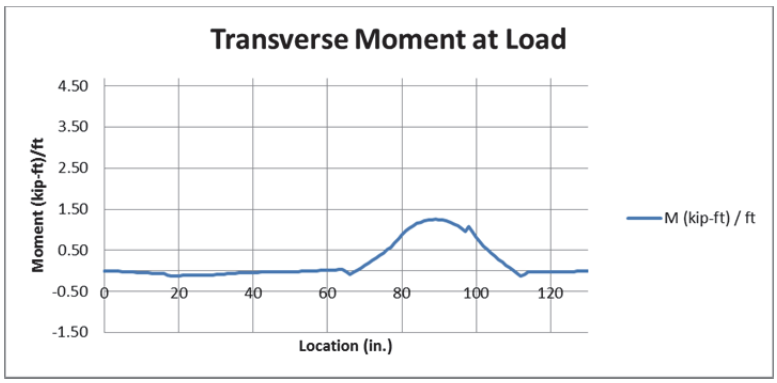

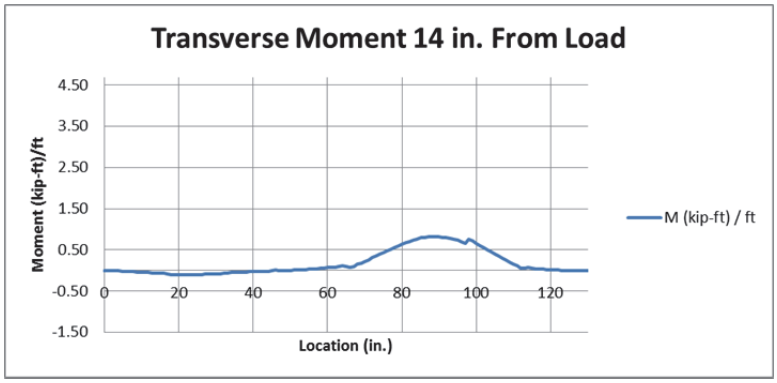
Transverse Moment 14 in. From Load
Moment (kip-ft)/ft
4.50
3.50
2.50
1.50
0.50
-0.50
-1.50
0
20
40
60
80
100
120
Location (in.)
M (kip-ft) / ft

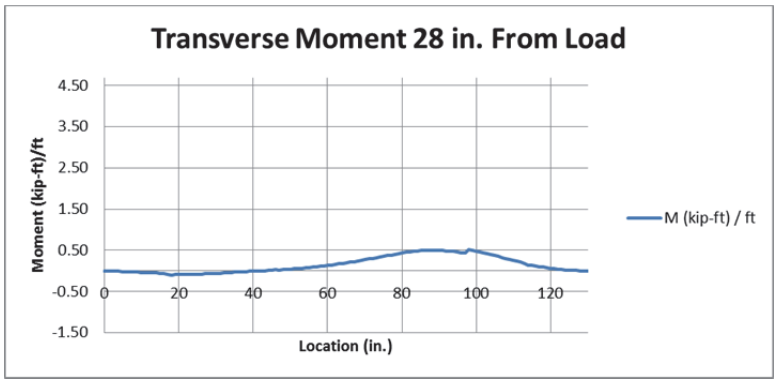
Transverse Moment 28 in. From Load
Moment (kip-ft)/ft
4.50
3.50
2.50
1.50
0.50
-0.50
-1.50
0
20
40
60
80
100
120
Location (in.)
M (kip-ft) / ft

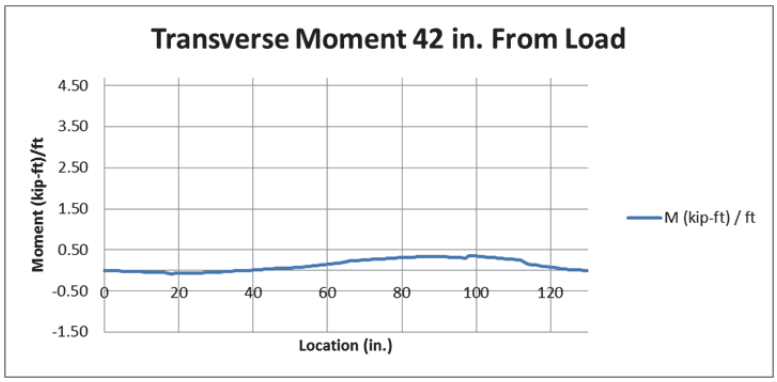
Transverse Moment 42 in. From Load
Moment (kip-ft)/ft
4.50
3.50
2.50
1.50
0.50
-0.50
-1.50
0
20
40
60
80
100
120
Location (in.)
M (kip-ft) / ft

Test 3 Moments: Midspan Service Two Point Loads

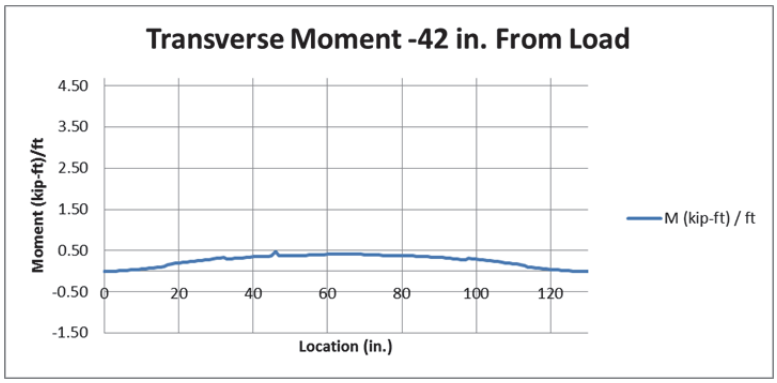

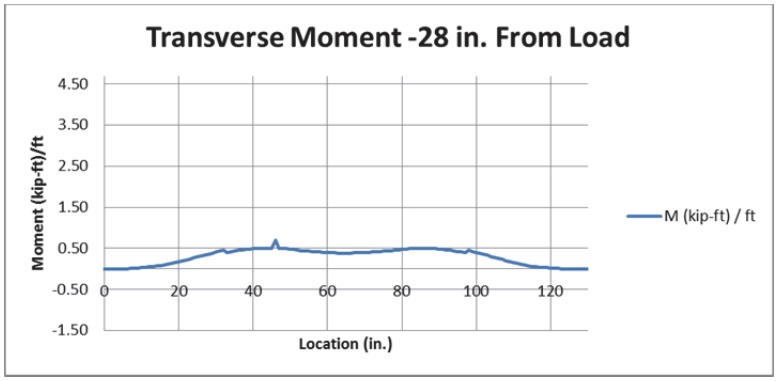

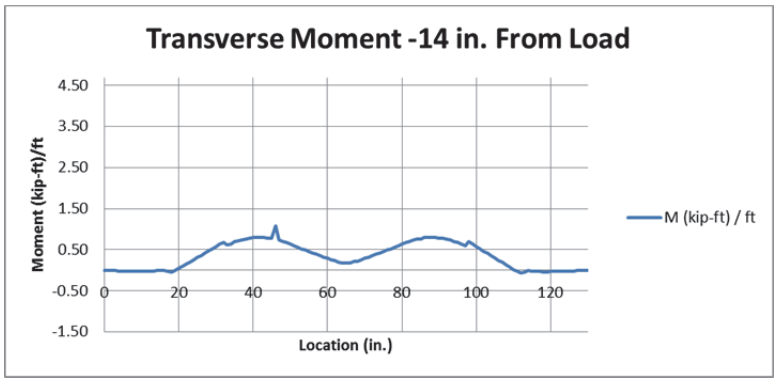

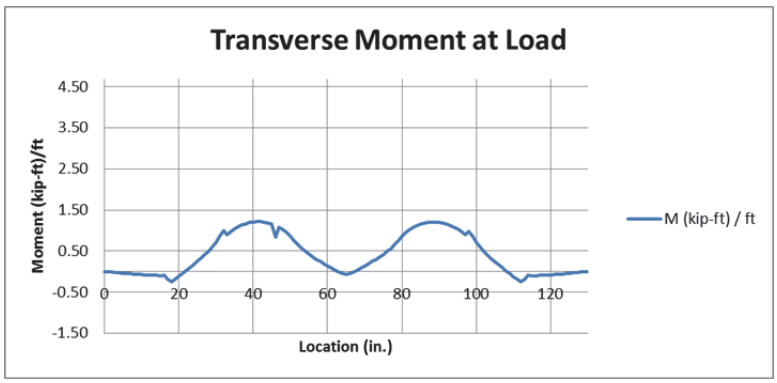

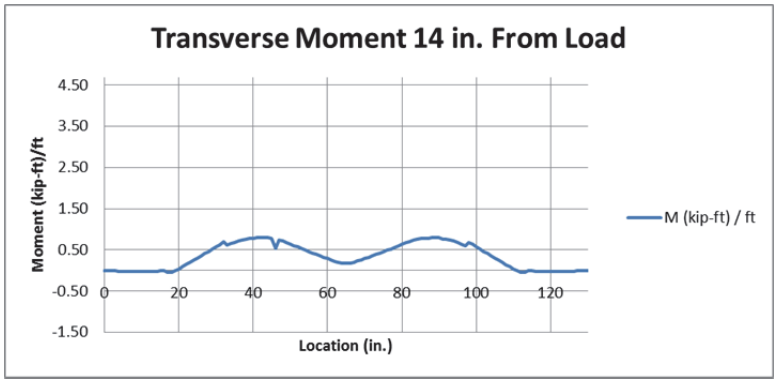
Transverse Moment 14 in. From Load
Moment (kip-ft)/ft
4.50
3.50
2.50
1.50
0.50
-0.50
-1.50
0
20
40
60
80
100
120
Location (in.)
M (kip-ft) / ft

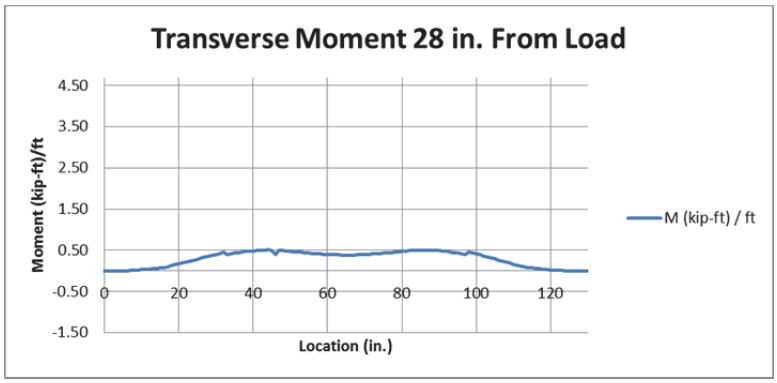
Transverse Moment 28 in. From Load
Moment (kip-ft)/ft
4.50
3.50
2.50
1.50
0.50
-0.50
-1.50
0
20
40
60
80
100
120
Location (in.)
M (kip-ft) / ft

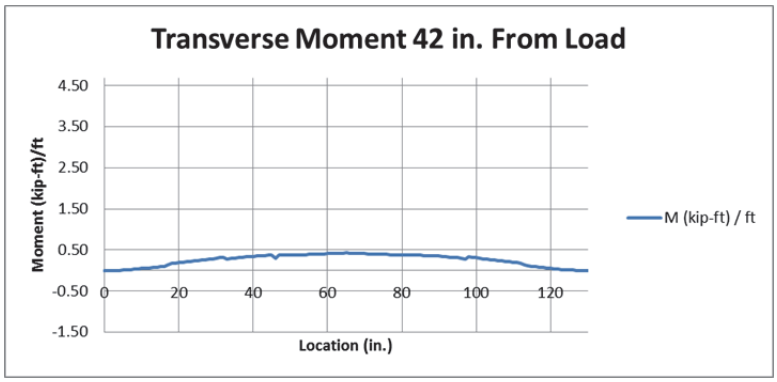
Transverse Moment 42 in. From Load
Moment (kip-ft)/ft
4.50
3.50
2.50
1.50
0.50
-0.50
-1.50
0
20
40
60
80
100
120
Location (in.)
M (kip-ft) / ft

Test 4 Moments: Midspan Strength Two Point Loads

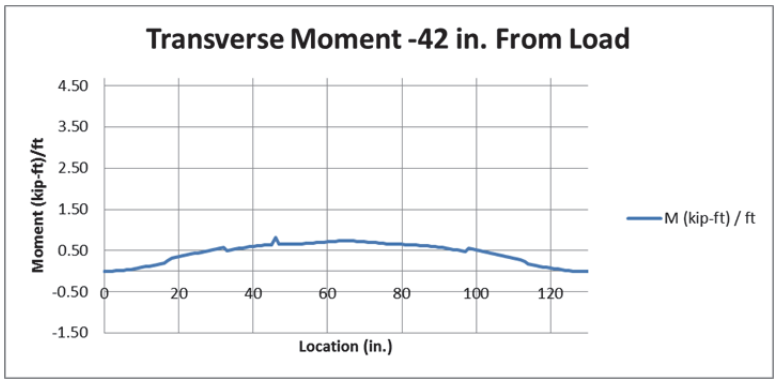

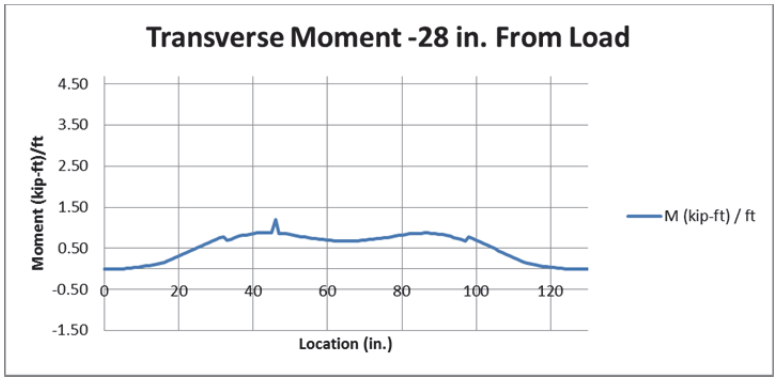

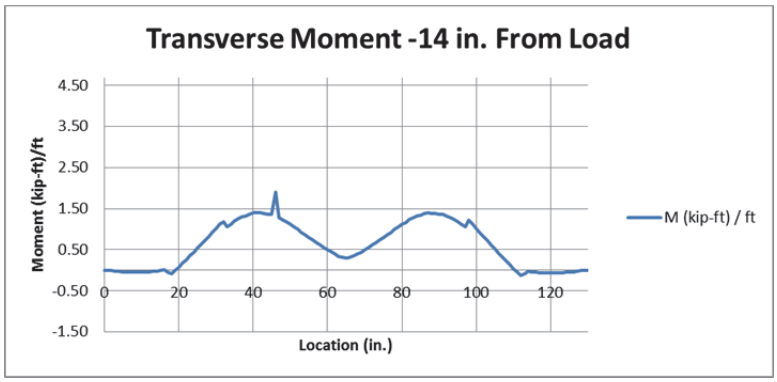

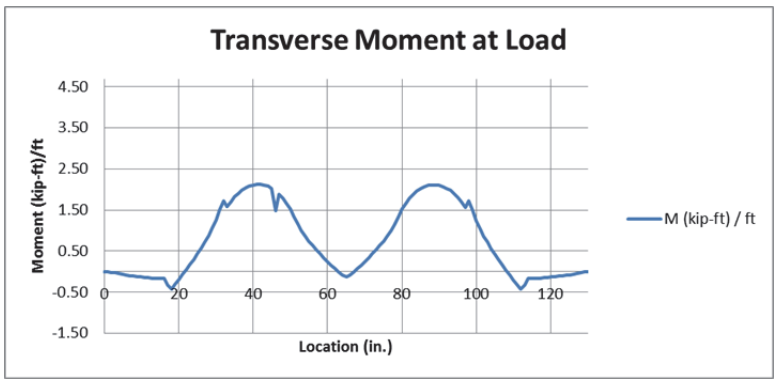

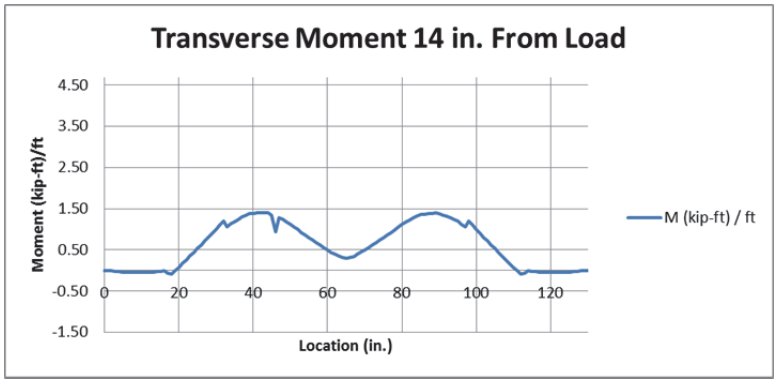
Transverse Moment 14 in. From Load
Moment (kip-ft)/ft
4.50
3.50
2.50
1.50
0.50
-0.50
-1.50
0
20
40
60
80
100
120
Location (in.)
M (kip-ft) / ft

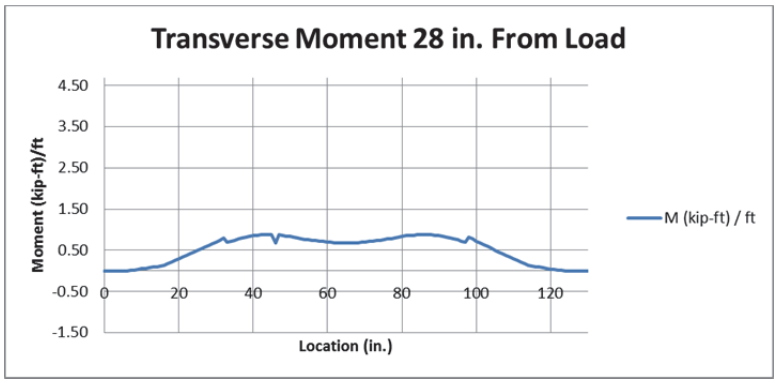
Transverse Moment 28 in. From Load
Moment (kip-ft)/ft
4.50
3.50
2.50
1.50
0.50
-0.50
-1.50
0
20
40
60
80
100
120
Location (in.)
M (kip-ft) / ft

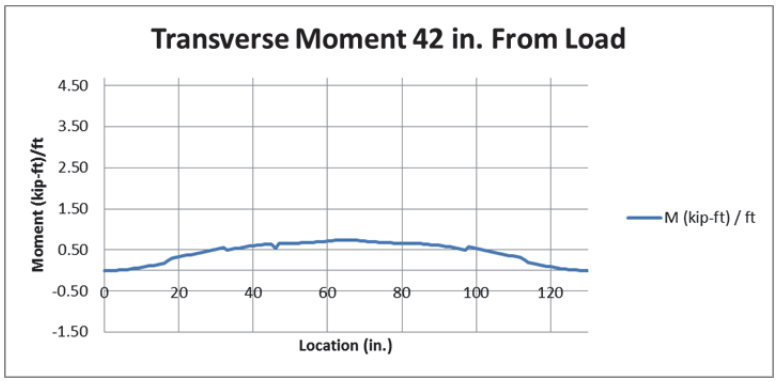
Transverse Moment 42 in. From Load
Moment (kip-ft)/ft
4.50
3.50
2.50
1.50
0.50
-0.50
-1.50
0
20
40
60
80
100
120
Location (in.)
M (kip-ft) / ft

Test 5 Moments: Quarter Point Service Single Point Load on East Side

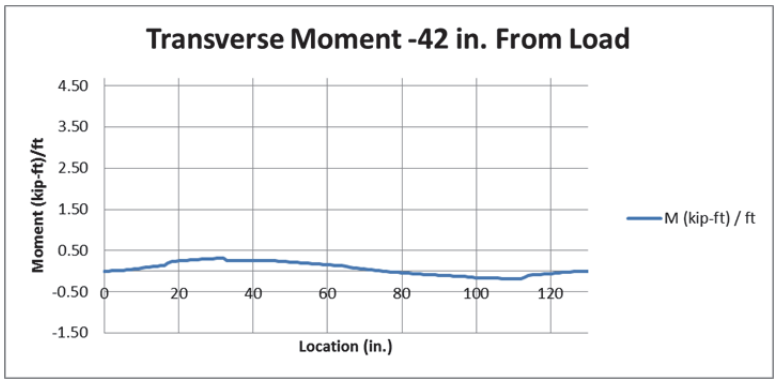

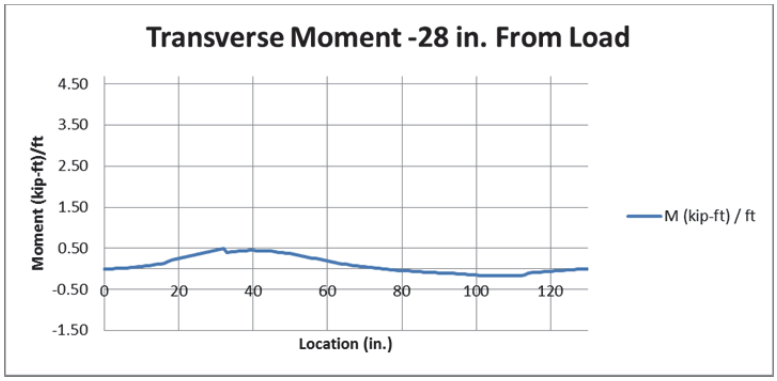

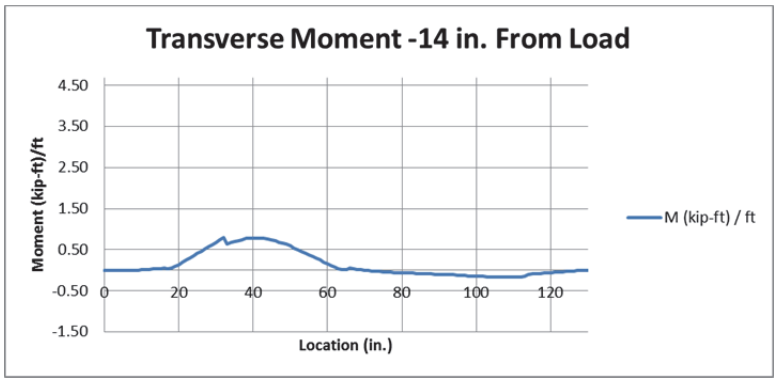

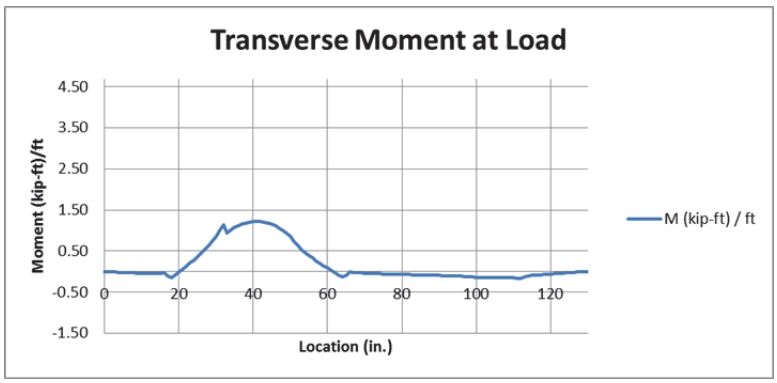

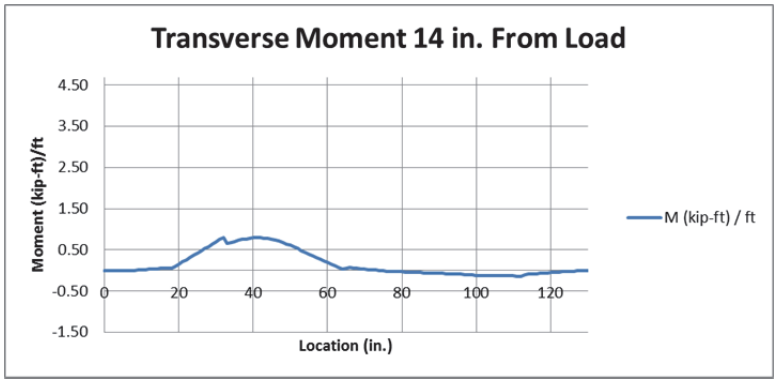
Transverse Moment 14 in. From Load
Moment (kip-ft)/ft
4.50
3.50
2.50
1.50
0.50
-0.50
-1.50
0
20
40
60
80
100
120
Location (in.)
M (kip-ft) / ft

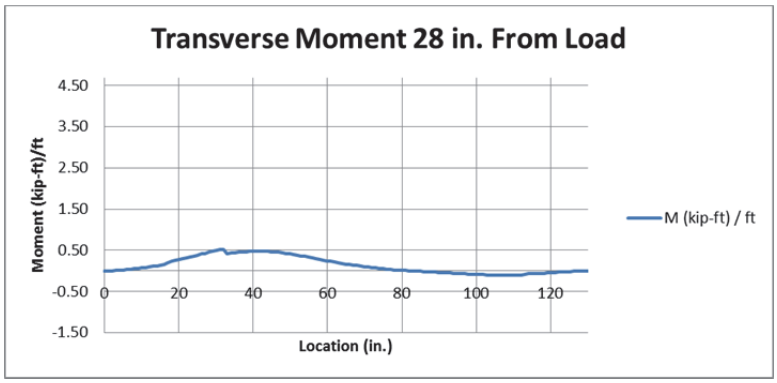
Transverse Moment 28 in. From Load
Moment (kip-ft)/ft
4.50
3.50
2.50
1.50
0.50
-0.50
-1.50
0
20
40
60
80
100
120
Location (in.)
M (kip-ft) / ft

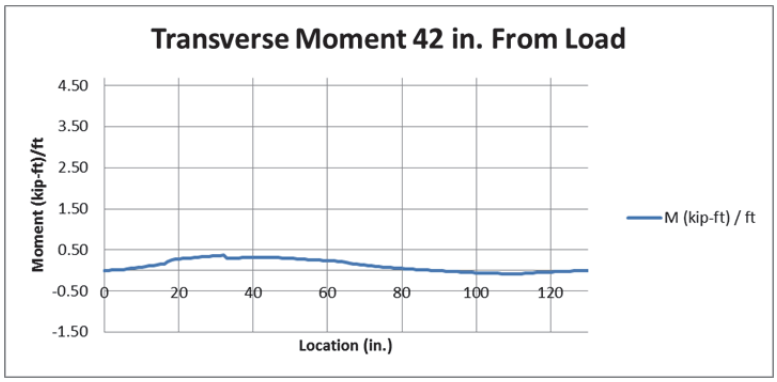
Transverse Moment 42 in. From Load
Moment (kip-ft)/ft
4.50
3.50
2.50
1.50
0.50
-0.50
-1.50
0
20
40
60
80
100
120
Location (in.)
M (kip-ft) / ft

Test 6 Moments: Quarter Point Service Single Point Load on West Side

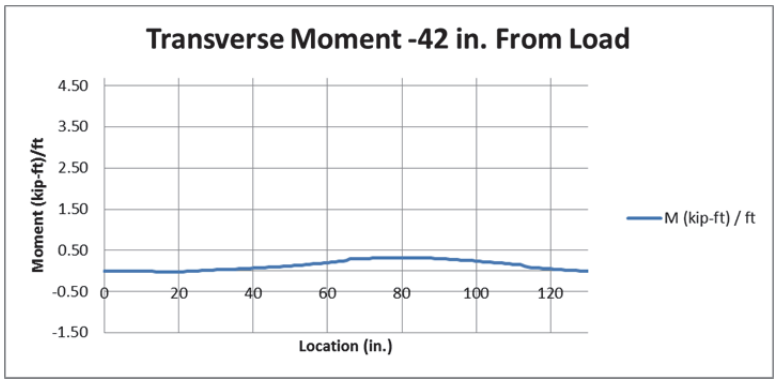

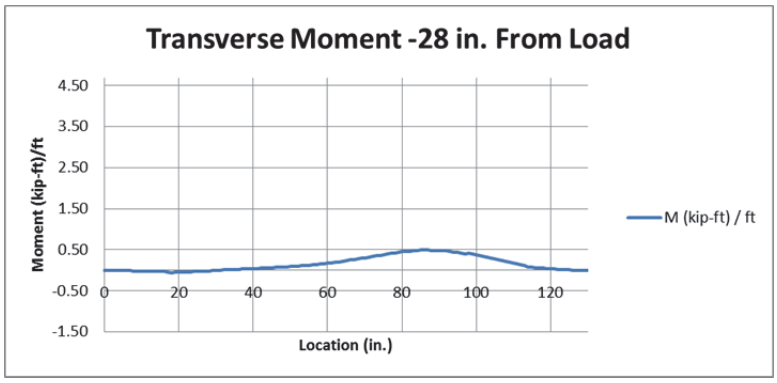

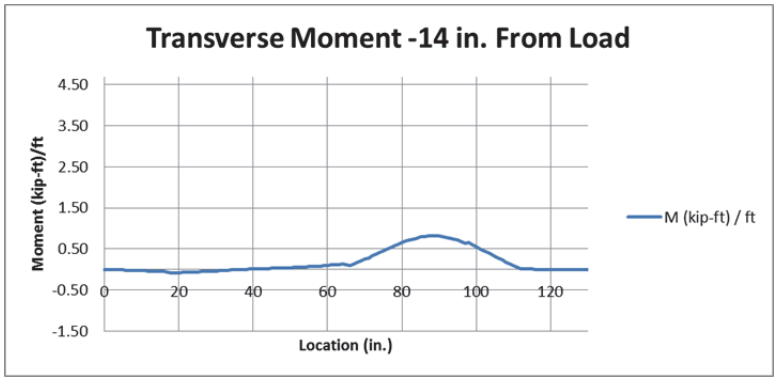

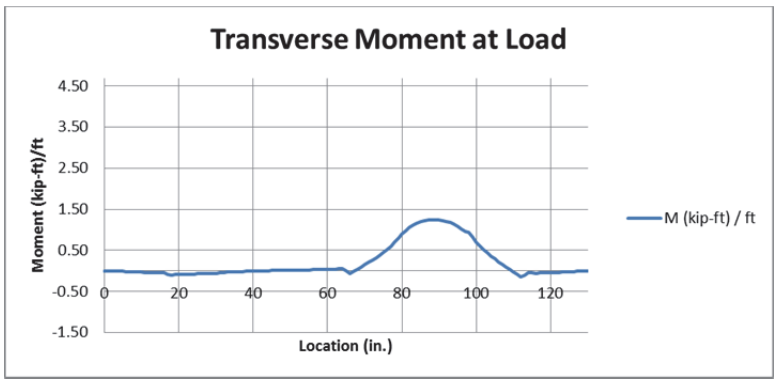

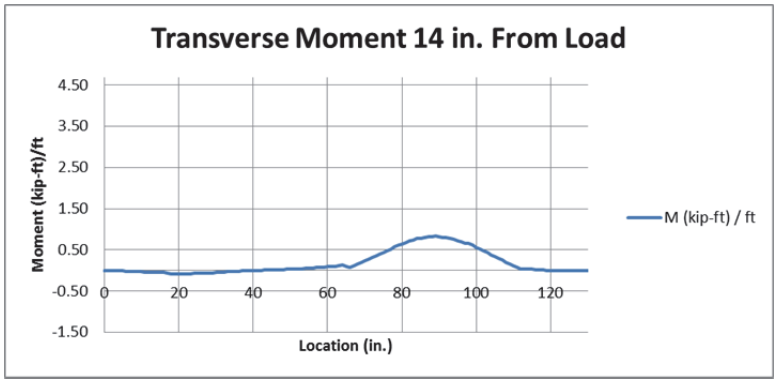
Transverse Moment 14 in. From Load
Moment (kip-ft)/ft
4.50
3.50
2.50
1.50
0.50
-0.50
-1.50
0
20
40
60
80
100
120
Location (in.)
M (kip-ft) / ft

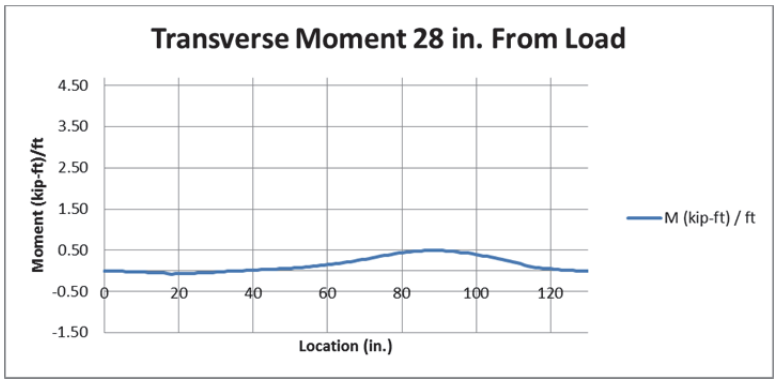
Transverse Moment 28 in. From Load
Moment (kip-ft)/ft
4.50
3.50
2.50
1.50
0.50
-0.50
-1.50
0
20
40
60
80
100
120
Location (in.)
M (kip-ft) / ft

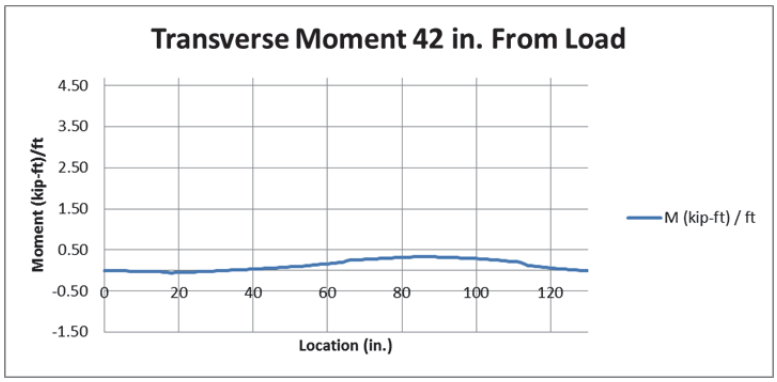
Transverse Moment 42 in. From Load
Moment (kip-ft)/ft
4.50
3.50
2.50
1.50
0.50
-0.50
-1.50
0
20
40
60
80
100
120
Location (in.)
M (kip-ft) / ft

Test 7 Moments: Quarter Point Service Two Point Loads

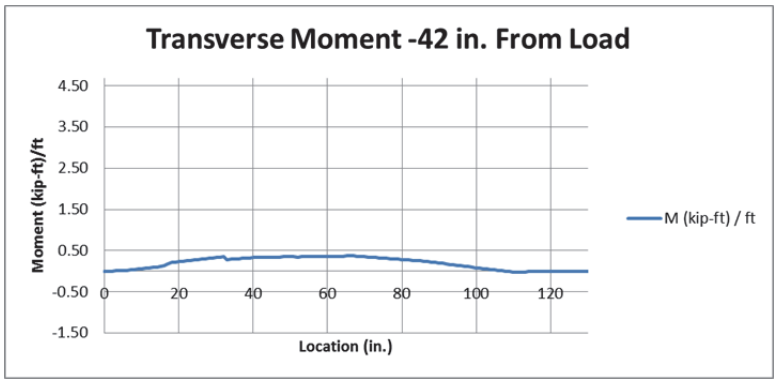

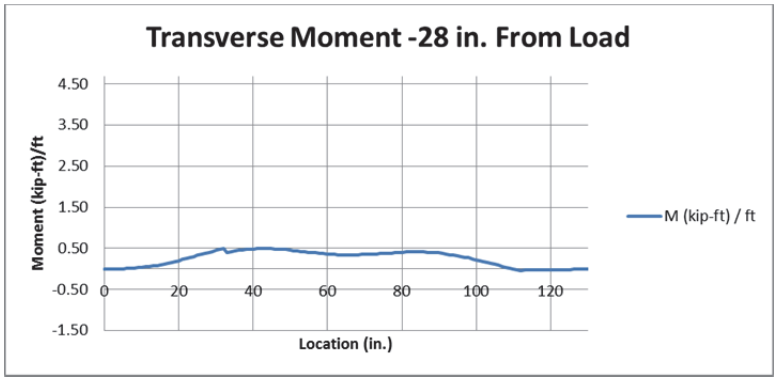

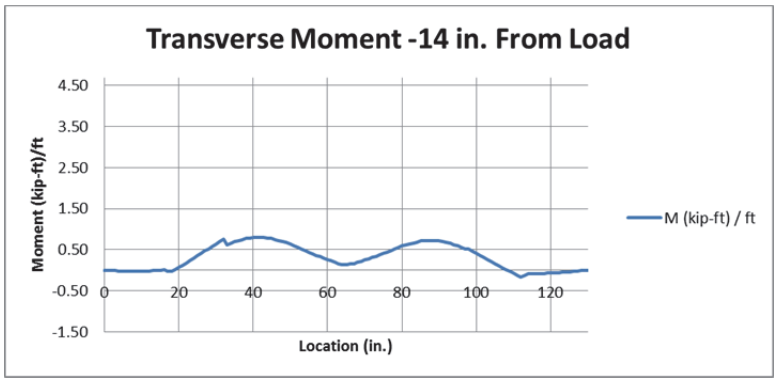

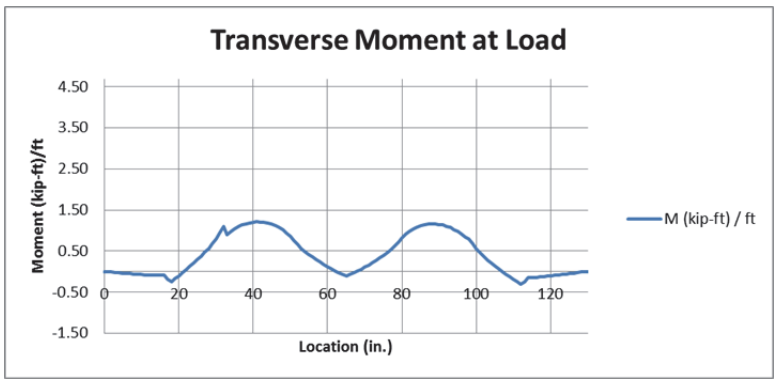

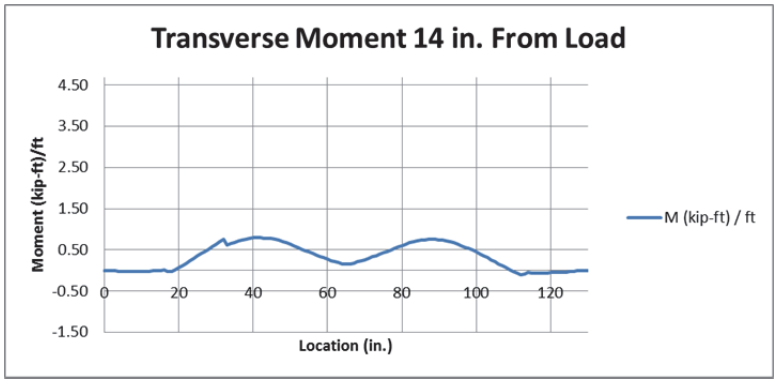
Transverse Moment 14 in. From Load
Moment (kip-ft)/ft
4.50
3.50
2.50
1.50
0.50
-0.50
-1.50
0
20
40
60
80
100
120
Location (in.)
M (kip-ft) / ft

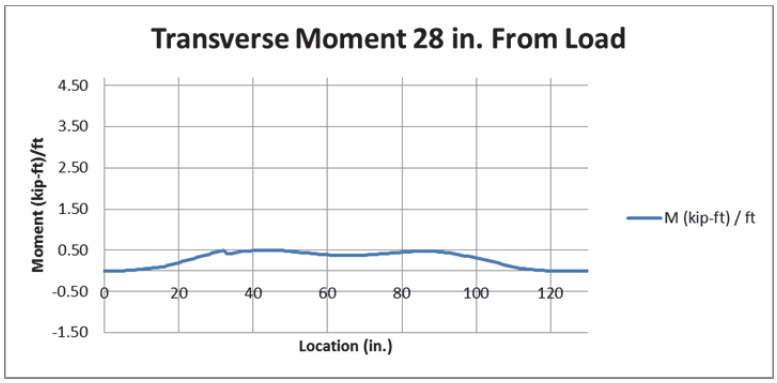
Transverse Moment 28 in. From Load
Moment (kip-ft)/ft
4.50
3.50
2.50
1.50
0.50
-0.50
-1.50
0
20
40
60
80
100
120
Location (in.)
M (kip-ft) / ft

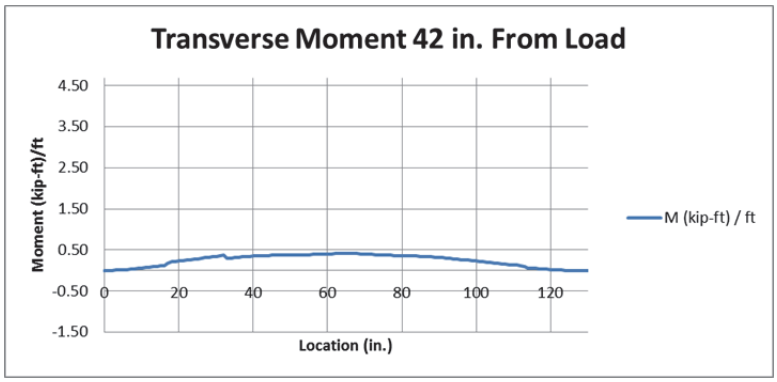
Transverse Moment 42 in. From Load
Moment (kip-ft)/ft
4.50
3.50
2.50
1.50
0.50
-0.50
-1.50
0
20
40
60
80
100
120
Location (in.)
M (kip-ft) / ft

Test 8 Moments: Quarter Point Strength Two Point Loads

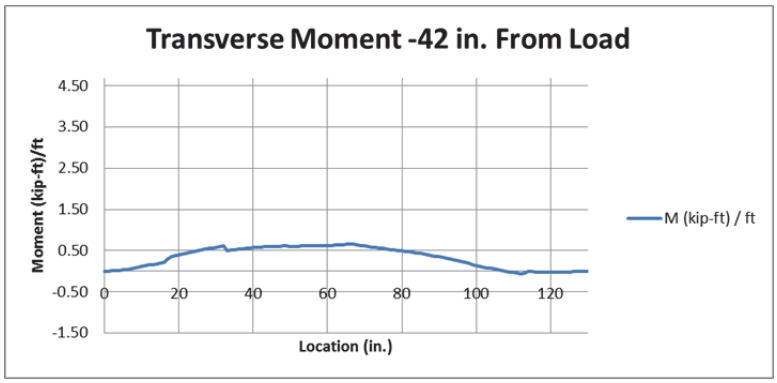

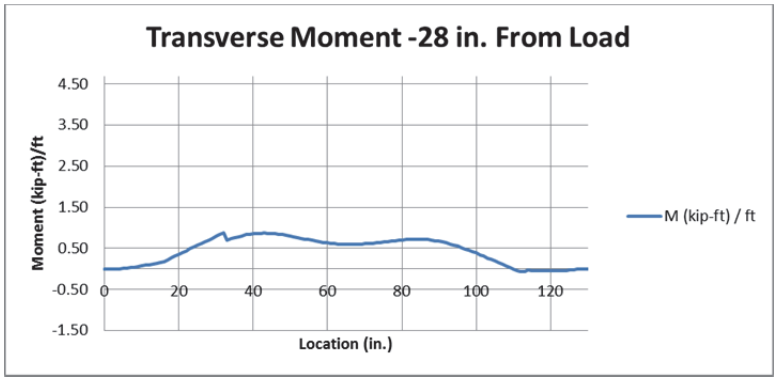

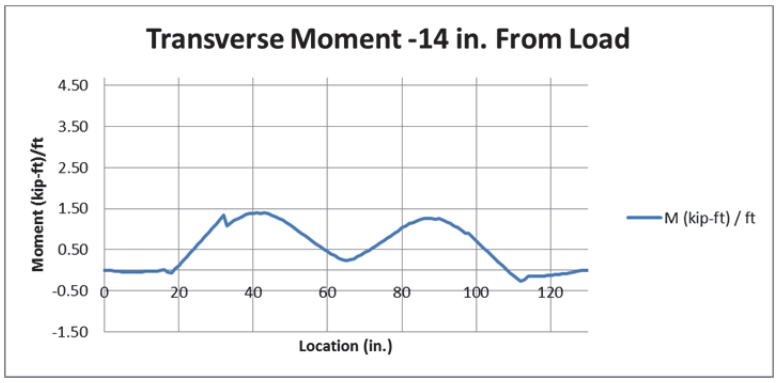

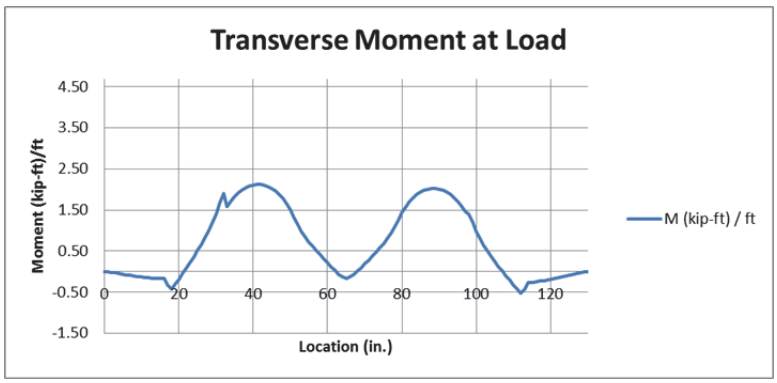

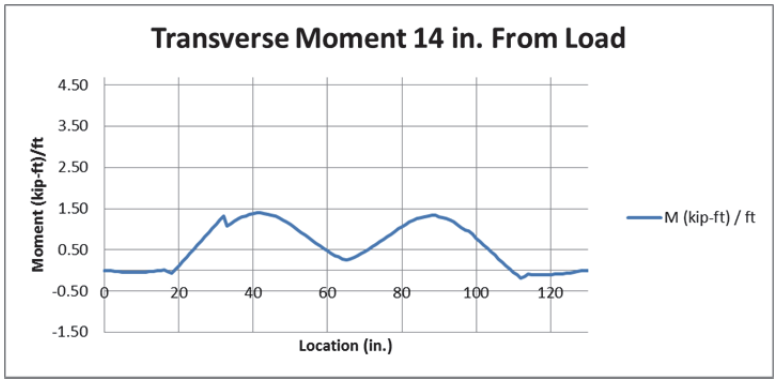
Transverse Moment 14 in. From Load
Moment (kip-ft)/ft
4.50
3.50
2.50
1.50
0.50
-0.50
-1.50
0
20
40
60
80
100
120
Location (in.)
M (kip-ft) / ft

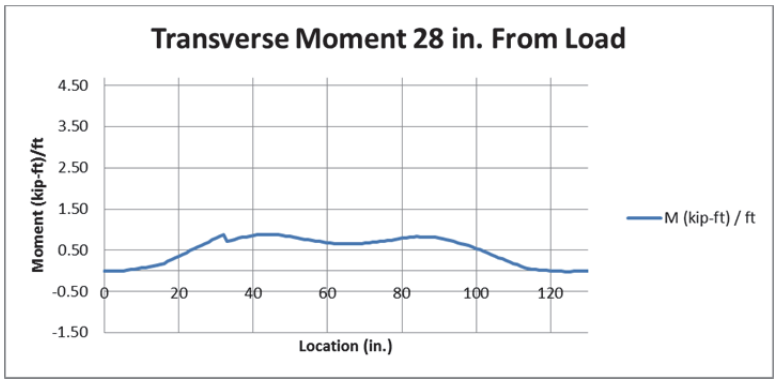
Transverse Moment 28 in. From Load
Moment (kip-ft)/ft
4.50
3.50
2.50
1.50
0.50
-0.50
-1.50
0
20
40
60
80
100
120
Location (in.)
M (kip-ft) / ft

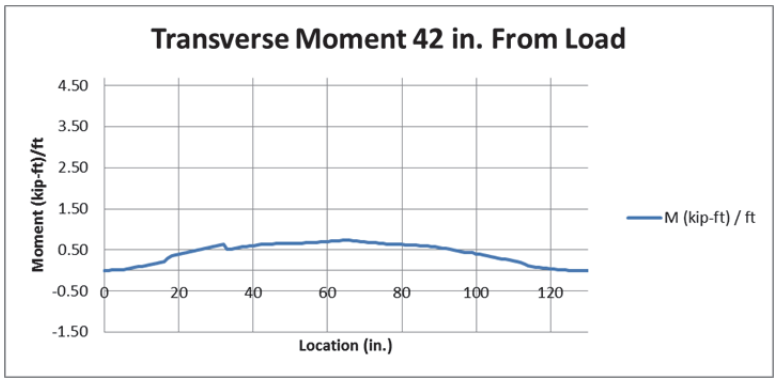
Transverse Moment 42 in. From Load
Moment (kip-ft)/ft
4.50
3.50
2.50
1.50
0.50
-0.50
-1.50
0
20
40
60
80
100
120
Location (in.)
M (kip-ft) / ft

APPENDIX D: STRAINS

Comparing Test Strains to Abaqus Strains

Test 1 Strains: Midspan Service Single Point Load on East Side

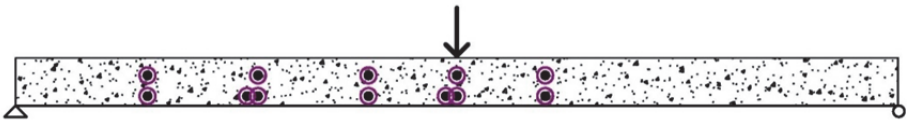

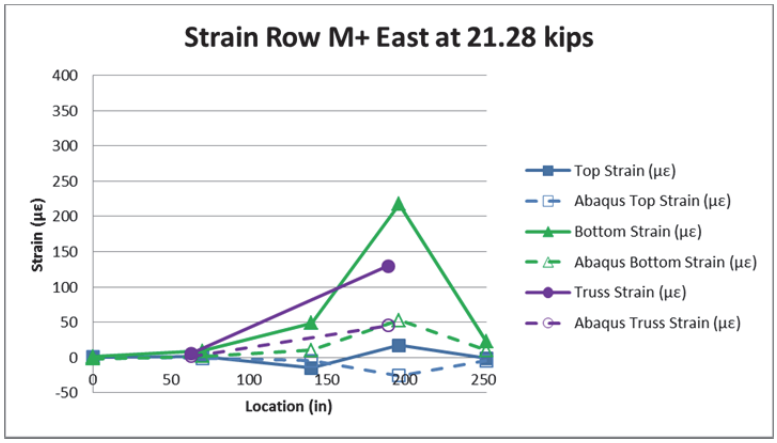

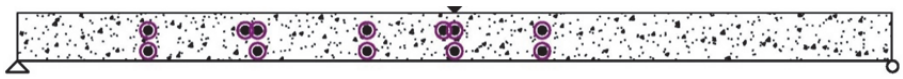

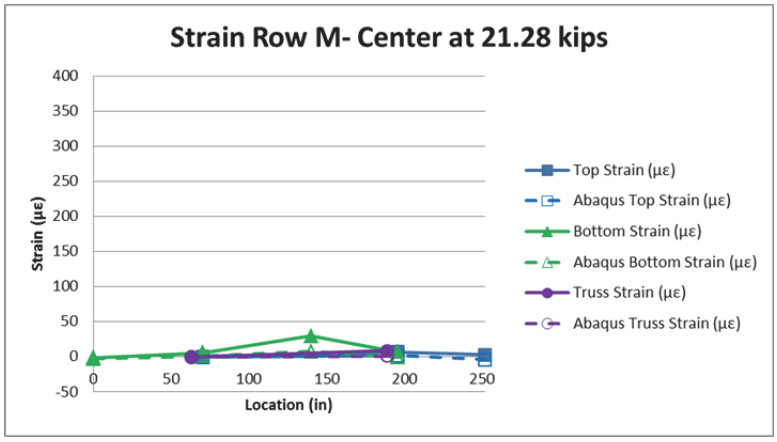

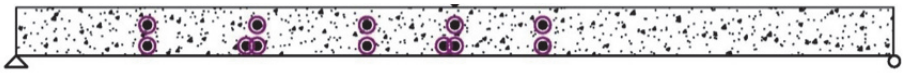

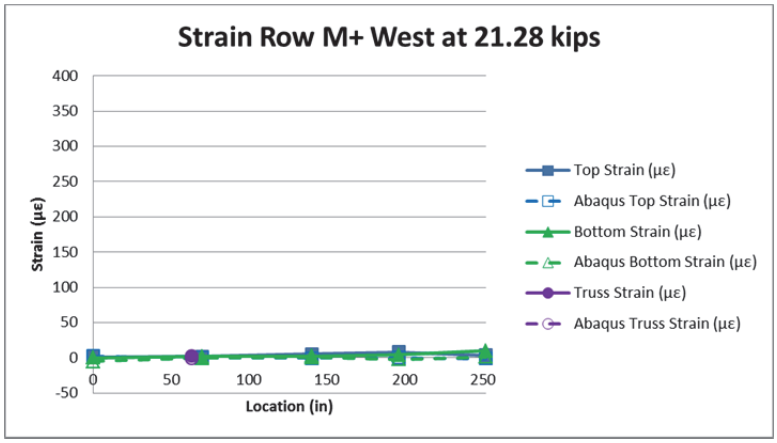

Test 2 Strains: Midspan Service Single Point Load on West Side

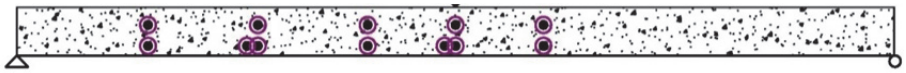

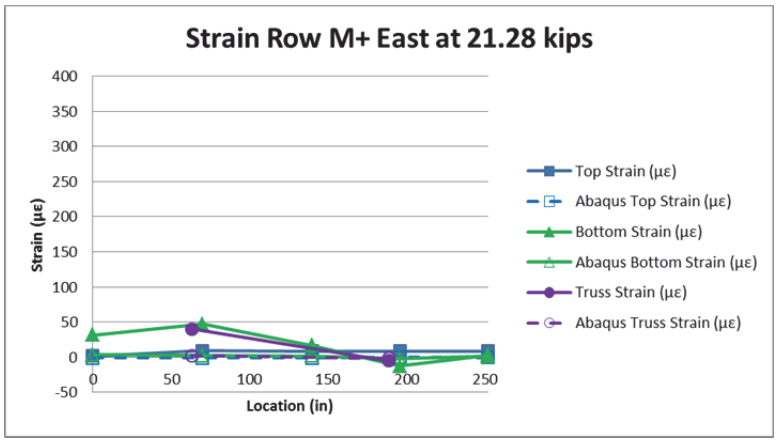

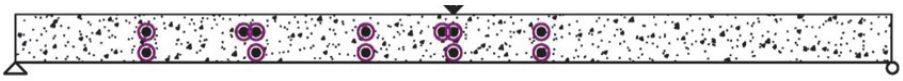

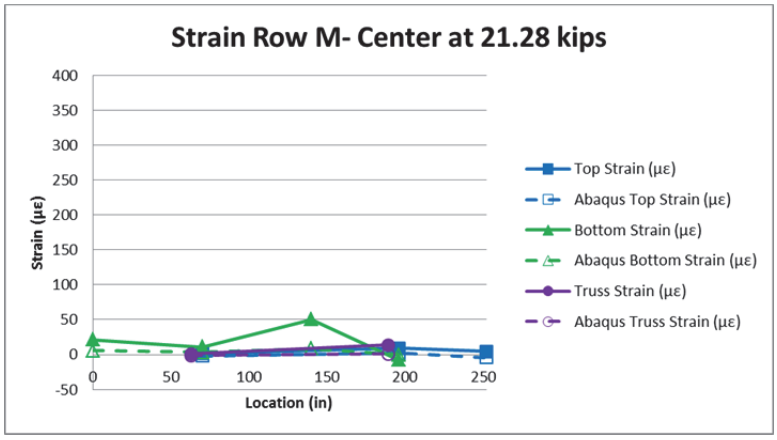
Strain Row M- Center at 21.28 kips
400
350
300
250
200
150
100
50
0
-50
Strain (με)
0
50
100
150
200
250
Location (in)
Top Strain (με)
Abaqus Top Strain (με)
Bottom Strain (με)
Abaqus Bottom Strain (με)
Truss Strain (με)
Abaqus Truss Strain (με)

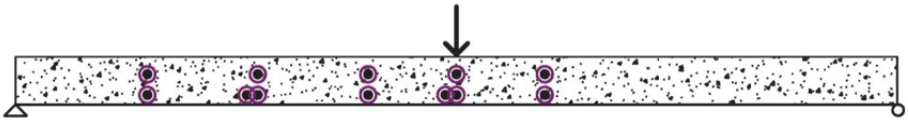

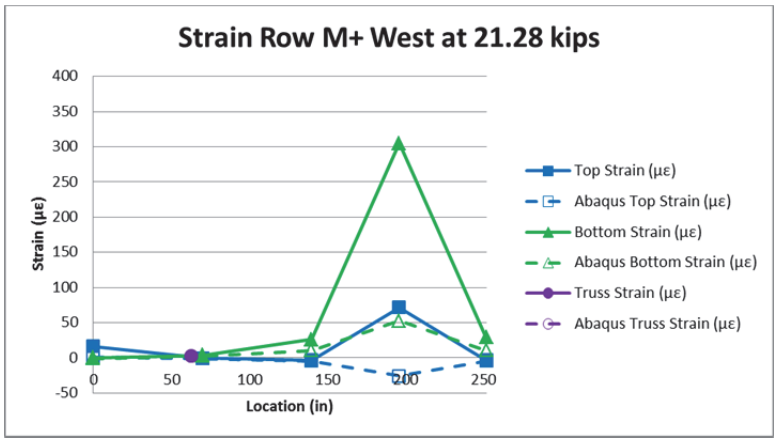
Strain Row M+ West at 21.28 kips
400
350
300
250
200
150
100
50
0
-50
Strain (με)
0
50
100
150
200
250
Location (in)
Top Strain (με)
Abaqus Top Strain (με)
Bottom Strain (με)
Abaqus Bottom Strain (με)
Truss Strain (με)
Abaqus Truss Strain (με)

Test 3 Strains: Midspan Service Two Point Loads

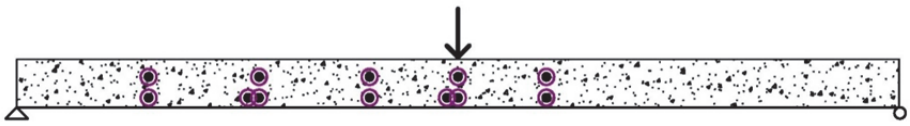

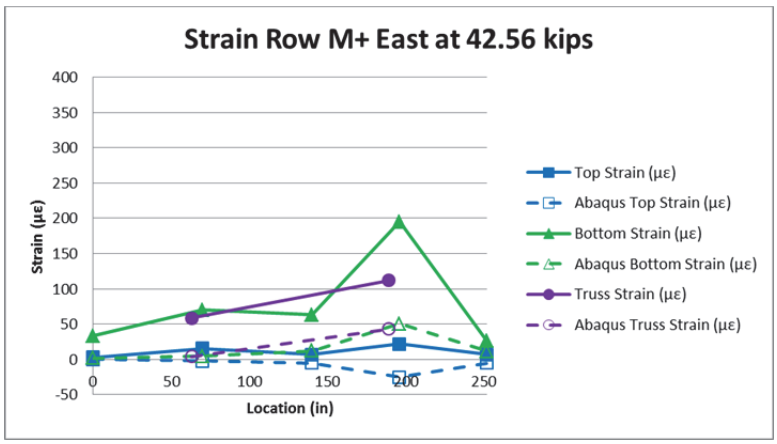

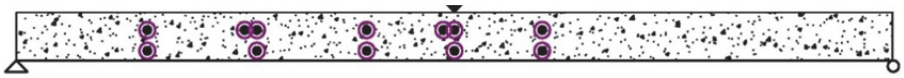

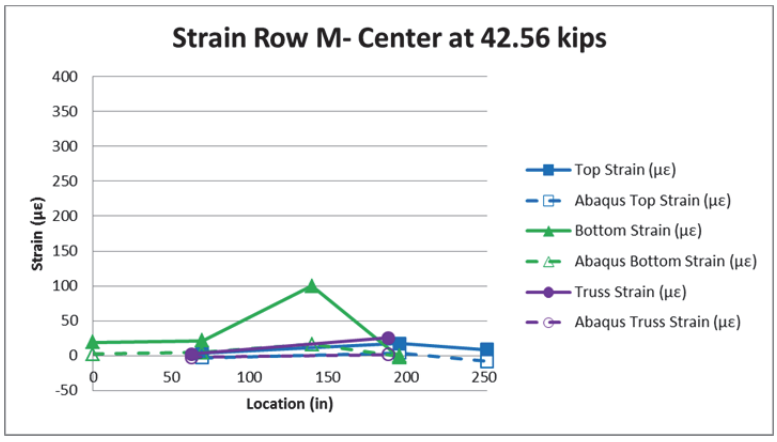

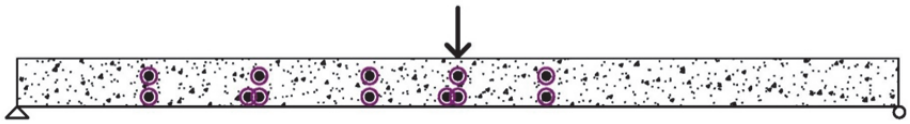

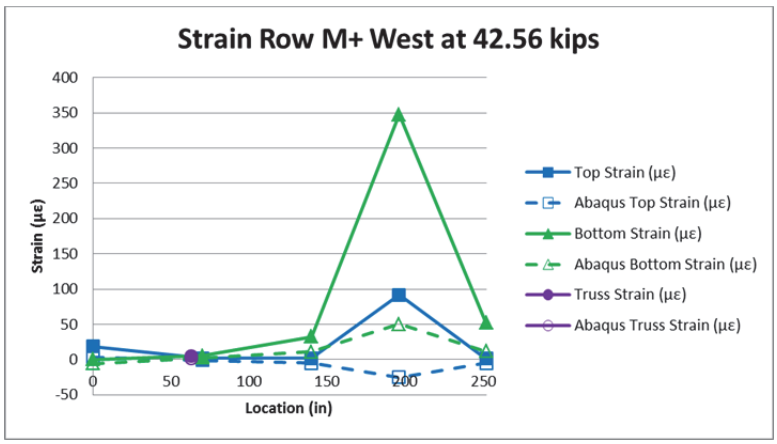

Test 4 Strains: Midspan Strength Two Point Loads

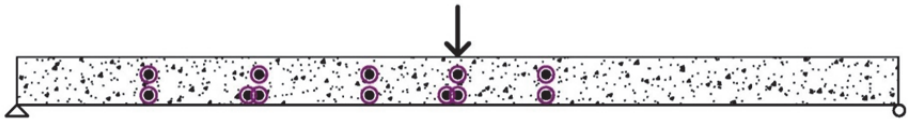

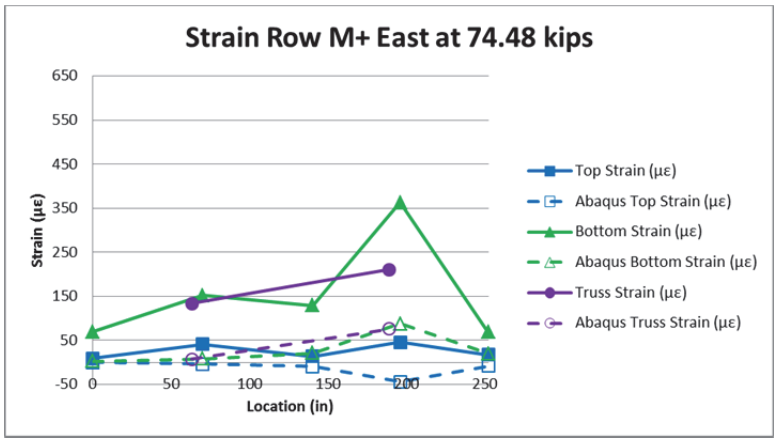

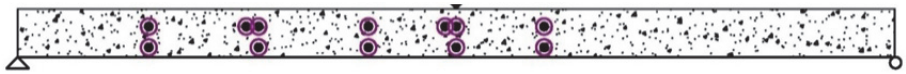

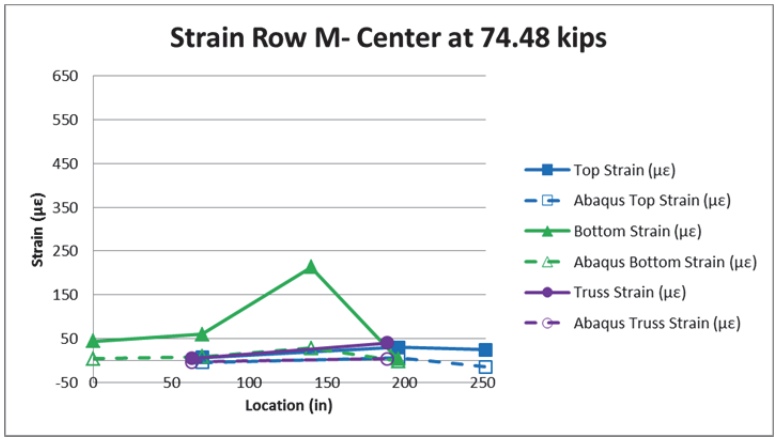
Strain Row M- Center at 74.48 kips
650
550
450
350
250
150
50
-50
Strain (με)
0
50
100
150
200
250
Location (in)
Top Strain (με)
Abaqus Top Strain (με)
Bottom Strain (με)
Abaqus Bottom Strain (με)
Truss Strain (με)
Abaqus Truss Strain (με)

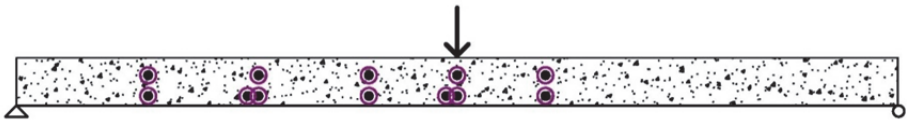

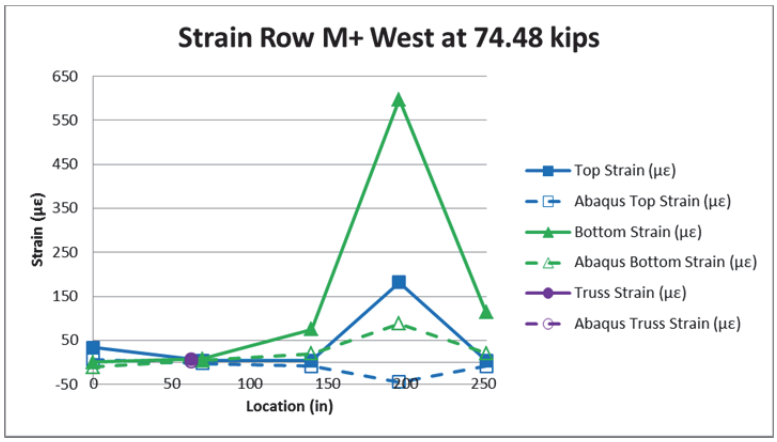
Strain Row M+ West at 74.48 kips
650
550
450
350
250
150
50
-50
Strain (με)
0
50
100
150
200
250
Location (in)
Top Strain (με)
Abaqus Top Strain (με)
Bottom Strain (με)
Abaqus Bottom Strain (με)
Truss Strain (με)
Abaqus Truss Strain (με)

Test 5 Strains: Quarter Point Service Single Point Load on East Side

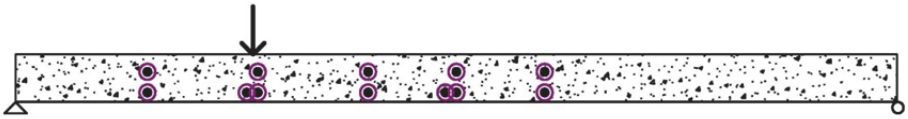

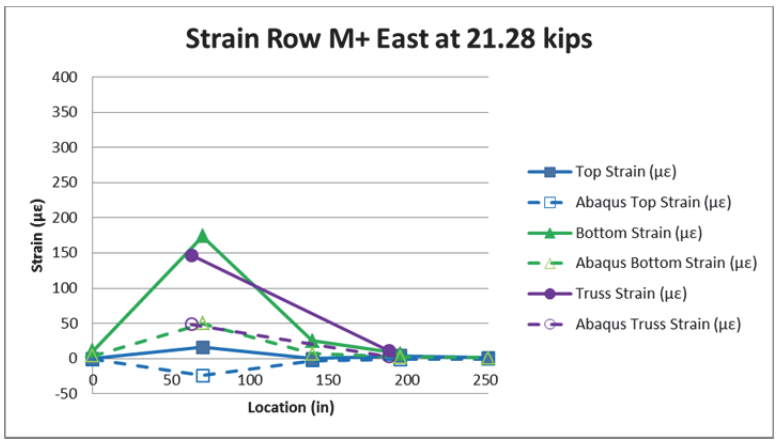

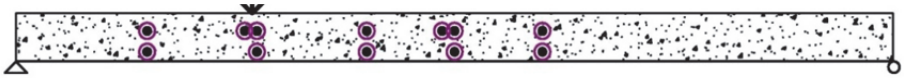

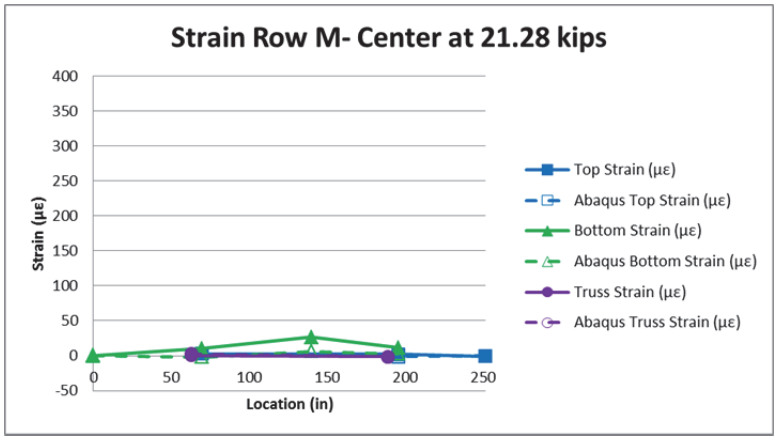

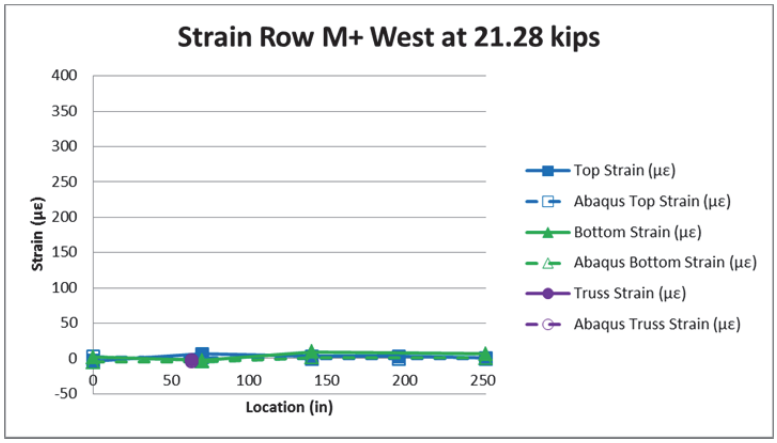

Test 6 Strains: Quarter Point Service Single Point Load on West Side

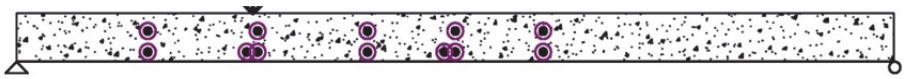

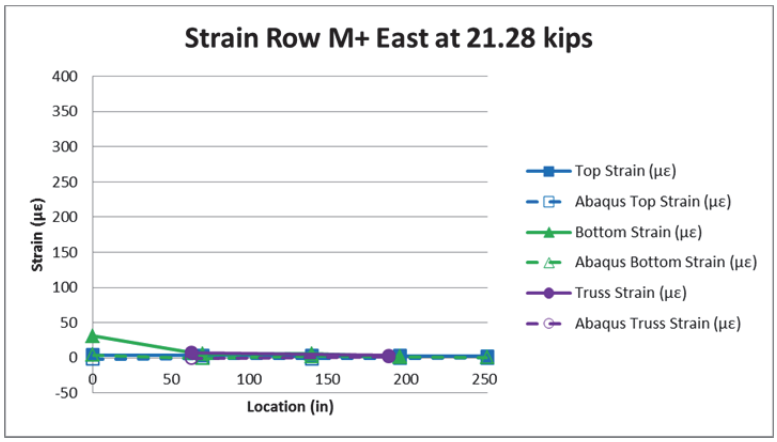

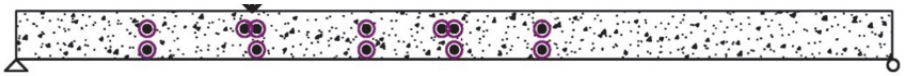

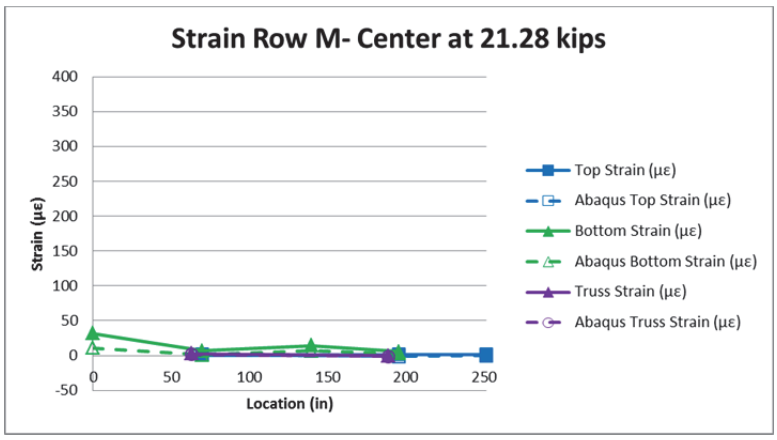
Strain Row M- Center at 21.28 kips
400
350
300
250
200
150
100
50
0
-50
Strain (με)
0
50
100
150
200
250
Location (in)
Top Strain (με)
Abaqus Top Strain (με)
Bottom Strain (με)
Abaqus Bottom Strain (με)
Truss Strain (με)
Abaqus Truss Strain (με)

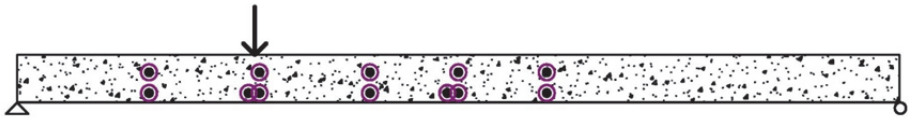

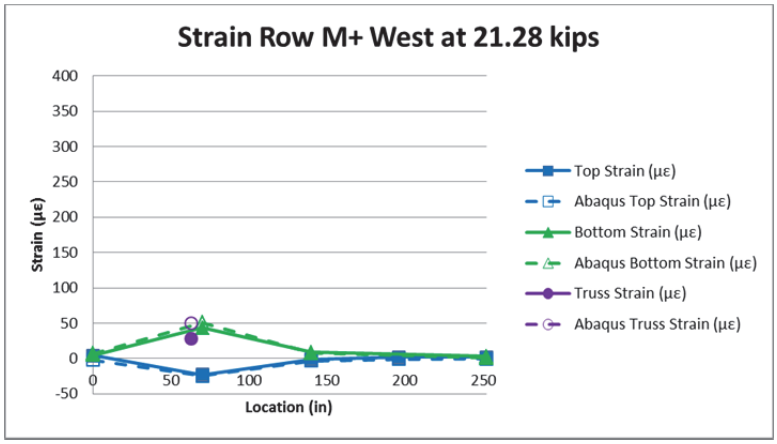
Strain Row M+ West at 21.28 kips
400
350
300
250
200
150
100
50
0
-50
Strain (με)
0
50
100
150
200
250
Location (in)
Top Strain (με)
Abaqus Top Strain (με)
Bottom Strain (με)
Abaqus Bottom Strain (με)
Truss Strain (με)
Abaqus Truss Strain (με)

Test 7 Strains: Quarter Point Service Two Point Loads

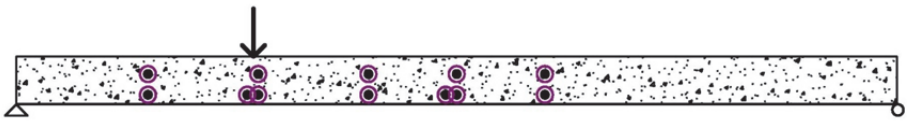

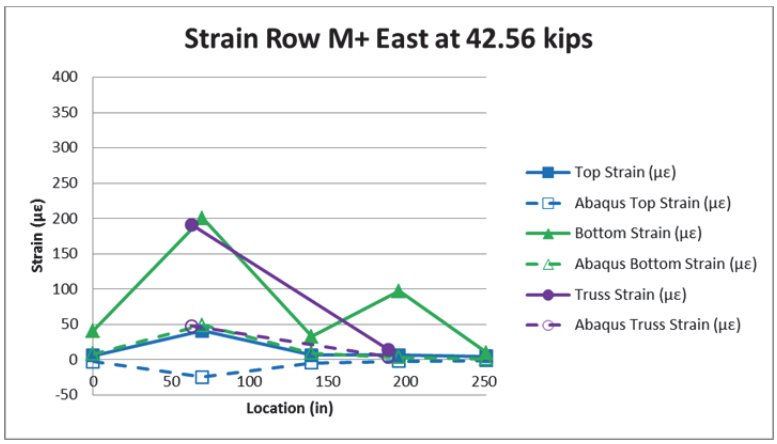

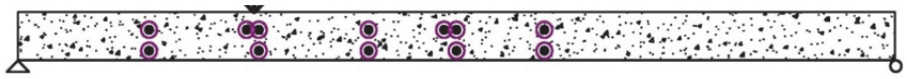

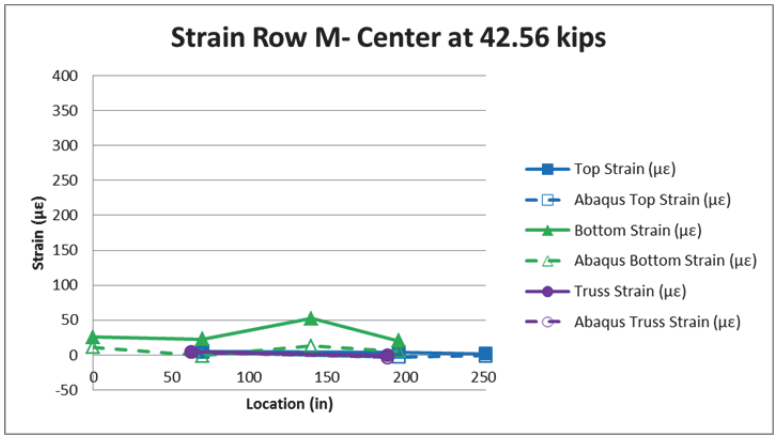

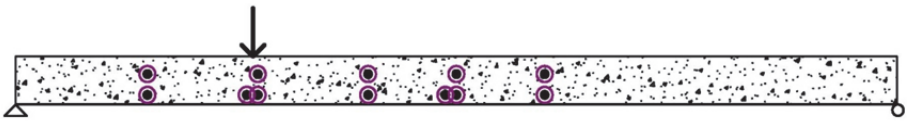

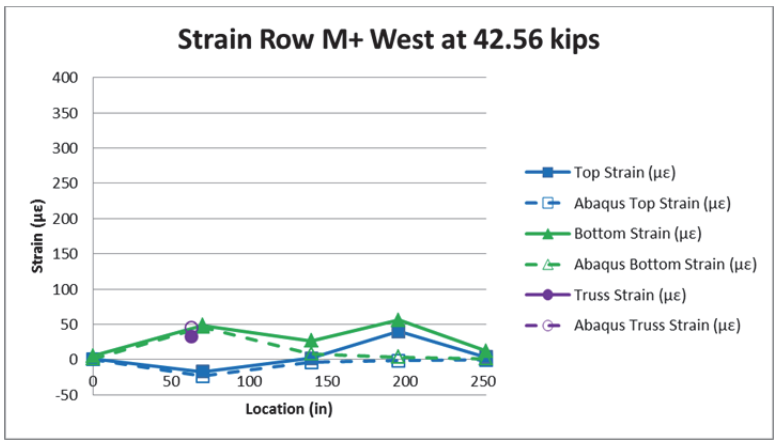

Test 8 Strains: Quarter Point Strength Two Point Loads

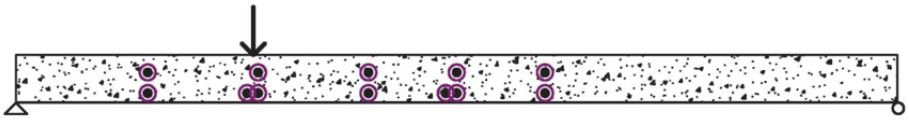

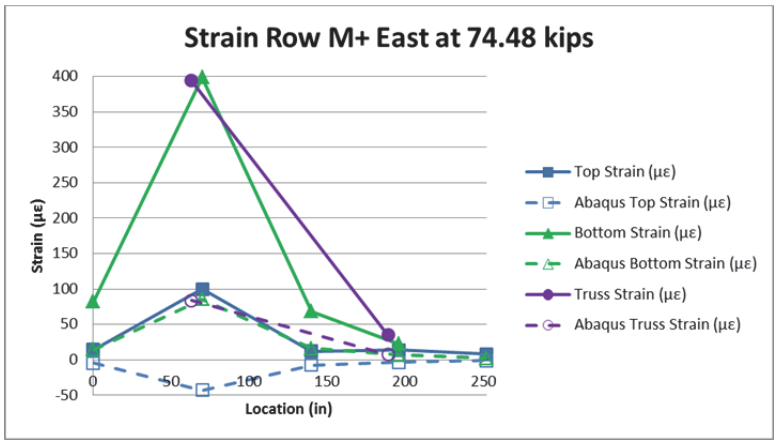

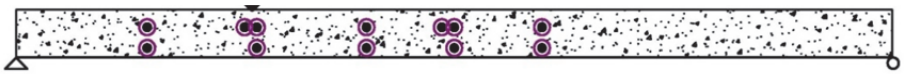

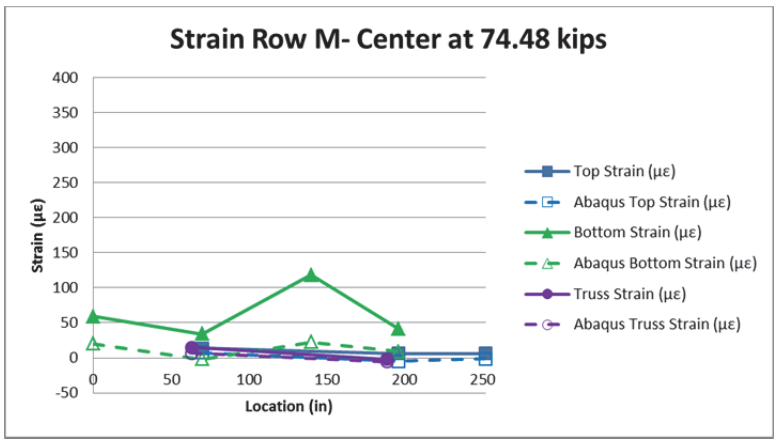
Strain Row M- Center at 74.48 kips
400
350
300
250
200
150
100
50
0
-50
Strain (με)
0
50
100
150
200
250
Location (in)
Top Strain (με)
Abaqus Top Strain (με)
Bottom Strain (με)
Abaqus Bottom Strain (με)
Truss Strain (με)
Abaqus Truss Strain (με)

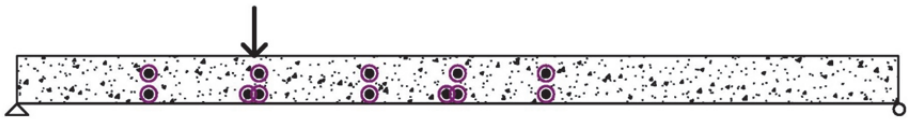

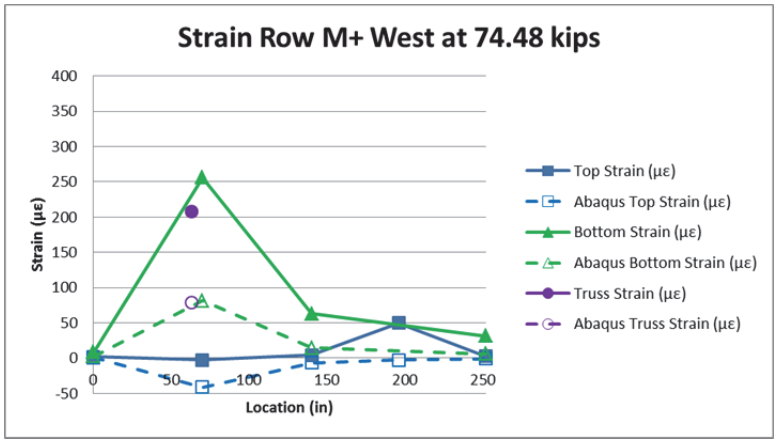
Strain Row M+ West at 74.48 kips
400
350
300
250
200
150
100
50
0
-50
Strain (με)
0
50
100
150
200
250
Location (in)
Top Strain (με)
Abaqus Top Strain (με)
Bottom Strain (με)
Abaqus Bottom Strain (με)
Truss Strain (με)
Abaqus Truss Strain (με)

APPENDIX E: DEFLECTIONS

Test 1 Maximum Deflection Experimental and Abaqus Values

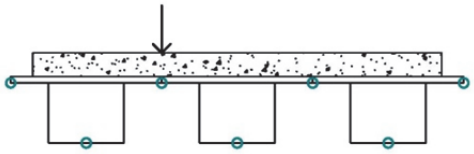

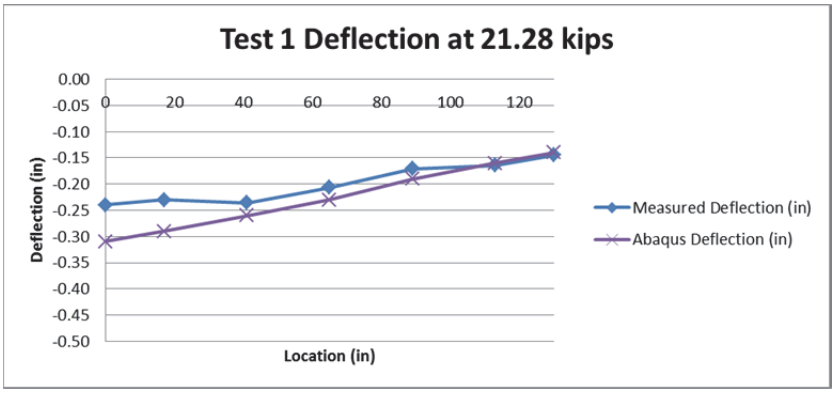

Test 2 Maximum Deflection Experimental and Abaqus Values

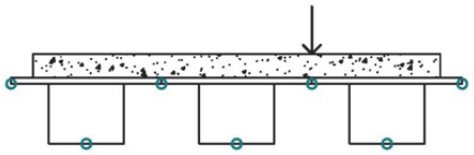

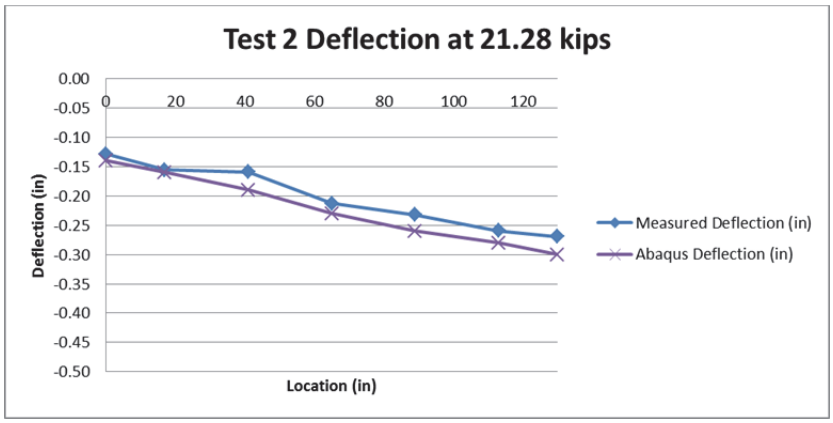

Test 3 Maximum Deflection Experimental and Abaqus Values

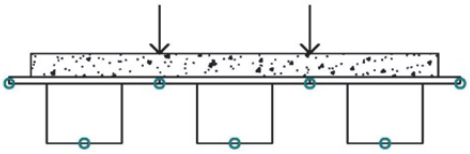

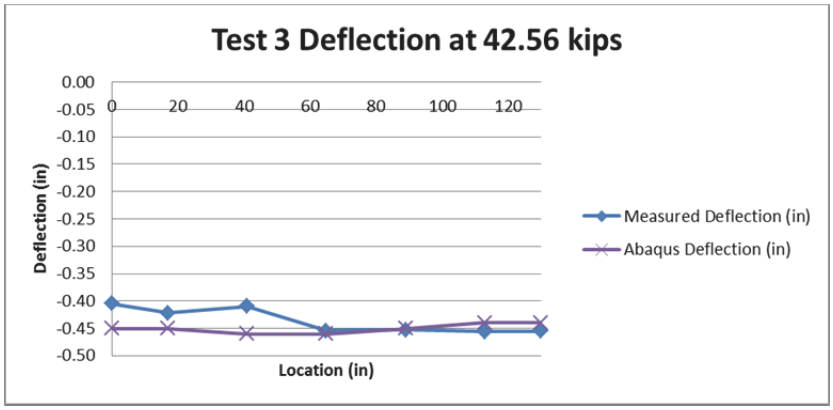

Test 4 Maximum Deflection Experimental and Abaqus Values

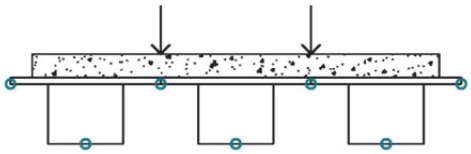

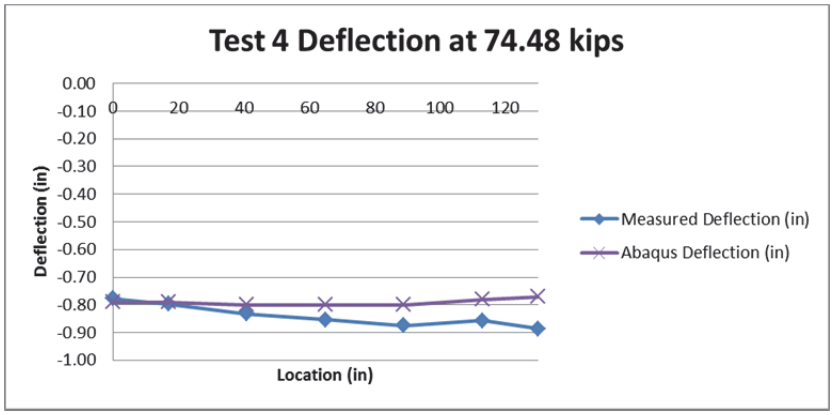

Test 5 Maximum Deflection Experimental and Abaqus Values

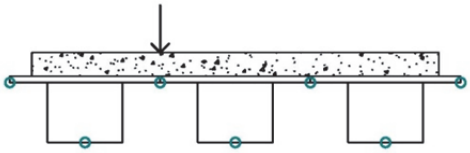

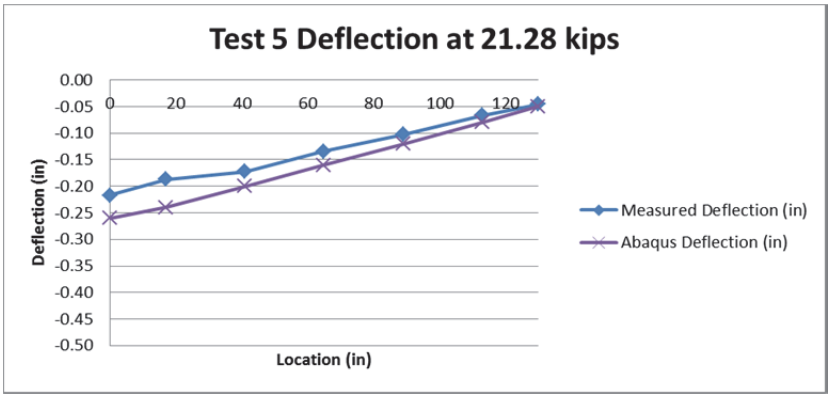

Test 6 Maximum Deflection Experimental and Abaqus Values

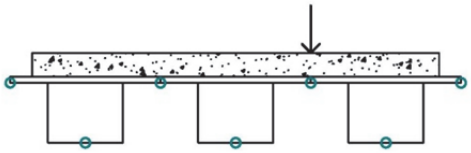

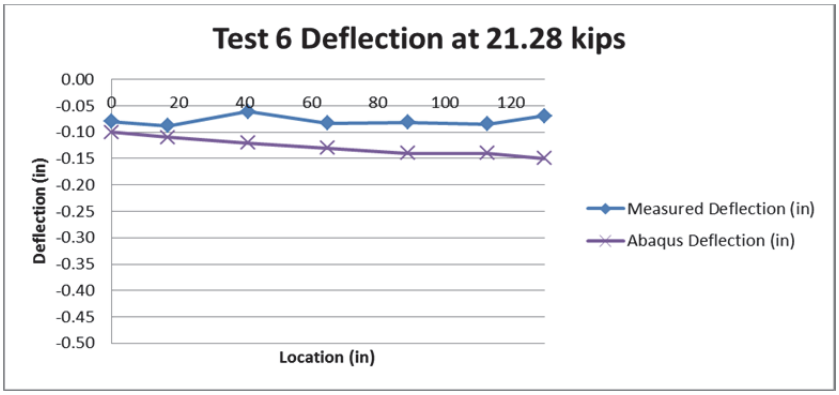

Test 7 Maximum Deflection Experimental and Abaqus Values

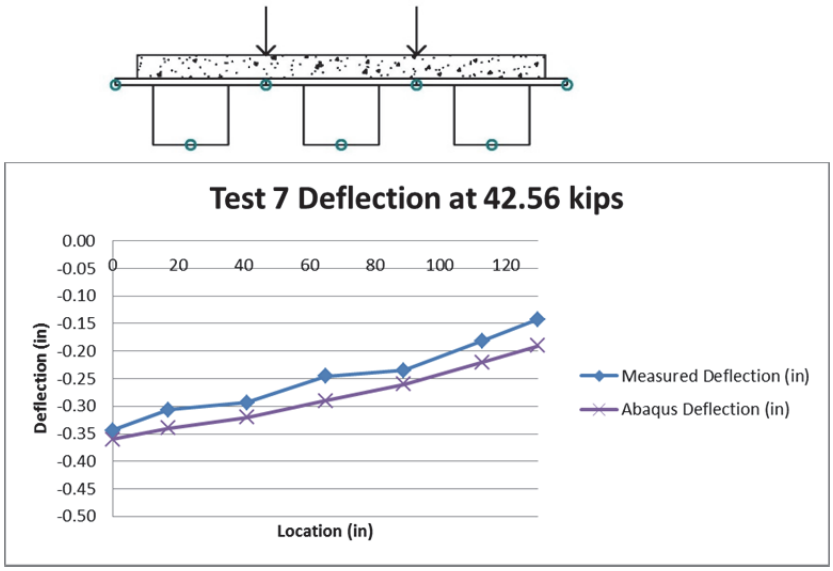

Test 8 Maximum Deflection Experimental and Abaqus Values

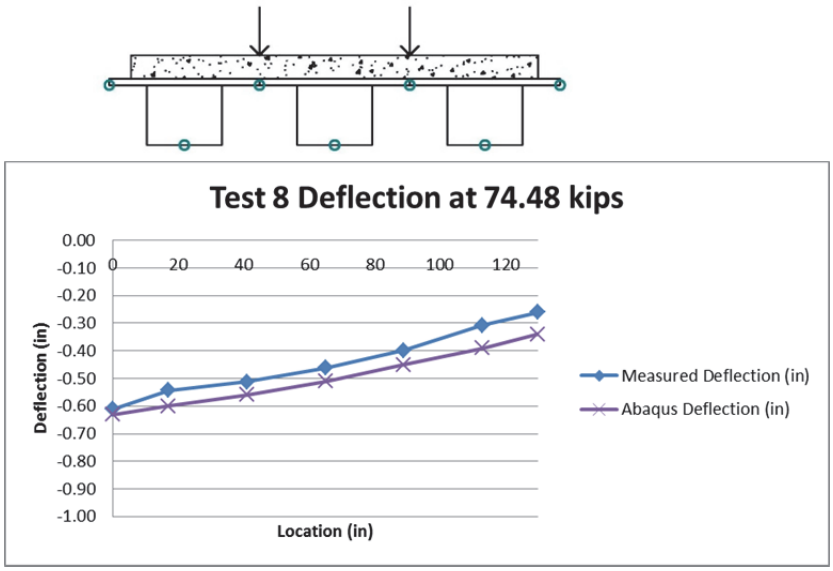

Test 9 Maximum Deflection Experimental and Abaqus Values

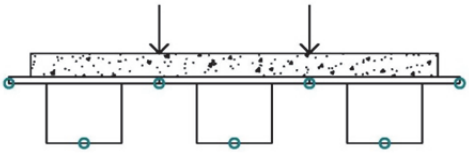

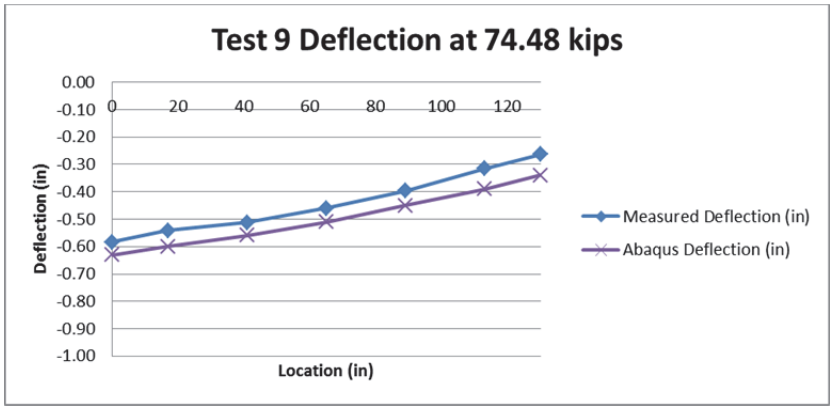

APPENDIX F: NEW DESIGN CALCULATIONS

Loads Chosen

When using the strip method, the moments are moved around until the maximum moment is found. In order to find the loading position with the maximum moment, influence lines were created for the maximum positive and negative moments for the Tide Mill Bridge.

Influence Line for Positive Moment Between the Beams:

Influence Line for Negative Moment over the support:

The influence of the load diminishes as it is applied further away from the place in question.

The test bridge only had 3 beams and therefore it has only 2 spans when using the strip method.

In order to get the maximum positive moment, a point load would be placed at the center of the span and the other would be 6 ft away right over the center of a beam. Therefore, only the load at the midspan is shown below.

To get the maximum negative moment, two truck loads would be used with one wheel from each truck near the center of the two spans adjacent to the support where the maximum negative moment is desired. Therefore, one wheel load from each truck is shown below applied at the center of each span.

Transverse Positive Moment Reinforcement

Beam Spacing: $S := 4 \cdot ft$

Proposed Effective Width: $SW_{ppos} := 6 \cdot ft$

AASHTO Effective Width: $SW_{AASHTOpos} := \left(26 + 6.6 \cdot \frac{S}{ft}\right) \cdot in = 4.4\,ft$

Maximum Moment Using Point Loads:

$P := 21.3 \cdot kip$

One Span Loaded:

$M_{pos\_point} := \frac{13}{64} \cdot P \cdot S = 17.3 \cdot kip \cdot ft$

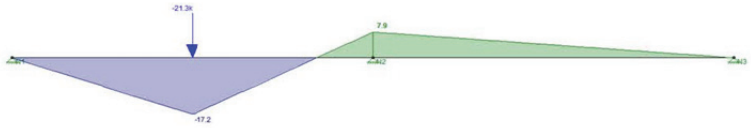

$M_{pos\_point2} := \frac{M_{pos\_point}}{SW_{ppos}} = 2.9 \cdot \frac{kip \cdot ft}{ft}$

Two Spans Loaded:

$Factored\_M_{pospoint} := 1.75 \cdot M_{pos\_point2} = 5.0 \cdot \frac{kip \cdot ft}{ft}$

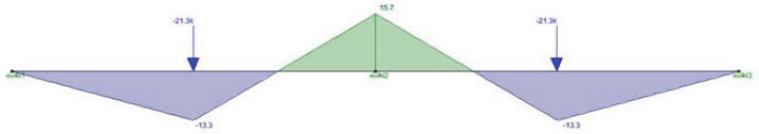

$M_{pos\_pointb} := \frac{13.3}{SW_{ppos}} \cdot kip \cdot ft = 2.2 \cdot \frac{kip \cdot ft}{ft}$

$Factored\_M_{pospointb} := 1.75 \cdot M_{pos\_pointb} = 3.9 \cdot \frac{kip \cdot ft}{ft}$

Maximum Moment Using Distributed Load in RISA 2D:

One Span Loaded:

$M_{pos\_dist} := 2.2 \cdot \frac{kip \cdot ft}{ft}$ from RISA shown below

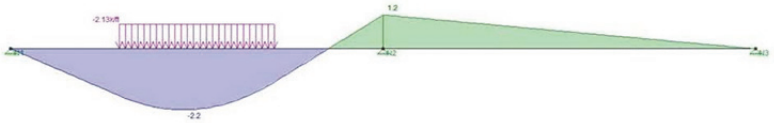

$Factored\_M_{posdist} := 1.75 \cdot M_{pos\_dist} = 3.9 \cdot \frac{kip \cdot ft}{ft}$

Two Spans Loaded:

$M_{pos\_distb} := 0.7 \cdot \frac{kip \cdot ft}{ft}$ from RISA shown below

$Factored\_M_{posdistb} := 1.75 \cdot M_{pos\_distb} = 1.2 \cdot \frac{kip \cdot ft}{ft}$

Positive Moment Rebar Design:

The biggest factored moment is from the single point load application:

$Factored\_M_{pospoint} = 5.0 \cdot \frac{kip \cdot ft}{ft}$

$d := 5.75 \cdot in \quad \phi := 0.9 \quad f_y := 60 \cdot \frac{kip}{in^2} \quad f_c := 4 \cdot \frac{kip}{in^2}$

Try No. 4 Bars at 12 in.

$A_{sNo4} := 0.2 \cdot in^2$

$s := 12 \cdot in$

$A_s := A_{sNo4} \cdot \frac{12 \cdot in}{s} = 0.2 \cdot in^2$

$a := \frac{A_s \cdot f_y}{0.85 \cdot f_c \cdot 12 \cdot in} = 0.3 \cdot in$

$\phi M_n := \phi \cdot A_s \cdot f_y \cdot \left(d - \frac{a}{2} \right) = 5.0 \cdot kip \cdot ft$ per foot

this is equal to the required factored moment, therefore the design is okay

For Positive Moment Reinforcement, use No. 4 bars spaced at 12 in.

Transverse Negative Moment Reinforcement

Proposed Effective Width: $SW_{pneg} := 14.4 \cdot ft$

AASHTO Effective Width: $SW_{AASHTOneg} := \left(48 + 3 \cdot \frac{S}{ft}\right) \cdot in = 5.0\,ft$

Maximum Moment Using Point Loads:

$P := 21.3 \cdot kip$

$M_{neg\_point} := -\frac{3}{16} \cdot P \cdot S = -16.0 \cdot kip \cdot ft$

$M_{neg\_point2} := \frac{M_{neg\_point}}{SW_{pneg}} = -1.1 \cdot \frac{kip \cdot ft}{ft}$

$Factored\_M_{negpoint} := 1.75 \cdot M_{neg\_point2} = -1.9 \cdot \frac{kip \cdot ft}{ft}$

Maximum Moment Using Distributed Load in RISA 2D:

$M_{neg\_dist} := -1 \cdot \frac{kip \cdot ft}{ft}$ from RISA shown below

$Factored\_M_{negdist} := 1.75 \cdot M_{neg\_dist} = -1.8 \cdot \frac{kip \cdot ft}{ft}$

Negative Moment Rebar Design:

The biggest factored moment is from the double point load application:

$$\text{Factored\_M}_{negpoint} = -1.9 \cdot \frac{kip \cdot ft}{ft}$$

This is the moment right above the center of the beam. The design section is really at the face of the beams, so the factored moment used was linear interpolated to be:

$$\text{Factored\_M}_{negpoint} := -1.2 \cdot \frac{kip \cdot ft}{ft}$$

$$d := 4.5 \cdot in$$

Try No. 4 Bars at 18 in . to satisfy temperature and shrinkate spacing requirements

$$A_{sNo4} := 0.2 \cdot in^2$$

$$s := 18 \cdot in$$

$$A_s := A_{sNo4} \cdot \frac{12 \cdot in}{s} = 0.1 \cdot in^2$$

$$a := \frac{A_s \cdot f_y}{0.85 \cdot f_c \cdot 12 \cdot in} = 0.2 \cdot in$$

$$\phi M_n := \phi \cdot A_s \cdot f_y \cdot \left(d - \frac{a}{2} \right) = 2.6 \cdot kip \cdot ft$$ per foot — this is greater than the required factored moment, therefore the design is okay

For Negaive Moment Reinforcement, use No. 4 bars spaced at 18 in.

Crack Control Calculations:

Define Variables:

$f_y := 60 \cdot ksi$ $f_c := 4 \cdot ksi$

$E_s := 29000 ksi$ $E_c := 4381 \cdot ksi$

$n := \frac{E_s}{E_c} = 6.619$

$b := 12 \cdot in$ $h := 7.5 \cdot in$

$M_{upos} := 5 \cdot kip \cdot ft$

$M_{uneg} := 1.2 \cdot kip \cdot ft$

$cover_{top} := 2.75 \cdot in$ $cover_{bot} := 1.5 \cdot in$

$d_{no4} := 0.5 \cdot in$

$d_{pos} := h - cover_{bot} - \frac{1}{2} \cdot d_{no4} = 5.75 \cdot in$

$d_{neg} := h - cover_{top} - \frac{1}{2} \cdot d_{no4} = 4.5 \cdot in$

$\gamma_e := 0.75$

Check Crack Control at Service I

Positive Moment:

$$A_{spos} := 0.2\cdot in^2\cdot\frac{b}{7\cdot in} = 0.343\cdot in^2$$

$$d_c := h - d_{pos} = 1.75\cdot in$$

$$\rho := \frac{A_{spos}}{b\cdot d_{pos}} = 4.969\times 10^{-3}$$

$$k := -n\cdot\rho + \sqrt{(n\cdot\rho)^2 + 2\cdot n\cdot\rho} = 0.226$$

$$j := 1 - \frac{1}{3}\cdot k = 0.925$$

$$f_{ss} := \frac{M_{upos}}{j\cdot A_{spos}\cdot d_{pos}}\cdot\frac{12\cdot in}{1\cdot ft} = 32.911\cdot ksi$$

$$\beta_s := 1 + \frac{d_c}{0.7\cdot(h - d_c)} = 1.435$$

$$s_{max} := \frac{700\cdot\gamma_e}{\beta_s\cdot\frac{f_{ss}}{ksi}}\cdot in - 2\cdot d_c = 7.618\cdot in$$

Negative Moment:

$$A_{sneg} := 0.2\cdot in^2\cdot\frac{b}{11\cdot in} = 0.218\cdot in^2$$

$$d_{neg} := h - d_{neg} = 3\cdot in$$

$$\rho := \frac{A_{sneg}}{b\cdot d_{neg}} = 4.04\times 10^{-3}$$

$$k := -n\cdot\rho + \sqrt{(n\cdot\rho)^2 + 2\cdot n\cdot\rho} = 0.206$$

$$j := 1 - \frac{1}{3}\cdot k = 0.931$$

$$f_{ss} := \frac{M_{uneg}}{j\cdot A_{sneg}\cdot d_{neg}}\cdot\frac{12\cdot in}{1\cdot ft} = 15.748\cdot ksi$$

$$\beta_s := 1 + \frac{d_c}{0.7\cdot(h - d_c)} = 1.952$$

$$s_{max} := \frac{700\cdot\gamma_e}{\beta_s\cdot\frac{f_{ss}}{ksi}}\cdot in - 2\cdot d_c = 11.075\cdot in$$

$$NewDesignSteel := \frac{0.2\cdot in^2}{7\cdot in} + \frac{0.2\cdot in^2}{11\cdot in} = 0.561\cdot\frac{in^2}{ft}$$

$$OriginalDesignSteel := \frac{0.31\cdot in^2}{14\cdot in}\cdot 2 + \frac{0.31\cdot in^2}{14\cdot in} = 0.797\cdot\frac{in^2}{ft}$$

$$PercentSaved := 100\cdot\left(1 - \frac{NewDesignSteel}{OriginalDesignSteel}\right) = 29.619$$